JOINT DESIGN OF PAPR, PICR, AND OBP IN OFDM SYSTEMS

by

Kewei Yuan

A thesis submitted to the faculty of graduate studies
Lakehead University
in partial fulfillment of the requirements for the degree of
Masters of Science in Engineering

Department of Control Engineering

Lakehead University

August 2008

Copyright © Kewei Yuan 2008

Library and Archives Canada

Published Heritage Branch

395 Wellington Street
Ottawa ON K1A 0N4
Canada

Bibliothèque et Archives Canada

Direction du Patrimoine de l'édition

395, rue Wellington
Ottawa ON K1A 0N4
Canada

Your file Votre référence
ISBN: 978-0-494-43439-0
Our file Notre référence
ISBN: 978-0-494-43439-0

NOTICE:
The author has granted a non-exclusive license allowing Library and Archives Canada to reproduce, publish, archive, preserve, conserve, communicate to the public by telecommunication or on the Internet, loan, distribute and sell theses worldwide, for commercial or non-commercial purposes, in microform, paper, electronic and/or any other formats.

The author retains copyright ownership and moral rights in this thesis. Neither the thesis nor substantial extracts from it may be printed or otherwise reproduced without the author's permission.

AVIS:
L'auteur a accordé une licence non exclusive permettant à la Bibliothèque et Archives Canada de reproduire, publier, archiver, sauvegarder, conserver, transmettre au public par télécommunication ou par l'Internet, prêter, distribuer et vendre des thèses partout dans le monde, à des fins commerciales ou autres, sur support microforme, papier, électronique et/ou autres formats.

L'auteur conserve la propriété du droit d'auteur et des droits moraux qui protège cette thèse. Ni la thèse ni des extraits substantiels de celle-ci ne doivent être imprimés ou autrement reproduits sans son autorisation.

In compliance with the Canadian Privacy Act some supporting forms may have been removed from this thesis.

While these forms may be included in the document page count, their removal does not represent any loss of content from the thesis.

Conformément à la loi canadienne sur la protection de la vie privée, quelques formulaires secondaires ont été enlevés de cette thèse.

Bien que ces formulaires aient inclus dans la pagination, il n'y aura aucun contenu manquant.

Canada

Contents

List of Tables v

List of Fingures vii

Abbreviations viii

Symbols ix

Acknowledgments xii

Abstract xiii

1 Introduction 1
- 1.1 Previous Work 2
- 1.2 Scope and Contributions of the Thesis 4

2 Fundamentals of OFDM 7
- 2.1 Wireless Multipath Channel 7
- 2.2 OFDM Techniques 9

3 PAPR, PICR, and OBP Problems in OFDM Systems 14
- 3.1 PAPR Reduction 14
- 3.2 PICR Reduction 15
- 3.3 OBP Reduction 16
- 3.4 Techniques to Reduce PAPR and PICR 19
  - 3.4.1 Partial Transmit Sequence Technique 19
  - 3.4.2 Selective Mapping Technique 22

4 Joint Design of PAPR and PICR in OFDM Systems 23
- 4.1 Joint PAPR and PICR Design 23
  - 4.1.1 Joint Constrained PAPR-PICR Reduction Problem 24
  - 4.1.2 Joint Weighted PAPR-PICR Reduction Problem 27
- 4.2 Simulation Results 30
- 4.3 Conclusion 32

5 Joint Design of PAPR, PICR, and OBP in OFDM Systems 38
5.1 System Model 38
5.2 PAPR, PICR, and OBP Problems for the System Model in Section 5.1 40
5.3 Joint PAPR, PICR, and OBP Design 41
5.3.1 Problem Formulation 43
5.3.2 Algorithm Based on Phase Rotation Approach 44
5.3.3 Algorithm Based on the Constellation Extension Approach . . 50
5.4 Simulation Results 58
5.4.1 Algorithm Based on Phase Rotation Approach 59
5.4.2 Algorithm Based on Constellation Extension Approach 71
5.5 Conclusion 72

6 Conclusions 81

7 Future Work 82

References 83

A Basic Concepts and Properties of DFT and IDFT 88

B Some Derivations for OFDM 90
B.1 Cyclic Prefix in OFDM Signals 90
B.2 The Minimum Frequency Separation of Subcarriers in OFDM Signals 92
B.3 Matrix Representation of OFDM Received Signal 93

C Second Order Cone Programming 97

D Formulation of the Angle Constraint 100

Index 102

List of Tables

4.1 PTS based joint constrained PAPR-PICR reduction algorithm 26
4.2 The range of PICR values of OFDM signals 29

5.1 The threshold values by using phase rotation based algorithm 60
5.2 The threshold values by using constellation extension based algorithm with M=4 72

List of Figures

2.1 Illustration of ISI in a wireless channel 8
2.2 Principle of OFDM 9
2.3 Block diagram of an OFDM system 11

3.1 The spectrum of an OFDM signal 17
3.2 The PTS technique at transmitter end 19
3.3 The PTS technique at the receiver end 20

4.1 CCDF of PICR for an fast time-varying frequency-selective Rayleigh fading channel (joint weighted PAPR-PICR problem). 34
4.2 CCDF of PAPR for an fast time-varying frequency-selective Rayleigh fading channel (joint weighted PAPR-PICR problem). 35
4.3 CCDF of PICR for an fast time-varying frequency-selective Rayleigh fading channel with $\gamma = 7,\ 8,\ 9$ dB (joint constrained PAPR-PICR problem). 36
4.4 CCDF of PAPR for an fast time-varying frequency-selective Rayleigh fading channel with $\gamma = 7,\ 8,\ 9$ dB (joint constrained PAPR-PICR problem). 37

5.1 The PSD of an OFDM system with $N = 12$, $M = 4$, and $K_1 = K_2 = 7$ 42
5.2 Phase rotation approach 44
5.3 Relaxed solution region 48
5.4 Feasible region of 8PSK for the constellation extension approach. . . . 51
5.5 Feasible region of 16QAM for the constellation extension approach. . 52
5.6 CCDFs for individual optimal problems with 16QAM (phase rotation approach) 62
5.7 CCDFs for joint problem as a function of θ (phase rotation approach) 63
5.8 Phase rotation based PICR reduction for OFDM systems with 16QAM 64
5.9 Phase rotation based PAPR reduction for OFDM systems with 16QAM 65
5.10 Phase rotation based OBP reduction for OFDM systems with 16QAM 66
5.11 Phase rotation based PICR reduction for OFDM systems with 8PSK modulation 67
5.12 Phase rotation based PAPR reduction for OFDM systems with 8PSK modulation 68

5.13 Phase rotation based OBP reduction for OFDM systems with 8PSK modulation 69
5.14 Power spectrum of the joint designed and the original OFDM symbols with 8PSK modulation (phase rotation approach) 70
5.15 CCDFs for individual problems with 16QAM (constellation extension approach) 73
5.16 Constellation extension based PICR reduction for OFDM systems with 16QAM 74
5.17 Constellation extension based PAPR reduction for OFDM systems with 16QAM 75
5.18 Constellation extension based OBP reduction for OFDM systems with 16QAM 76
5.19 Constellation extension based PICR reduction for OFDM systems with 8PSK modulation 77
5.20 Constellation extension based PAPR reduction for OFDM systems with 8PSK modulation 78
5.21 Constellation extension based OBP reduction for OFDM systems with 8PSK modulation 79
5.22 The constellations of optimal symbols 80

C.1 Second order cones of dimension k=1, 2, and 3 98

Abbreviations

ADC	Analogue to digital converter
AWGN	Additive white Gaussian noise
BER	Bit-error rate
BPSK	Binary phase shift keying
CCDF	Complimentary cumulative density functions
CFO	Carrier frequency offset
CP	Cyclic prefix
DAB	Digital audio broadcasting
DAC	Digital to analogue converter
DFT	Discrete Fortier transformer
DVB	Digital video broadcasting
FDM	Frequency-division multiplexing
FTV	Fast time-varying
ICI	Inter-carrier interference
ICR	Interference-to-carrier ratio
IDFT	Inverse discrete Fourier transformer
ISI	Inter-symbol interference
MPSK	M-ary phase-shift keying
MQAM	M-ary quadrature amplitude modulation
OBP	Out-of-band power
OFDM	Orthogonal frequency division multiplexing
P/S	Parallel to series
PA	Power amplifiers
PAPR	Peak-to-average power ratio
PICR	Peak interference-to-carrier ratio
PTS	Partial transmit sequences
QAM	Quadrature amplitude modulation
QS	Quasi-static
SLM	Selective mapping
SOCP	Second order cone programming
TDL	Tapped delay line
TI	Tone insertion
TR	Tone reservation
WSSUS	Wide-sense stationary uncorrelated scattering

Symbols

A :	The amplitude of a rectangular pulse
$\mathbf{A}_\varepsilon$:	The matrix which is defined as $\mathbf{F}_\varepsilon^{\mathbf{H}}\mathbf{HF}$
$\mathbf{A}_\varepsilon^{\mathbf{0}}$:	The matrix which is obtained by replacing all diagnal elements with zeros in $\mathbf{A}_\varepsilon$
$\mathbf{b}$:	The phase rotatin factor vector used in the PTS technique
$\mathbf{b}_\mathbf{k}^\mathbf{T}$:	The column vector which is the k^{th}row of$\mathbf{A}_\varepsilon^{\mathbf{0}}$
$\widehat{\mathbf{B}}_\mathbf{k}^\mathbf{T}$:	The matrix obtained by $\mathbf{b}_\mathbf{k}^\mathbf{T}$and defined in (5.17)
$\widetilde{\mathbf{B}}_\mathbf{k}^\mathbf{T}$:	The matrix obtained by $\widehat{\mathbf{B}}_\mathbf{k}^\mathbf{T}$and defined in (5.18)
$\widetilde{\mathbf{B}}_\mathbf{k}^\mathbf{q}$:	The matrix used for the 16QAM modulation scheme and defined in (5.34)
$\mathbf{c}^\mathbf{m}$:	The column vector which is used in the PTS technique and defined in (3.16)
$\overline{\mathbf{c}}^\mathbf{m}$:	The column vector which is formed by $\mathbf{c}^\mathbf{m}$
$\mathbf{c}_\mathbf{rk}$:	The column vector which is defined by (5.18)
$(\mathbf{c}_\mathbf{ek}^\mathbf{q})^\mathbf{T}$:	The k^{th}row of the matrix $\widetilde{\mathbf{R}}^\mathbf{q}$
$\mathbf{d}_\mathbf{e}$:	The column vector which is defined by (5.28)
$\mathbf{d}_\mathbf{r}$:	The column vector which is defined by (5.18)
$\mathbf{D}_\varepsilon$:	Diagnal matrix with diagnals $[1, \ , e^{j2\pi\varepsilon/N}, \cdot, e^{j2\pi\varepsilon(N-1)/N}]$
$\widehat{\mathbf{D}}^\mathbf{T}$:	The matrix which is defined in (5.17)
$\widetilde{\mathbf{D}}_\mathbf{r}^\mathbf{T}$:	The matrix which is defined in (5.18)
$\widetilde{\mathbf{D}}_\mathbf{e}^\mathbf{p}$:	The matrix which is defined in (5.30)
$\widetilde{\mathbf{D}}_\mathbf{e}^\mathbf{q}$:	The matrix which is defined in (5.33)
$E\{X_n\}$:	The expectation of r.v. X_n
$\mathbf{E}$:	The matrix with all elements being ones
f :	Frequency
f_n :	The frequency of the nth subcarriers
$\Delta f'$:	The frequency offset
$\mathbf{f}_\mathbf{k}^\mathbf{T}$:	The column vector which is the k^{th}row of $\mathbf{F}$
$\widehat{\mathbf{f}}$:	The matrix which is defined in (5.17)
$\mathbf{F}$:	The DFT matrix
$\mathbf{F}^\mathbf{H}$:	The IDFT matrix
$\mathbf{F}_\varepsilon^\mathbf{H}$:	The IDFT matrix associated with ε and defined in (2.10)
$g(t)$:	The rectangular pulse
$\widehat{\mathbf{g}}$:	The column vector which is defined in (5.17)
$G(f)$:	The spectrum of g(t)
$\widehat{\mathbf{G}}$:	The matrix which is defined in (5.17)

$\widetilde{\mathbf{G}}$:	The matrix which is defined in (5.18)
$\widetilde{\mathbf{G}}^{\mathbf{q}}$:	The matrix which is defined in (5.34)
$h(n,l)$:	The channel matrix coefficients
$\mathbf{H}$:	The channel matrix
I_m :	The ICI on the m^{th}subcarriers caused by the other subcarriers
$\mathbf{I}^a$:	The index vector which is defined in page 56
$\mathbf{I}^b$:	The index vector which is defined in page 56
$\mathbf{I}^r$:	The index vector which is formed by $\mathbf{I}^a$
$\mathbf{I}^i$:	The index vector which is formed by $\mathbf{I}^b$
$\widetilde{\mathbf{I}}$:	The matrix which is defined by (5.18)
$\widetilde{\mathbf{I}}^q$:	The matrix which is defined by (5.34)
$\mathbf{J}$:	The index vector which is formed by $\mathbf{I}^r$ and $\mathbf{I}^i$
K :	The number of sidelobes which is desired to be suppressed
L_2 :	L_2 norm
L_∞ :	L_∞ norm
L :	The over sampling factor used for the PTS technique
m :	The number of possible values on which the carrier phase takes in MPSK
M :	The number of subbloks used in the PTS technique in Chapter 3 and 4
M :	The number of sidelobe cancellation subcarriers in Chapter 5
$\mathbf{n}$:	AWGN noise vector with zero mean and covariance matrix $2\sigma^2\mathbf{I}$
N :	The number of subcarriers of an OFDM system
N_0 :	$M/2$ with M being the number of sidelobe cancellation subcarriers
N_1 :	$M/2+N$ with M being the number of sidelobe cancellation subcarriers
N_2 :	$M+N$ with M being the number of sidelobe cancellation subcarriers
$\mathbf{N}_0$:	The frequency domain noise vector which is defined by $\mathbf{F}^H\mathbf{n}$
$\mathbf{0}$:	The zero matrix
$\mathbf{P}$:	The OFDM symbol vector used for the PTS technique and defined in (3.20)
$\mathbf{P}'$:	The vector obtained by picking up first N components in $\mathbf{P}$
$\widehat{\mathbf{P}}_{\mathbf{k}}^{\mathbf{T}}$:	The matrix obtained by $\mathbf{f}_{\mathbf{k}}^{\mathbf{T}}$and defined in (5.17)
$\widetilde{\mathbf{P}}_{\mathbf{k}}^{\mathbf{T}}$:	The matrix obtained by $\widehat{\mathbf{P}}_{\mathbf{k}}^{\mathbf{T}}$and defined in (5.18)
$\widetilde{\mathbf{P}}_{\mathbf{k}}^{\mathbf{q}}$:	The matrix used for the 16QAM modulation scheme and defined in (5.34)
Q :	The size of the modulation constellations
$\mathbf{r}_k$:	The rotation phasor on the k^{th}subcarriers
$\mathbf{R}_{\mathbf{m}}$:	The corresponding time domain column vector of $\mathbf{c}^m$
$\widetilde{\mathbf{R}}^{\mathbf{q}}$:	The matrix which is defined in (5.34)
$s(f)$:	The spectrum of an OFDM symbol
$s_n(f)$:	The spectrum of the nth subcarrier of an OFDM symbol
$S(f)$:	The power spectrum of an OFDM symbol which is defined in (3.11)
$\mathbf{s}$:	The spectrum vector of an OFDM symbol and which is defined in (3.15)
$sinc(f)$:	sinc function which is defined as $sinc(\pi f)/\pi f$
t :	The time instance
T_s :	The OFDM symbol duration

T_c : The delay between two adjacent multipaths
U : The length of each non-overlapping data blocks in the PTS technique
w : The weighting factor which is in $[0, 1]$
w_k : The normalized frequency at the middle point of a sidelobe
W : The size of the set of allowed phase factors in the PTS technique
$\mathbf{x}$: The corresponding time domain OFDM symbol vector of data subcarriers
$\mathbf{X}$: The expanded frequency domain OFDM symbol vector
$\overline{\mathbf{X}}$: The frequency domain OFDM symbol vector
$\widehat{\mathbf{x}}_{\mathbf{k}}$: The column vector which is defined in (5.18)
$\widehat{\mathbf{X}}$: The column vector which is defined in (5.17)
$\mathbf{X}_r$: The column vector which is defined in page 46
$\mathbf{X}_i$: The column vector which is defined in page 46
$\mathbf{y}$: The corresponding time domain vector of vector $\mathbf{Y}$
$\mathbf{Y}$: The frequency domain subcarrier modification vector
$\widehat{\mathbf{Y}}$: The column vector which is defined in (5.17)
$\mathbf{Y}_r$: The column vector which is defined in page 46
$\mathbf{Y}_i$: The column vector which is defined in page 46
$\widetilde{\mathbf{Y}}_{\mathbf{e}}^{\mathbf{q}}$: The column vector which is defined in (5.34)
$\mathbf{z}$: The corresponding time domain OFDM symbol vector at the receiver
$\mathbf{Z}$: The frequency domain OFDM symbol vector at the receiver
α : The parameter which is in $(0, 1)$ and is defined in page 43
β : The parameter which is in $(0, 1)$ and is used for limiting the transmission power
γ : The threshold for PAPR in Chapter 4
$\delta(t)$: The impulse response function
δ_k : The quantization angle which is in $\{-\theta, 0, \theta\}$
δ_k^* : The quantized optimal angle
ϵ : The normalized central frequency of a subcarrier
ε : The normalized frequency offset which is defined in (2.6)
$\mathcal{E}$: The average power of the original OFDM data symbol
η : The data transmission efficiency which is defined in (5.22)
θ : The rotation angle bound of the feasible area for $\mathbf{Y}$
μ : The number of multipaths of the channel
ξ : The PICR threshold variable
ξ_0 : The PICR threshold value obtained by solving (5.28) as $\mathbf{Y}_0 = \mathbf{0}$
τ : The threshold for PAPR in Chapter 5

Acknowledgments

I would like to thank my supervisor Dr. Zhiwei Mao for her theoretical and technical advice and guidance. Without her support and supervision, this thesis would not have been possibly done nicely.

I also would like to thank my co-supervisor Dr. Ruizhong Wei for his valuable suggestion and technical help.

I have spent a great time studying and working with my two supervisors. I have learnt a lot from them not only about knowledge and skills in doing research, but also about the attitude toward the work and life. Working with them, I feel my life was meaningful and rich.

Thank you to the both of my examiners, Dr. N. Yu and Dr. C. Christoffersen for your time in reviewing my thesis. Your comments are very valuable to me and make my thesis become perfect. Also I would like to thank Dr. K. Natarajan, as an acting-supervisor, and Dr. A. Tayebi, as the Control Engineering program coordinator, who take extra time and effort to organize my thesis defense after Dr. Zhiwei Mao left from lakehead University.

This work was supported by a Discovery Grant from the Natural Sciences and Engineering Research Council (NSERC) of Canada and an Ontario Graduate Scholarship (OGS). We gratefully acknowledge the organizations for their financing supports.

Abstract

Orthogonal frequency division multiplexing (OFDM) technique has been adopted by many existing and future wireless communication systems for high-speed data transmission. However, a major problem of OFDM systems is the high peak-to-average power ratio (PAPR) of OFDM signals, which results in inefficient operations of nonlinear devices in the system such as power amplifiers (PAs). On the other hand, at the receiver end, frequency offset, caused by Doppler frequency shifts, mismatched oscillators, or a fast fading channel, destroys the orthogonality among subcarriers and results in inter-carrier interference (ICI), thus degrades the detection performance of OFDM systems. Analogous to the definition of PAPR, the peak interference-to-carrier ratio (PICR) is defined to represent the effect of ICI. In addition, due to the sidelobes of modulated subcarriers, OFDM systems also suffer from high out-of-band power (OBP) radiations. High OBP results in the need for wide guard band and thus inefficient usage of frequency band.

In order to improve the performance of OFDM systems, PAPR, PICR, and OBP should be reduced. The PAPR and PICR reduction problems have been studied extensively in literature. Methods of OBP reduction to make best use of spectral resources have also been studied. However, most of previous studies consider PAPR reduction, PICR reduction, or OBP reduction separately. Our simulation results show that if only one of the three problems is considered, the performance of the other two problems can be quite bad. Therefore, it is desirable to design an OFDM system considering PAPR, PICR, and OBP problems jointly so that the performance of the whole system is satisfactory.

In this thesis, two schemes are proposed for joint reduction of PICR and PAPR. Simulation results are presented to demonstrate efficacy of the proposed schemes in reducing PAPR and PICR. The low computational complexity makes them appropriate for practical OFDM systems.

In addition, the joint PAPR, PICR, and OBP design problem is also considered in this thesis. Two approaches, the phase rotation approach and the constellation extension approach, are proposed for this joint design problem. In each approach, this joint problem is modelled as a constrained optimization problem with continuous variables. The optimization problem is then relaxed into a second order cone programming (SOCP) problem, whose global optimal solution can be obtained efficiently. Simulation results show that the proposed schemes are effective and the optimized OFDM system has very good performance.

Chapter 1

Introduction

As an important high-speed data transmission technique in modern wireless communication systems, orthogonal frequency division multiplexing (OFDM) can reduce or eliminate inter-symbol interference (ISI) appeared in frequency-selective channels due to multipath propagation, and thus considerably increase data transmission rate. OFDM has been adopted by many existing and future wireless systems such as IEEE WiFi systems, IEEE WiMax systems, European digital audio broadcasting (DAB) and digital video broadcasting (DVB) systems, etc. [1]-[4].

A major problem of OFDM is the high peak-to-average power ratio (PAPR) of OFDM signals [5]. High PAPR of OFDM signals forces nonlinear devices in the system, such as power amplifiers (PAs), to leave a large backoff capacity to ensure that the devices can always operate in their linear response regions and signal distortion is avoided. However, this results in inefficiency of the devices. Therefore, it is desirable to reduce the PAPR of OFDM signals.

On the other hand, Doppler frequency shifts, mismatched oscillators or timing synchronization errors at receiver cause carrier frequency offset (CFO). In addition, in a fast fading channel, the channel may be time-varying even within one OFDM symbol duration. CFO or/and fast time-varying fading channel destroy the

orthogonality among subcarriers and lead to inter-carrier interference (ICI), thus impair the detection performance at the receiver. Analogous to the definition of PAPR, the peak interference-to-carrier ratio (PICR) is defined in [14] to represent the effect of ICI at the receiver. High PICR of received signal degrades bit-error rate (BER) performance of OFDM systems and thus it is desirable to reduce the PICR of the OFDM received signals.

In addition, due to the sidelobes of modulated subcarriers, OFDM systems also suffer from high out-of-band power (OBP) radiations. Especially in an OFDM based overlay system, which fills frequency gaps left by existing legacy systems, a high OBP of the overlay system leads to significant interferences to the legacy systems. Therefore, high OBP results in the need for wide guard band and thus inefficient usage of frequency band. In order to make the best use of the spectral resource, it is also desirable to reduce the OBP of OFDM systems.

1.1 Previous Work

The PAPR reduction problem has been studied extensively in literature and many schemes have been proposed [6]. For instance, the coding techniques select the codewords that minimize or reduce the PAPR for transmission [7]-[9]. The selective mapping (SLM) techniques generate a set of candidate data blocks, all representing the same information block, and select the data block with the lowest PAPR for transmission [10]-[13]. The partial transmit sequences (PTS) techniques weight the disjointedly partitioned subblocks of the input data block with appropriate phases so that the PAPR of the combined signal is minimized [14]-[17]. The tone reservation (TR) technique sets aside a small subset of subcarriers unused for

information data transmission and sets appropriate symbols on those subcarriers for PAPR reduction [18]. In the tone insertion (TI) technique, the constellation size is increased so that each information symbol can be mapped into one of several equivalent constellation points. The symbol mappings are determined to reduce PAPR [18]. The signal distortion techniques reduce high peaks by modifying the modulation constellation [19]-[23].

In [21], the scheme is to scale the envelopes of the symbols on some subcarriers so that the PAPR is minimized. This method is suitable for m-ary phase-shift keying (MPSK) modulation schemes, where the envelopes of all symbols are equal and only the phases represent information. Since the modified symbols on all subcarriers have the same phases as the original ones even though the envelopes may be changed, the receiver can detect the received sequence without any side information.

In [22], the scheme is to reduce PAPR by modifying the modulation constellation in active subcarriers and setting appropriate symbols on unused subcarriers. To avoid from transmitting side information for recovering the original transmitted signal, the modified constellations should be in certain feasible areas.

From the above description, it is seen that in the signal distortion technique, some of the transmission power is consumed solely for PAPR reduction but not for information data transmission. Thus the BER performance will degrade if the total transmission power is kept constant.

The SLM and the PTS techniques have also been proposed to reduce PICR to improve BER performance of the system [14]. These techniques involve with finding the optimal phase factors by using an exhaustive search over the combinations of

phase factors which are restricted to finite set of values. Apparently, to get better performance, the size of the phase factor set or the number of phase combinations needs to be increased, which leads to dramatic increase in search complexity. In addition, these techniques require the transmission of side information.

In [20], the signal distortion technique is used for ICI reduction in an OFDM system using quadrature amplitude modulation (QAM) schemes.

In order to make the best use of the spectral resource, reducing OBP of OFDM systems has been discussed recently in some papers [24] [25]. One method is to reduce the sidelobe radiation by inserting a few weighted cancellation carriers by both sides of the OFDM signal spectrum.

1.2 Scope and Contributions of the Thesis

As discussed above, in OFDM systems, high PAPR of OFDM signal results in inefficient operations of nonlinear devices used in the system. High PICR of the received signal degrades BER performance of the receiver. And high OBP radiations decrease efficiency of the frequency band usage. Therefore, it is desirable to design the system considering PAPR, PICR and OBP problems jointly so that PAPR, PICR, and OBP are reduced and the performance of the system is improved. However, most of previous studies consider PAPR problem, PICR problem, or OBP problem solely, and most schemes in literature reduce PAPR, PICR, or OBP only. As shown later by simulation results in this thesis, when one of the problems is considered alone, the performance of the other two problems of the same system can be quite bad. Thus, in this thesis, the joint design problem is considered.

The joint PAPR and PICR design problem was considered in [26] and [27].

The block coding method is used in [26] to reduce both PAPR and PICR in an OFDM system. An exhaustive search was performed to find the best block code which reduces both PAPR and PICR for signal transmission. But no solid selection criterion is available in [26]. In addition, the block coding method suffers from high computational complexity and large storage space requirements, especially for systems with a large number of subcarriers. The joint PAPR and OBP reduction problem considered in [25] needs to choose an appropriate trade-off weighting factor.

The rest of this thesis is organized as follows. Chapter 2 provides the fundamentals of OFDM systems. The properties and model of wireless channels are also presented in this chapter. The PAPR, PICR, and OBP reduction problems are formulated in Chapter 3. The existing techniques used for reducing PAPR or PICR, such as PTS technique and SLM technique are also introduced in this chapter.

In Chapter 4, we formulate a joint constrained and a joint weighted PAPR and PICR reduction problems, which provide solid design criteria. Algorithms are also developed to jointly reduce both PAPR and PICR. Simulation results are presented to demonstrate efficacy of the proposed algorithms in reducing PAPR and PICR. With the extremely low computational complexity properties, it is possible to apply these algorithms to practical OFDM systems.

In Chapter 5, based on the phase rotation approach and the constellation extension approach, the PAPR, PICR, and OBP joint design problem is first modelled as a constrained optimization problem with continuous variables. The optimization problem is then relaxed into a second order cone programming (SOCP) problem, whose global optimal solution can be obtained efficiently. Simulation results show that the proposed schemes are effective in reducing PAPR, PICR, and OBP, and

the optimized system has very good performance.

Chapter 2

Fundamentals of OFDM

2.1 Wireless Multipath Channel

Assume a transmitter is transmitting a signal to the receiver through a wireless channel. The receiver may receive multiple copies of this signal from multiple paths with different delays due to the phenomena such as reflection, refraction, and scattering. The channel impulse response is used to described this property. Due to multipath propagation, inter-symbol interference (ISI) appears, which would limit the data transmission rate considerably if no measure is adopted to overcome this problem. Figure 2.1 shows an example which illustrates how ISI happens.

Assume a channel has an impulse response at time t as shown in Figure 2.1(a). If the transmitter sends a symbol at t_0, then the receiver will receive the first copy of the transmitted symbol at $t_0 + \tau_0$. The second copy with delay τ_1 and the third copy with longer delay τ_2 will be received consequently. The symbol and its copies are shown in Figure 2.1(b). In fact, in a symbol duration, the received signal should be the sum of all these copies which is shown in Figure 2.1(c).

The next symbol will be transmitted consequently from the transmitter. Assume the duration of a symbol is T_s and the second symbol is transmitted at $t_1 = t_0 + T_s$.

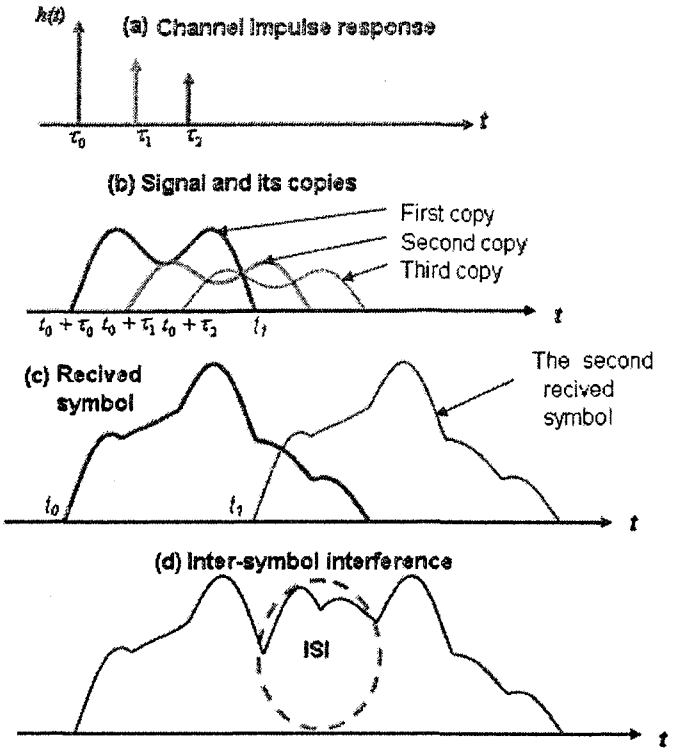

Figure 2.1: Illustration of ISI in a wireless channel

The second received symbol is also shown in Figure 2.1(c). Therefore, ISI happens. At the receiver end, the received symbols are corrupted by ISI, which is shown in Figure 2.1(d).

Based on the channel impulse response delay profile, the coherence bandwidth of a wireless channel can be defined [28]. If the wireless channel has a coherence bandwidth which is greater than the bandwidth of the transmitted signal, which is directly related to the transmitted symbol duration and thus the transmission data rate, then the received signal will undergo flat fading. Therefore, the spectra characteristics of the transmitted signal are preserved at the receiver, but the strength of the received signal may change with time. If the channel coherence bandwidth is

less than the transmitted signal bandwidth, then the received signal will undergo frequency-selective fading. In time domain, this means when the channel delay spread is great compared with the transmitted signal duration, ISI happens and the received signal is distorted, as shown in Figure 2.1.

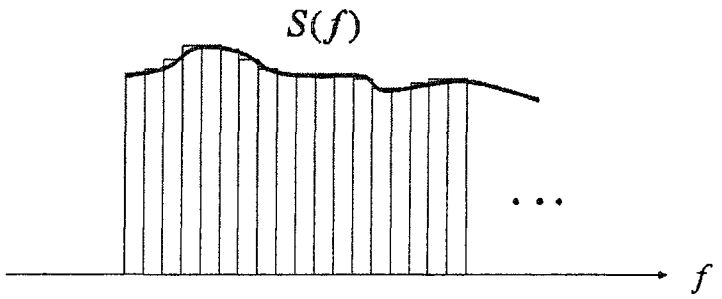

Figure 2.2: Principle of OFDM

2.2 OFDM Techniques

As shown in Figure 2.2, as a digital multi-carrier modulation method, in OFDM systems, a large number of closely-spaced orthogonal subcarriers are used to transmit data in a frequency-division multiplexing (FDM) manner. The information data stream is divided into several parallel data substreams, one for each subcarrier. Each subcarrier can be modulated using single-carrier modulation schemes in its associated bandwidth. Since the wideband system is broken into multiple subsystems with channel bandwidth being much less than the coherence bandwidth of the wireless channel, each subchannel undergoes relatively flat fading and the ISI problem is overcome. Thus, a high-speed data transmission can be achieved.

Figure 2.3 shows the block diagram of an OFDM system. Suppose that we consider an OFDM system of N subcarriers. At the transmitter, information bits are

first modulated using MPSK or m-ary quadrature amplitude modulation (MQAM), resulting in a complex symbol X. By passing through a series to parallel (S/P) converter, the series symbol stream is then converted to a block of N parallel symbols, which correspond to the symbols transmitted over each of the N subcarriers and are the frequency components of OFDM signals. By an inverse discrete Fourier transformer (IDFT), the frequency domain symbol block is transformed into the time domain OFDM symbol sample block $[x_0\ x_1\ \cdots\ x_{N-1}]^T$, where

$$x_n = \frac{1}{\sqrt{N}} \sum_{i=0}^{N-1} X_i e^{j2\pi ni/N} \qquad n = 0, \cdots, N-1. \tag{2.1}$$

where x_n denotes the time-domain signal at the nth sampling instant and $j^2 = -1$. In a matrix form, equation (2.1) can be expressed as

$$\mathbf{x} = \mathbf{F}\mathbf{X} \tag{2.2}$$

where $\mathbf{X} = [X_0\ X_1\ \cdots\ X_{N-1}]^T$, $\mathbf{x} = [x_0\ x_1\ \cdots\ x_{N-1}]^T$, and $\mathbf{F}$ is the IDFT matrix with the (n,i)th element $F(n,i) = \frac{1}{\sqrt{N}} e^{j2\pi ni/N}$ for $n, i = 0, \cdots, N-1$.

The OFDM symbol sample block is then converted to the sample stream by a parallel to series (P/S) converter. A cyclic prefix (CP) sequence is added to remove the remaining ISI. After passing through a digital to analogue converter (DAC), the sample stream becomes a continuous baseband signal $x(t)$ which is then upconverted into the passband signal $s(t)$ by the carrier signal $\cos(2\pi f_c t)$. Then $s(t)$ is transmitted through the channel.

In this thesis, a doubly frequency selective fading channel model is adopted [28]. Thus a wide-sense stationary uncorrelated scattering (WSSUS) channel is considered, whose impulse response is given by

$$h(t;\tau) = \sum_{d=0}^{\mu} h(t;\tau_d)\,\delta(\tau - \tau_d) \tag{2.3}$$

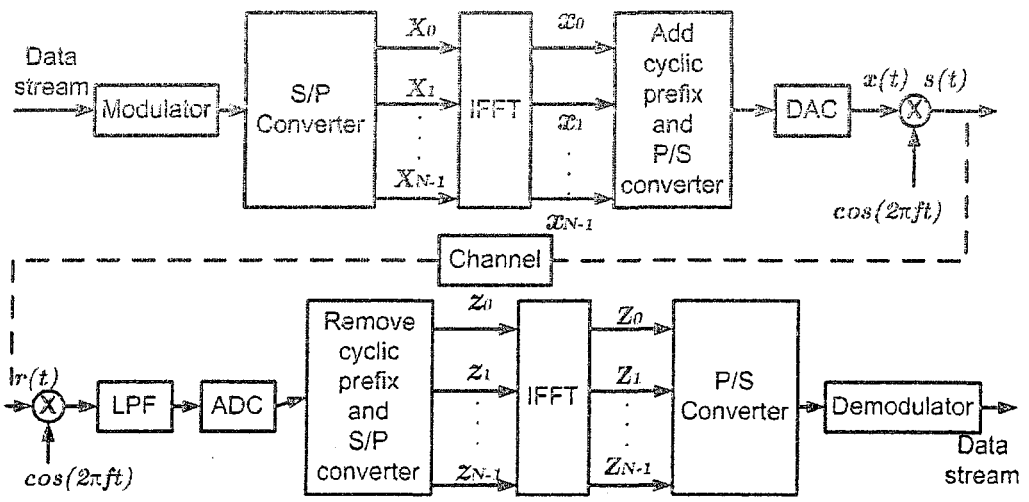

Figure 2.3: Block diagram of an OFDM system

where τ_d is the delay of the dth path with $\tau_0 < \tau_1 < \cdots < \tau_\mu$ and $\delta(\cdot)$ represents an impulse function. For a multipath fading channel, $h(t;\tau_d)$ is a complex random process. The number of multipaths is $\mu + 1$. A discrete version of the WSSUS channel in (2.3) can be expressed as a tapped delay line (TDL) filter with random taps

$$h\,(n,l) = h(nT_c; lT_c) \tag{2.4}$$

where $h(n,l)$ denotes the channel coefficient for the lth tap at the nth sampling instant and the delay between two taps is T_c, with $T_c = T_s/N$ being the duration of each sample and T_s being the OFDM symbol duration. For the sake of simplicity, we assume that the length of CP is greater than or at least equal to the maximum delay of the channel, ISI is thus not in presence in the received signal. We also consider the uncorrelated fading, which means all taps are independent each other.

At the receiver, the received signal $r(t)$ is first down-converted and filtered to obtain the baseband analog received signal. An analogue to digital converter (ADC) samples the analog received signal to obtain the sample stream. The first μ samples

in the sample stream are corrupted by ISI associated with the last μ samples of the transmitted signal in the previous block and are removed without any loss of original information. Therefore, the discrete demodulated signal can be expressed as

$$z_n = e^{j2\pi n\varepsilon/N} \sum_{k=0}^{\mu} x_{n-k} h(n,k) + v_n \qquad n = 0, \cdots, N-1 \tag{2.5}$$

where v_n is a complex additive white Gaussian noise (AWGN) process with independent real and imaginary components, each of which has zero mean and variance σ^2. ε is the normalized frequency offset which is defined as

$$\varepsilon = \Delta f' \cdot T_s \tag{2.6}$$

with $\Delta f'$ being the frequency offset of the receiver local carrier frequency above the correct carrier frequency [29].

As shown in Appendix B.3, the matrix form of (2.5) is written as

$$\mathbf{z} = \mathbf{D}_\varepsilon \mathbf{H} \mathbf{x} + \mathbf{n} \tag{2.7}$$

where $\mathbf{z} = [z_0 \ z_1 \ \cdots \ z_{N-1}]^T$ denotes the time-domain received signal, $\mathbf{n} = [v_0 \ v_1 \ \cdots \ v_{N-1}]^T$ denotes the AWGN noise with zero mean and covariance matrix $2\sigma^2\mathbf{I}$, $\mathbf{D}_\varepsilon = \text{diag}\{1, \ e^{j2\pi\varepsilon/N}, \ \ldots, \ e^{j2\pi\varepsilon(N-1)/N}\}$, and $\mathbf{H}$ is given by

$$\begin{bmatrix} h(0,0) & 0 & 0 & \cdots & 0 & h(0,\mu) & h(0,\mu-1) & \cdots & h(0,1) \\ h(1,1) & h(1,0) & 0 & \cdots & 0 & 0 & h(1,\mu) & \cdots & h(1,2) \\ \vdots & \vdots & \ddots & \ddots & \ddots & \ddots & \ddots & \ddots & \vdots \\ h(\mu,\mu) & h(\mu,\mu-1) & \cdots & \cdots & h(\mu,0) & 0 & 0 & \cdots & 0 \\ 0 & h(\mu+1,\mu) & \cdots & \cdots & h(\mu+1,1) & h(\mu+1,0) & 0 & \cdots & 0 \\ \vdots & \vdots & \ddots & \ddots & \ddots & \ddots & \ddots & \ddots & \vdots \\ 0 & 0 & 0 & \cdots & h(N-1,\mu) & h(N-1,\mu-1) & \cdots & \cdots & h(N-1,0) \end{bmatrix}. \tag{2.8}$$

Note that when $h(t;\tau)$ in (2.3) remains constant within one OFDM symbol dura-

tion, we have

$$\begin{cases} h(0,0) &= h(1,0) = \cdots = h(N-1,0) \\ h(0,1) &= h(1,1) = \cdots = h(N-1,1) \\ & \vdots \\ h(0,\mu) &= h(1,\mu) = \cdots = h(N-1,\mu) \end{cases} \tag{2.9}$$

and the channel is called quasi-static(QS). On the other hand, when $h(t;\tau)$ in (2.3) changes within one OFDM symbol duration, the channel is called fast time-varying (FTV).

The stream $\{z_n\}$ is converted into a block of N parallel data by a S/P and then transformed into a block of frequency domain symbols by passing through a discrete Fortier transformer (DFT). Then we have

$$\mathbf{Z} = \mathbf{F^H z} = \mathbf{F^H}(\mathbf{D}_\varepsilon \mathbf{H x} + \mathbf{n}) = \mathbf{A}_\varepsilon \mathbf{X} + \mathbf{N}_0 \tag{2.10}$$

where $\mathbf{A}_\varepsilon = \mathbf{F}_\varepsilon^H \mathbf{HF}$, $\mathbf{F}_\varepsilon^H = \mathbf{F^H D}_\varepsilon$ is an $N \times N$ matrix with the (n,i)th element $F_\varepsilon^H(n,i) = \frac{1}{\sqrt{N}} e^{-j2\pi(n-\varepsilon)i/N}$ $(n,i = 0,\cdots,N-1)$, and $\mathbf{N}_0 = \mathbf{F}^H\mathbf{n}$. After being converted to a serial symbol stream, the signal is ready for detection.

Chapter 3

PAPR, PICR, and OBP Problems in OFDM Systems

3.1 PAPR Reduction

The modulated symbols, X_i $(n = 0, \cdots, N-1)$ are statistically independent. If N is large, then the central limit theorem is applicable and the corresponding complex-valued time-domain samples of OFDM signal x_n $(n = 0, \cdots, N-1)$ are approximately complex Gaussian distributed. The magnitude of OFDM signal is thus approximately Rayleigh distributed. This results that the PAPR of signal $\mathbf{x}$, which is defined as

$$\text{PAPR} = \frac{\|\mathbf{x}\|_\infty^2}{E\left\{\|\mathbf{x}\|_2^2/N\right\}} \tag{3.1}$$

can be very high. In (3.1), $E\{\cdot\}$ denotes expectation, and $\|\cdot\|_2$ and $\|\cdot\|_\infty$ denote the L_2 and L_∞ norms of a vector, respectively. We can achieve PAPR reduction by minimizing (3.1).

3.2 PICR Reduction

It can be seen from (2.10) that the received signal on the mth subcarrier can be expressed as

$$Z_m = X_m A_\varepsilon(m,m) + \sum_{k=0,k\neq m}^{N-1} X_k A_\varepsilon(m,k) + N_{o,m} \qquad m = 0, \cdots, N-1 \tag{3.2}$$

where $A_\varepsilon(m,k)$ denotes the (m,k)th elements of $\mathbf{A}_\varepsilon$ and $N_{0,m}$ denotes the mth element of $\mathbf{N}_0$.

In (3.2), the first term represents the desired signal on the mth subcarrier, the second term, denoted as I_m, represents the ICI caused by other subcarriers, and the last term is the noise. Note that only when $\varepsilon = 0$ and (2.9) is satisfied, $\mathbf{A}_\varepsilon$ is reduced to a diagonal matrix such that $I_m = 0$. Otherwise, $\mathbf{A}_\varepsilon$ is not diagonal and $I_m \neq 0$. In other words, ICI can be caused by fast time-varying channel or the frequency offset at the receiver, or more likely, both. A high interference-to-carrier ratio (ICR) of the received signal $\mathbf{Z}$ on any subcarrier m, which is defined as

$$\mathrm{ICR}_m = \frac{|I_m|^2}{|X_m A_\varepsilon(m,m)|^2} \tag{3.3}$$

degrades the detection performance of OFDM on that subcarrier. Similar to the definition of PAPR in (3.1), the PICR of the received signal $\mathbf{Z}$ is defined in [14] as

$$\mathrm{PICR} = \max_{0\leq m\leq N-1} \mathrm{ICR}_m \tag{3.4}$$

which specifies the worst-case ICI effect on any subcarrier.

As shown from [14] and [30], an upper bound for the BER of binary phase shift keying (BPSK) signal can be expressed as

$$\mathrm{BER} \leq \frac{1}{4}\left[\mathrm{erfc}\left(\lambda\left(1-\sqrt{\mathrm{PICR}}\right)\right) + \mathrm{erfc}\left(\lambda\left(1+\sqrt{\mathrm{PICR}}\right)\right)\right] \tag{3.5}$$

where $\lambda = |A_\varepsilon(m^*, m^*)|/\sqrt{2}\sigma$ and $\mathrm{erfc}(x) = 1 - \frac{2}{\sqrt{\pi}}\int_0^x e^{-t^2}dt$, with

$$m^* = \arg \max_{0 \le m \le N-1} \mathrm{ICR}_m.$$

From (3.5), it can be seen that in general, we can improve BER performance of OFDM systems by reducing PICR or by minimizing (3.4).

3.3 OBP Reduction

From the above discussion, the transmitted signal at the transmitter end is given by

$$\begin{aligned} s(t) &= \frac{1}{\sqrt{N}} \sum_{n=0}^{N-1} X_n g(t) e^{j2\pi(f_c + n\Delta f)t} \\ &= \frac{1}{\sqrt{N}} \sum_{n=0}^{N-1} X_n g(t) e^{j2\pi f_n t} \end{aligned} \tag{3.6}$$

where f_c is the carrier frequency, $f_n = f_c + n\Delta f$ is the center frequency of the nth subcarrier for $n = 0, \ldots, N-1$, and $g(t)$ is the transmitted pulse.

For a rectangular pulse

$$g(t) = \begin{cases} A, & -T_s/2 \le t \le T_s/2 \\ 0, & \text{otherwise} \end{cases},$$

the frequency spectrum of $g(t)$ is given by

$$G(f) = \int_{-T_s/2}^{T_s/2} A e^{-j2\pi f t} dt = \frac{AT_s \sin(\pi f T_s)}{\pi f T_s} = AT_s \operatorname{sinc}(fT_s). \tag{3.7}$$

By using the IDFT to transform OFDM signals from frequency domain to time domain, a rectangular pulse shaping filter is implicitly applied. Therefore, the spectrum of the nth subcarrier at frequency f is given by

$$s_n(f) = \frac{AT_s}{\sqrt{N}} X_n \operatorname{sinc}((f - f_n)T_s) \qquad n = 0, \ldots, N-1 \tag{3.8}$$

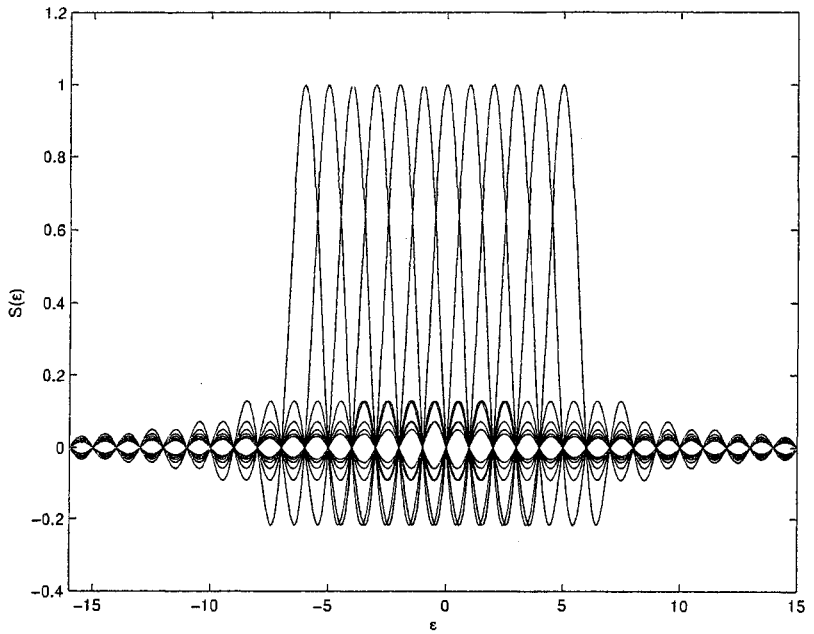

Figure 3.1: The spectrum of an OFDM signal

Figure 3.1 shows the spectrum of each of the 12 subcarriers in an OFDM system.

Let $A = \sqrt{N}/T_s$ for simplicity and define the normalized frequency as

$$\epsilon = f \cdot T_s \tag{3.9}$$

Accordingly, $\epsilon_n = f_n \cdot T_s$ is defined as the normalized center frequency of the nth subcarrier. Then (3.8) can also be expressed as

$$s_n(\epsilon) = X_n \mathrm{sinc}(\epsilon - \epsilon_n) \qquad n = 0, \ldots, N-1.$$

The spectrum of the transmitted OFDM symbol is the superposition of the spectra of all individual subcarriers, which is expressed as

$$s(\epsilon) = \sum_{n=0}^{N-1} s_n(\epsilon). \tag{3.10}$$

For zero mean independent random variable X_n $(n = 0, \ldots, N-1)$ with variance $E\left(|X_n|^2\right)$, the power spectrum of an OFDM signal is shown to be [34]

$$S(f) = \sum_{n=0}^{N-1} S_n(f) = \sum_{n=0}^{N-1} E\left(|X_n|^2\right) \frac{|s_n(f)|^2}{T_s} \tag{3.11}$$

where $s_n(f)$ is the spectrum of the nth subcarrier. The power spectrum of the nth subcarrier is given by

$$\begin{aligned} S_n(f) &= E\left(|X_n|^2\right) \frac{|X_n \operatorname{sinc}((f-f_n)T_s)|^2}{T_s} = E\left(|X_n|^2\right) \frac{|X_n|^2}{T_s} |\operatorname{sinc}((f-f_n)T_s)|^2 \\ S_n(\epsilon) &= E\left(|X_n|^2\right) \frac{|X_n|^2}{T_s} |\operatorname{sinc}(\epsilon - \epsilon_n)|^2 . \end{aligned} \tag{3.12}$$

Note that at the middle point of two adjacent zero crossings of $\operatorname{sinc}(\epsilon)$, we have

$$|\operatorname{sinc}(\epsilon)|^2 = \left|\frac{\sin(\pi(k+k+1)/2)}{\pi\epsilon}\right|^2 = \left|\frac{\sin(\pi/2 + k\pi)}{\pi\epsilon}\right|^2 = \frac{1}{\pi^2\epsilon^2} \tag{3.13}$$

where k is an integer. Therefore the sidelobe power spectrum in (3.12) decays approximate $1/\epsilon^2$ and results in a high out-of-band radiation.

It is usually sufficient to represent the spectrum in (3.10) by a certain number of sampling values which span a certain frequency range over a few sidelobes. In order to reduce the computational complexity, only one sample in the middle of each sidelobe is considered. In our discussion, we consider K_1 and K_2 samples on the left and right hand side sidelobes respectively, with $K_1 + K_2 = K$. That is, $s_k = s(w_k)$ with

$$w_k = \begin{cases} -(1.5 + K_1 - 1 - k) - f_N T_s/2 & \text{for } k = 0, \cdots, K_1 - 1 \\ f_{N/2-1} T_s + 1.5 - K_1 + k & \text{for } k = K_1, \cdots, K-1. \end{cases} \tag{3.14}$$

In matrix form, equation (3.10) can be expressed as

$$\mathbf{s} = \mathbf{G}\mathbf{X} \tag{3.15}$$

where $\mathbf{s} = [s_0 \; s_2 \; \cdots \; s_{K-1}]^T$, $\mathbf{G} \in \mathbb{R}^{K \times N_2}$ is a real matrix with the (k,n)th element $G(k,n) = \operatorname{sinc}(w_k - \epsilon_n)$. We can suppress OBP radiations by minimizing $\|\mathbf{s}\|_2$.

3.4 Techniques to Reduce PAPR and PICR

3.4.1 Partial Transmit Sequence Technique

Figure 3.2 shows the block diagram of the PTS technique at transmitter end.

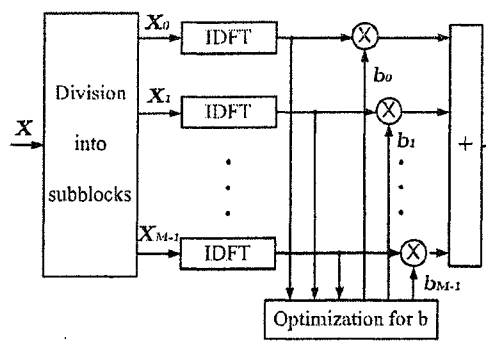

Figure 3.2: The PTS technique at transmitter end

In the PTS technique [15][16], the input data block $\mathbf{X}$ is partitioned into M disjoint subblocks $\mathbf{X}_m = [X_{mU}\ X_{mU+1}\ \cdots\ X_{mU+U-1}]^T$ $(m = 0,\ \ldots,\ M-1;\ UM = N)$. Each subblock is zero padded to make its length as N and to form a new vector denoted as $\mathbf{c}^m = \left[c_0^m\ c_1^m\ \cdots\ c_{N-1}^m\right]^T$ $(m = 0, \ldots, M-1)$ such that

$$\sum_{m=1}^{M} \mathbf{c}^m = \mathbf{X}. \tag{3.16}$$

The NL oversampled time domain signal of $\mathbf{c}^m$, denote by $\mathbf{R}_m = \left[R_0^m\ R_1^m\ \cdots\ R_{LN-1}^m\right]^T$ $(m = 0, \ldots, M-1)$ is obtained by taking an IDFT of length NL on $\mathbf{c}^m$, where $L \geq 1$ is the oversampling factor. Especially, when $L = 1$, the Nyquist-rate sampling is obtained.

$\mathbf{R}_m$ $(m = 0, 1, \ldots, M-1)$ is called the *partial transmit sequence.* Each partial transmit sequence is weighted by a phase factor $b_m = e^{j\alpha_m}$ $(m = 0, \ldots, M-1)$,

then the time domain signal at the kth sampling instant becomes

$$x'_k = \mathbf{R}_m \cdot \mathbf{b} = \sum_{m=0}^{M-1} R_k^m b_m \quad k = 0, \ldots, LN-1 \tag{3.17}$$

In a matrix form, (3.17) can be expressed as

$$\mathbf{x}' = \sum_{m=0}^{M-1} \mathbf{R}_m b_m = \mathbf{R}\mathbf{b} \tag{3.18}$$

where $\mathbf{x}' = [x'_0\ x'_1\ \cdots\ x'_{M-1}]^T$, $\mathbf{b} = [b_0\ b_1\ \cdots b_{M-1}]^T$, and $\mathbf{R} = [\mathbf{R}_0\ \mathbf{R}_1\ \cdots\ \mathbf{R}_{M-1}]^T$.

The phase factors are usually restricted to a finite set of values. For example, $\alpha_m \in \{\frac{2\pi l}{W} | l = 0, \ldots, W-1\}$ with W being the size of the set of phase factors and the PAPR reduction problem is expressed as

$$\begin{aligned} \{b_0^*, b_1^*, \ldots, b_{M-1}^*\} &= \arg\min_m \left(\max_{0 \le k \le NL-1} \left| x'_k \right| \right) \\ &= \arg\min_m \left(\max_{0 \le k \le NL-1} \left| \sum_{m=0}^{M-1} R_k^m b_m \right| \right). \end{aligned} \tag{3.19}$$

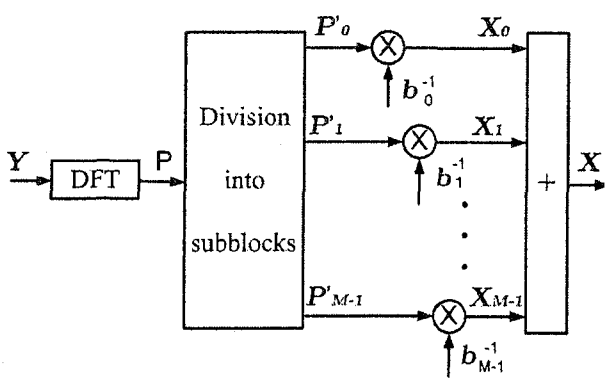

Figure 3.3: The PTS technique at the receiver end

For the simplicity of description, we ignore the noise and the effect of the channel. Therefore, as shown in Figure 3.3, at the receiver end, after passing the received

signal through a DFT, we have $\mathbf{P} = [P_0\ P_1\ \cdots\ P_{LN-1}]^T$ where

$$\begin{aligned} P_n &= \frac{1}{\sqrt{LN}} \sum_{k=0}^{LN-1} x'_k e^{-j\frac{2\pi}{NL}kn} \\ &= \frac{1}{\sqrt{LN}} \sum_{k=0}^{LN-1} \left(\sum_{m=0}^{M-1} R_k^m b_m \right) e^{-j\frac{2\pi}{NL}kn} \\ &= \sum_{m=0}^{M-1} b_m \left(\frac{1}{\sqrt{LN}} \sum_{k=0}^{LN-1} R_k^m e^{-j\frac{2\pi}{NL}kn} \right) \\ &= \sum_{m=0}^{M-1} b_m Q_n^m \quad n = 0, \ldots, LN-1 \end{aligned} \tag{3.20}$$

In a matrix form, equation (3.20) can be expressed as

$$\mathbf{P} = \left[\mathbf{Q}^0\ \mathbf{Q}^1\ \cdots\ \mathbf{Q}^{M-1}\right] \mathbf{b} \tag{3.21}$$

where $\mathbf{Q}^m = [\mathbf{c}^m\ \underbrace{0\ \cdots\ 0}_{(L-1)N}]^T$. Therefore, in order to recover the original information symbol, we pick up the first N components in $\mathbf{P}$ to obtain $\mathbf{P}'$. Then $\mathbf{P}'$ is partitioned into M disjoint subblocks $\mathbf{P}'_m = [P_{mU}\ \cdots\ P_{mU+U-1}]^T$ $(m = 0, \ldots, M-1; UM = N)$.

Therefore,

$$\begin{aligned} \mathbf{X}_0 &= b_0^{-1}\mathbf{P}'_0 \\ \mathbf{X}_1 &= b_1^{-1}\mathbf{P}'_1 \\ &\vdots \\ \mathbf{X}_{M-1} &= b_{M-1}^{-1}\mathbf{P}'_{M-1}. \end{aligned} \tag{3.22}$$

From the above description, for the PTS technique, the computational complexity in terms of the number of complex multiplications in exhaustive search is given by [16]

$$N_c = O\left(W^{M-1}LN\right).$$

Therefore the complexity will increase dramatically with the increase of W and M. In order to get a good performance, the value of W usually needs to be set large enough.

3.4.2 Selective Mapping Technique

The SLM technique has also been proposed for the reduction of PAPR and PICR. In the SLM approach, each input symbol is multiplied by a phase factor $b_n = e^{j\varphi_n}$ $(n = 0, \ \ldots, \ N-1)$ and then transmitted through the OFDM system. That is, in the SLM approach, the transmitted symbols are $X_n e^{j\varphi_n}$ $(n = 0, \ \ldots, \ N-1)$. The phase factor vector $\mathbf{b} = [b_0 \ b_1 \ \cdots \ b_{N-1}]^T$ is chosen to minimize (3.1). It can be seen that the SLM approach can be considered as a special case of the PTS approach by setting $M = N$.

Chapter 4

Joint Design of PAPR and PICR in OFDM Systems

4.1 Joint PAPR and PICR Design

It is noted that high PAPR of OFDM signals results in inefficient operations of nonlinear devices in the system and high PICR of received signal degrades BER performance of OFDM systems. As discussed above, most of previous studies consider either PAPR problem or PICR problem, and most schemes in literature reduce either PAPR or PICR. However, as shown later in Section 4.2, when PAPR (or PICR) problem is considered alone and schemes are adopted to reduce PAPR (or PICR) solely, PICR (or PAPR) of the same system can be quite high. Therefore, it is desirable to design the system considering both PAPR and PICR problems so that both PAPR and PICR are reduced and the performance of the system is improved. Thus, we define new joint design problems by taking both PAPR and PICR of the OFDM signals into account.

4.1.1 Joint Constrained PAPR-PICR Reduction Problem

Problem Formulation

It is noted that in a practical OFDM system, the PAPR of the OFDM signal needs to be lower than a specific threshold such that nonlinear devices in the system always operate in their linear response regions [31]. On the other hand, the value of PICR is related to the BER performance of the system. In general, the lower the PICR, the better the system BER performance [14][30]. Therefore, the PICR needs to be reduced as much as it can be. Thus, based on these observations, a joint constrained PAPR-PICR reduction problem is defined as

$$\min \quad \text{PICR} \tag{4.8a}$$

$$\text{subject to: PAPR} \leq \gamma. \tag{4.8b}$$

The parameter γ in (4.8b) is chosen according to the specifications of the nonlinear devices used in the system to ensure that the nonlinear devices operate in their linear response regions.

A Joint Constrained PAPR-PICR Reduction Algorithm

As discussed in Section 4.1, the PTS approach has been proposed for the reduction of and PICR. We will apply this approach for the joint PAPR and PICR design problems. The phase factor vector $\mathbf{b} = [b_1 \ b_2 \ \cdots \ b_M]^T$ is chosen to optimize the design objective. Therefore, the joint constrained PAPR-PICR reduction problem is re-formulated as

$$\mathbf{b}^* = \arg\min_{\mathbf{b}} \text{PICR}(\mathbf{b}) \tag{4.9a}$$

$$\text{subject to: PAPR}(\mathbf{b}) \leq \gamma \tag{4.9b}$$

where

$$\mathrm{PICR}(\mathbf{b}) = \max_{l=0,\ldots,N-1} \frac{\left|\sum_{m=1}^{M}\sum_{k=0,k\neq l}^{N-1} c_k^m b_m A_\varepsilon(l,k)\right|^2}{\left|\sum_{m=1}^{M} c_l^m b_m A_\varepsilon(l,l)\right|^2}$$

$$\mathrm{PAPR}(\mathbf{b}) = \max_{l=0,\ldots,LN-1}\left[\frac{\left|\sum_{m=1}^{M}\sum_{k=0}^{LN-1}\overline{c}_k^m b_m F(l,k)\right|^2}{\frac{1}{LN}\sum_{l=0}^{LN-1}\left|\sum_{m=1}^{M}\sum_{k=0}^{LN-1}\overline{c}_k^m b_m F(l,k)\right|^2}\right]$$

denote PICR and PAPR of the OFDM signal adopting the PTS approach respectively with L being the over-sampling coefficient, $\left[c_0^m\ c_1^m\ \cdots\ c_{N-1}^m\right]^T$ is defined as in Section 4.1.1, $\left[\overline{c}_0^m\ \overline{c}_1^m\ \cdots\ \overline{c}_{LN-1}^m\right]^T$ $(m = 1,\ldots,M)$ is defined as

$$\overline{\mathbf{c}}^m = [\mathbf{c}^m\ \underbrace{0\ \cdots\ 0}_{(L-1)N}]^T,$$

and $\mathbf{F} \in \mathbb{C}^{(LN)\times(LN)}$ is the IDFT matrix with the (l,k)th element $F(l,k) = \frac{1}{\sqrt{LN}}e^{j2\pi lk/LN}$ for $l,k = 0,\ldots,LN$.

The problem in (4.9) is a nonlinear optimization problem whose solution is generally very difficult to obtain. As a suboptimal solution, N_a distinct phase factor vectors $\mathbf{b}^i = [b_1^i\ b_2^i\ \cdots\ b_M^i]^T$ are generated with $b_m^i = e^{j\varphi_{mi}}$ and φ_{mi} being a uniformly distributed random variable (r.v.) over $[0, 2\pi)$ $(i = 1,\ \cdots,\ N_a;\ m = 1,\ \cdots,\ M)$. Therefore, the problem in (4.9) can be solved as

$$\mathbf{b}^* = \arg\min_{\mathbf{b}^i, 1\le i\le N_a} \mathrm{PICR}(\mathbf{b}^i) \tag{4.10a}$$

$$\text{subject to: } \mathrm{PAPR}(\mathbf{b}^i) \le \gamma. \tag{4.10b}$$

Among $\mathbf{b}^i$ $(i = 1,\ \cdots,\ N_a)$, those satisfying (4.10b) are identified first. Then, from the chosen vectors, the one optimizes the objective in (4.10a) will be identified as the solution to this problem.

It is noted that sometimes no $\mathbf{b}^i$ for $i = 1,\ \cdots,\ N_a$ satisfies the constraint in (4.10b) for a given γ, especially when N is very large. Although increasing the value

Table 4.1: PTS based joint constrained PAPR-PICR reduction algorithm

Step 1. Generate N_a distinct phase factor vectors $\mathbf{b}^i = [b_1^i \ b_2^i \ \cdots b_M^i]^T$ with $b_m^i = e^{j\varphi_{mi}}$ and φ_{mi} a uniformly distributed r.v. over $[0, 2\pi)$ $(i = 1, \ \cdots, \ N_a; m = 1, \ \cdots, \ M)$.

Step 2. Among the N_a phase factor vectors $\mathbf{b}^i$, identify those satisfying (4.10b). If no vector is found, then go to step 3. Otherwise, go to step 4.

Step 3. Among the N_a phase factor vectors $\mathbf{b}^i$, identify the one that minimizes the PAPR value as in (4.11) as the final solution, and go to step 5.

Step 4. Among the vectors picked up, identify the one that optimizes the objective in (4.10a) as the final solution, and go to step 5.

Step 5. Record the PAPR and PICR values of the OFDM signal using the solution phase factor vector and stop.

of N_a can in general decrease the possibility that this phenomenon happens, we cannot eliminate it completely by increasing N_a only. Therefore, in this situation, we propose to identify the solution as the one that minimizes PAPR. That is,

$$\mathbf{b}^* = \arg \min_{\mathbf{b}^i, 1 \le i \le N_a} \text{PAPR}(\mathbf{b}^i). \tag{4.11}$$

In this way, PAPR is minimized while the value of PICR may be large and the BER performance may be degraded significantly. From the simulation results we obtained, since the phenomenon that no $\mathbf{b}^i$ among the N_a candidate vectors satisfies the constraint in (4.10b) happens quite infrequently when γ and N_a are set appropriately, the performance of PICR reduction, thus the BER performance of the system, is not affected much.

Therefore, the PTS approach based algorithm for the joint constrained PAPR-PICR reduction problem is summarized in Table 4.1.

4.1.2 Joint Weighted PAPR-PICR Reduction Problem

Problem Formulation

The problem in (4.9) is a standard constrained optimization problem, which can be solved using the Lagrange method. Define the Lagrange equation as

$$J(\mathbf{b}) = \mathrm{PICR}(\mathbf{b}) - \lambda\left(\gamma - \mathrm{PAPR}(\mathbf{b})\right) \tag{4.12}$$

with λ being the non-negative Lagrangian multiplier. A local optimal phase factor vector $\mathbf{b}^*$ and Lagrangian multiplier λ^* should satisfy

$$\nabla\mathrm{PICR}(\mathbf{b}^*) - \lambda^*\nabla\left(\gamma - \mathrm{PAPR}(\mathbf{b}^*)\right) = 0 \tag{4.13}$$

where

$$\begin{aligned}
\nabla\mathrm{PICR}(\mathbf{b}) &= \left[\frac{\partial\mathrm{PICR}(\mathbf{b})}{\partial b_1}\ \frac{\partial\mathrm{PICR}(\mathbf{b})}{\partial b_2}\ \cdots\ \frac{\partial\mathrm{PICR}(\mathbf{b})}{\partial b_M}\right]^T \\
\nabla\mathrm{PAPR}(\mathbf{b}) &= \left[\frac{\partial\mathrm{PAPR}(\mathbf{b})}{\partial b_1}\ \frac{\partial\mathrm{PAPR}(\mathbf{b})}{\partial b_2}\ \cdots\ \frac{\partial\mathrm{PAPR}(\mathbf{b})}{\partial b_M}\right]^T
\end{aligned}$$

Or equivalently, $\mathbf{b}^*$ and λ^* should satisfy

$$\nabla\mathrm{PICR}(\mathbf{b}^*) + \lambda^*\nabla\mathrm{PAPR}(\mathbf{b}^*) = 0. \tag{4.14}$$

The values of $\mathbf{b}^*$ and λ^* can be found through numerical search such that (4.14) and the constraint in (4.9b) are satisfied. However, in general, the numerical search is rather difficult. In addition, the solution $\mathbf{b}^*$ is only local optimal and might not provide a satisfactory performance.

Instead, from (4.14), we formulate an unconstrained optimization problem whose solution satisfies an equation similar to (4.14) as

$$\min \quad \mathrm{PICR}(\mathbf{b}) + \rho\mathrm{PAPR}(\mathbf{b}) \tag{4.15}$$

where $\rho \geq 0$ is a factor which is determined in advance and is adjusted according to system design requirement. Or equivalently, (4.15) can also be expressed as

$$\min \quad w\text{PICR}(\mathbf{b}) + (1-w)\text{PAPR}(\mathbf{b}) \tag{4.16}$$

with $w \in [0,1]$ being a weighting factor.

More generally, to include other PICR and PAPR reduction approaches, the unconstrained problem is expressed as

$$\min \quad w\text{PICR} + (1-w)\text{PAPR} \tag{4.17}$$

which is referred to as the joint weighted PAPR-PICR reduction problem. By solving (4.17), we jointly reduce PAPR and PICR. Note that the PAPR and PICR reduction problems can be considered as special cases of the joint problem in (4.17) with $w = 0$ and $w = 1$, respectively.

From the discussions above, the proposed joint weighted and joint constrained PAPR-PICR reduction problems can be used jointly to facilitate OFDM system design. Thus the system design is divided into two steps. First, according to the detection performance requirement of the receiver, we choose an appropriate value for w in the joint weighted PAPR-PICR reduction problem, thus choose an appropriate trade-off between PAPR and PICR reduction. By solving the joint weighted PAPR-PICR reduction problem, we can determine an appropriate value for the PAPR threshold γ, and then we can choose the nonlinear devices used in the system accordingly. This is the 'rough' design step. Next, based on the value of γ chosen, by solving the proposed joint constrained PAPR-PICR problem, we can obtain the system performance in terms of PAPR and PICR values. This is the 'fine' design step.

Table 4.2: The range of PICR values of OFDM signals

PICR (dB)						PAPR (dB)	
AWGN channel		QC channel		uncorrelated FTV channel			
PICR_L	PICR_H	PICR_L	PICR_H	PICR_L	PICR_H	PAPR_L	PAPR_H
-12	-5	-10	50	22	92	4	13

In addition, it is observed that the range of PICR values of OFDM signals is quite different from that of PAPR values. For instance, we consider an OFDM system with 8-PSK modulation, $N = 64$, and $\varepsilon = -0.1$. Using 10^5 OFDM symbol samples, in Table II, the ranges of PICR values of the original OFDM signals are given under AWGN channel, quasi-static and fast time-varying frequency-selective Rayleigh fading channels with $\mu = 10$ and with normalized total power in each path. The range of the PAPR values of the original OFDM signals, which is not dependent on the channel, is also included in the table. In Table II, PAPR_H, PAPR_L and PICR_H, PICR_L, denote the largest and smallest PAPR and PICR values in dB of the tested OFDM symbols, respectively. Thus, the two optimization objectives of PAPR and PICR reduction are significantly unequally weighted in (4.17).

Therefore, we propose to multiply PAPR by a coefficient α before minimizing (4.17), so that both optimization objectives of PAPR and PICR reduction are approximately equally weighted in the joint problem for the value of $w = 0.5$. The joint weighted PAPR-PICR reduction problem is thus expressed as

$$\min \quad w\text{PICR} + \alpha(1-w)\text{PAPR} \tag{4.18}$$

where α is given as

$$\alpha = \frac{\text{PICR}_0}{\text{PAPR}_0} \tag{4.19}$$

with PICR_0 and PAPR_0 being the PICR and PAPR values of the original OFDM

signal, respectively. That is, $\text{PICR}_0 = \text{PICR}(\mathbf{b} = \mathbf{1})$ and $\text{PAPR}_0 = \text{PAPR}(\mathbf{b} = \mathbf{1})$.

Joint Weighted PAPR-PICR Reduction Algorithm

By applying the PTS approach, among the N_a phase factor vectors $\mathbf{b}^i$ which are generated using the same method as described in Section 4.1.1, we choose the one that optimizes the objective in (4.18) as the solution. Thus, the joint weighted PAPR-PICR problem reduction in (4.18) is solved as

$$\mathbf{b}^* = \arg \min_{\mathbf{b}^i, 1 \le i \le N_a} \left\{ w\text{PICR}(\mathbf{b}^i) + \alpha(1-w)\text{PAPR}(\mathbf{b}^i) \right\} \tag{4.20}$$

Note that we can extend the PTS approach based algorithms developed in this section for both the joint constrained and the joint weighted PAPR-PICR reduction problems with ease adopting the SLM approach [12].

4.2 Simulation Results

Computer simulations were conducted to evaluate efficacy of the proposed PTS approach based algorithms in joint PAPR and PICR design. We considered an OFDM system with a fast time-varying frequency-selective fading channel, as described in Section 4.2.

We consider an OFDM system with subcarriers $N = 64$. Unless otherwise mentioned, $N_a = 16$ and $M = 8$ were used in our simulations. 10^6 OFDM symbols were used to obtain the results shown in this section. In order to increase the accuracy of the calculations of PAPR, the transmitted signals were over-sampled by a factor of 4 in our simulations. Note that simulations were carried out in other channel conditions, including AWGN channel and quasi-static frequency-selective Rayleigh fading channel, and similar results as shown in this section were obtained.

10^6 OFDM signals are transmitted and PICR and PAPR values of which exceed respective values, say, $PICR_0$, and $PAPR_0$ are countered. The probabilities that the PICR and PAPR are greater than those respective values then are respectively given by

$$\begin{aligned} Pr(\text{PICR} > PICR_0) &= \frac{\text{the numbers countered for PICR}}{10^6} \\ Pr(\text{PAPR} > PAPR_0) &= \frac{\text{the numbers countered for PAPR}}{10^6} \end{aligned}$$

To ensure the precision of the experiment results, usually the number of experiments used at least 10 times more than the target number of experiments, otherwise we can not say that the joint design performs better than the original design does. The target probability is chosen to be 10^{-4} in this problem.

Figures 4.1 and 4.2 show the logarithmic complimentary cumulative density functions (CCDFs) of PICR and PAPR of OFDM signals in the joint weighted problem as a function of w. It is shown from Figures 4.1 and 4.2 that the proposed joint weighted PAPR-PICR reduction algorithm is efficient in reducing both PAPR and PICR of OFDM signals. In addition, as w increases, the performance of PICR reduction becomes better and the performance of PAPR reduction becomes worse. When $w = 1$ (or $w = 0$), PICR (or PAPR) reduction gets the best possible result while PAPR (or PICR) gets the worst result. It can be seen that the weighting factor w provides a trade-off between PAPR and PICR reductions and can be adjusted according to the performance requirements of the nonlinear devices and the receiver in the OFDM system.

Figures 4.3 and 4.4 show the logarithmic CCDFs of PICR and PAPR of OFDM signals in the joint constrained problem with the PAPR threshold γ set as 7, 8, and

9 dB, respectively. The curve of PICR in Figure 4.3 with $\gamma = 8$ dB is very similar to the one shown in Figure 4.1 with $w = 0.5$. For instance, for the curve in Figure 4.3 with $\gamma = 8$ dB, 1 out of 10^4 OFDM symbols has PICR above 66.3 dB, whereas in the original OFDM signal, 1 out of 10^4 OFDM symbols has PICR above 75.9 dB. This represents a 9.6 dB reduction in PICR. Whereas the curve in Figure 4.1 with $w = 0.5$ represents a 10 dB reduction in PICR for 1 out of 10^4 OFDM symbols. However, the curve of PAPR in Figure 4.4 shows much better performance than the one shown in Figure 2 with $w = 0.5$. For instance, in Figure 4.4, 1 out of 10^4 OFDM symbols has PAPR exceeding 8 dB, whereas in the original OFDM signal, 1 out of 10^4 OFDM symbols has PAPR exceeding 11.4 dB. This represents at least 3.4 dB reduction in PAPR, which is about 2.1 dB more than the PAPR reduction in Figure 4.2 with $w = 0.5$. From the results in Figures 4.3 and 4.4, it can be seen that the proposed joint constrained PAPR-PICR reduction algorithm is also efficient in reducing both PAPR and PICR of OFDM signals.

Increasing N_a and M, which will increase the search space and the size of the set allowed phase factors respectively, thus makes the performance of the designed system better but increases the computation complexity at the same time. The values of N_a and M depend on the performance requirement of the PICR reduction in an OFDM system.

4.3 Conclusion

Considering both PAPR and PICR problems, new joint PAPR and PICR design problems, including the joint weighted and the joint constrained PAPR-PICR reduction problems, have been formulated, so that the performance of an OFDM

system is improved. Algorithms based on PTS approach have been proposed to solve the joint design problems. Simulation results have shown that the proposed algorithms are efficient in reducing both PAPR and PICR of OFDM signals. The proposed algorithms can also be used jointly to facilitate OFDM system design.

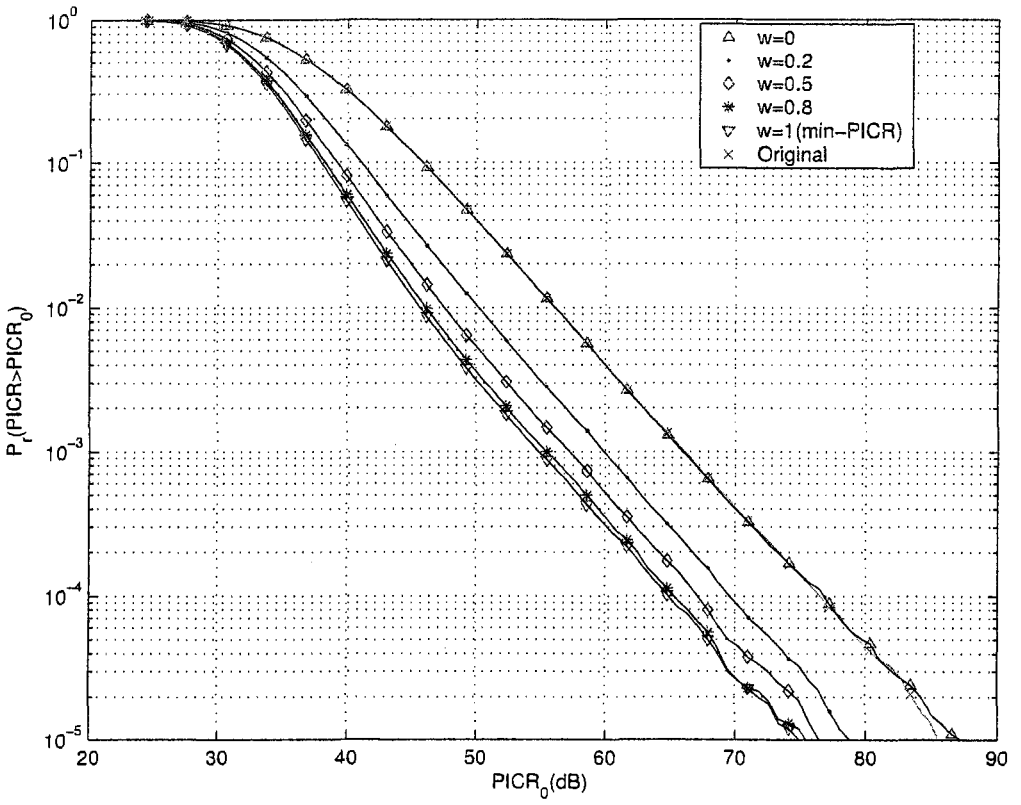

Figure 4.1: CCDF of PICR for an fast time-varying frequency-selective Rayleigh fading channel (joint weighted PAPR-PICR problem).

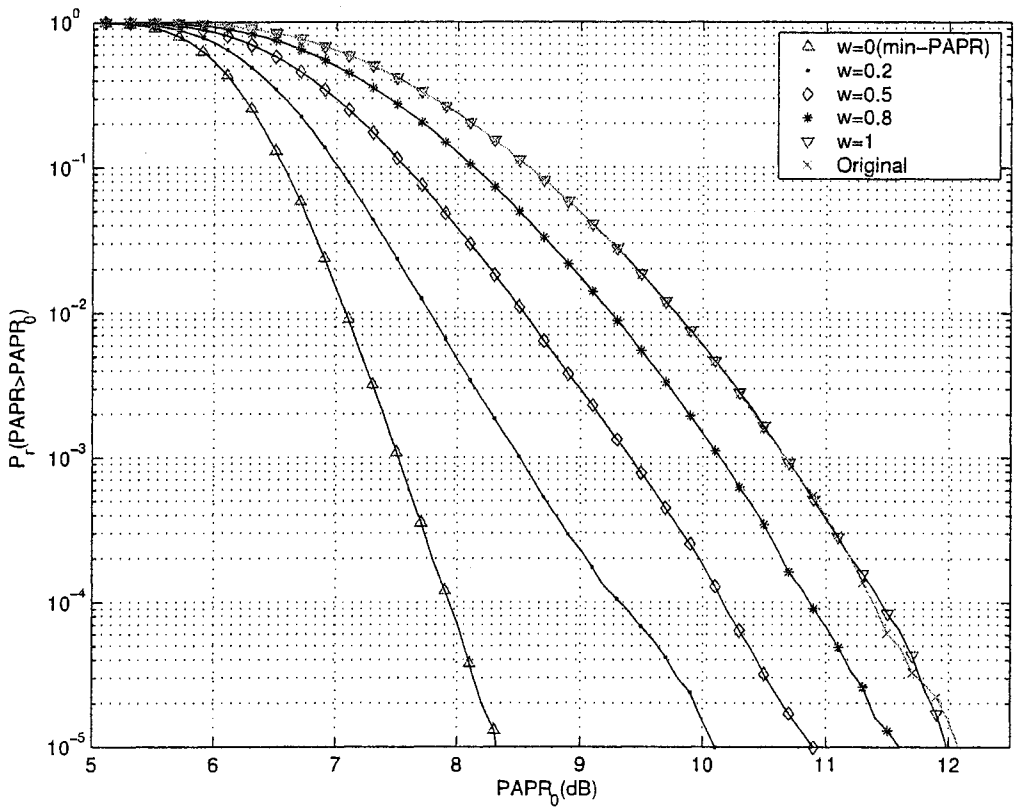

Figure 4.2: CCDF of PAPR for an fast time-varying frequency-selective Rayleigh fading channel (joint weighted PAPR-PICR problem).

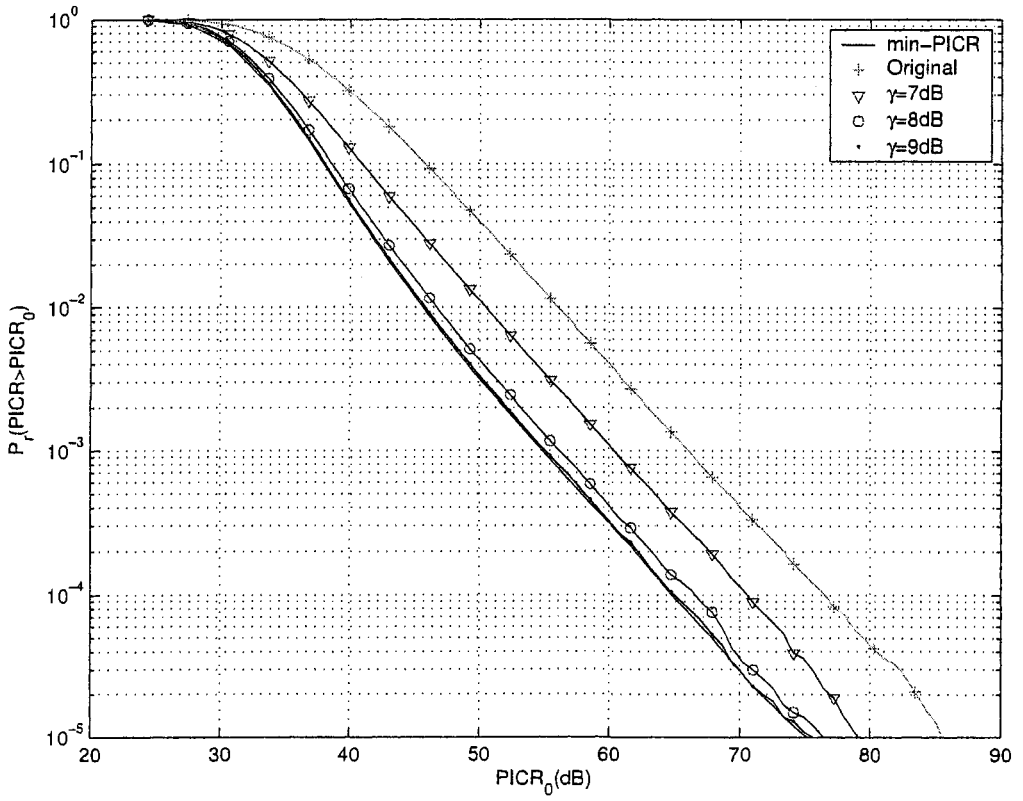

Figure 4.3: CCDF of PICR for an fast time-varying frequency-selective Rayleigh fading channel with $\gamma = 7,\ 8,\ 9$ dB (joint constrained PAPR-PICR problem).

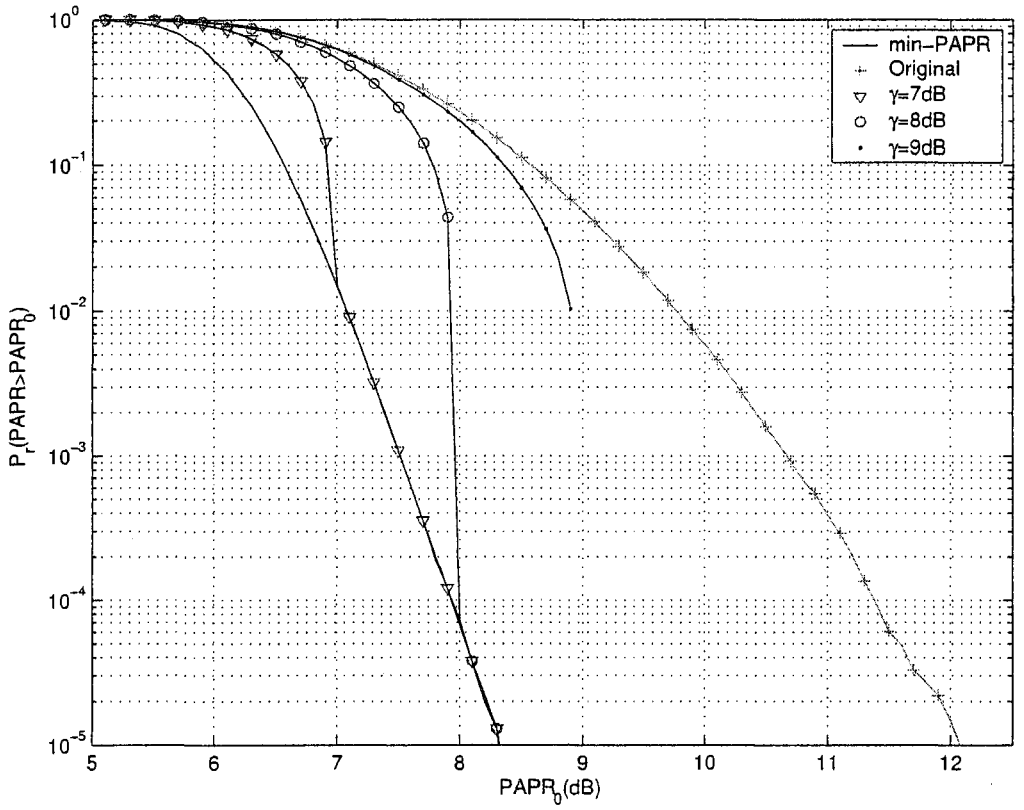

Figure 4.4: CCDF of PAPR for an fast time-varying frequency-selective Rayleigh fading channel with $\gamma = 7,\ 8,\ 9$ dB (joint constrained PAPR-PICR problem).

Chapter 5

Joint Design of PAPR, PICR, and OBP in OFDM Systems

5.1 System Model

We consider an OFDM system of N subcarriers, each of which is independently modulated using MPSK or MQAM to transmit N data sub-streams in parallel manner. On both sides of the N subcarriers, $M/2$ cancellation subcarriers are inserted to suppress sidelobes, to reduce PAPR, or/and to reduce PICR. Thus the subcarrier indices are denoted as $n = 0, \cdots, M/2-1, M/2, \cdots, M/2+N-1, M/2+N, \cdots, M+N-1$. Denoting the modulated symbol on the ith subcarrier by X_i ($i = M/2, \cdots, M/2+N-1$), we assume $\bar{\mathbf{X}} = \left[X_{M/2}\ X_{M/2+1}\ \cdots\ X_{M/2+N-1}\right]^T$ as the information symbol vector, and $\mathbf{X} = \left[\underbrace{0\ \cdots\ 0}_{M/2}\ \ \bar{\mathbf{X}}^T\ \underbrace{0\ \cdots\ 0}_{M/2}\right]^T$ as the expanded information symbol vector with cancellation subcarriers. Denoting

$$\mathbf{Y} = \left[Y_0\ \cdots\ Y_{M/2-1}\ Y_{M/2}\ \cdots\ Y_{M/2+N-1}\ Y_{M/2+N}\ \cdots\ Y_{M+N-1}\right]^T$$

as the modification vector to suppress sidelobes, to reduce PAPR, or/and to reduce PICR, we assume that the actual transmitted symbol vector is $\mathbf{X} + \mathbf{Y}$. For the convenience of the following discussion, we define $M/2 = N_0$, $M/2 + N = N_1$, and $M + N = N_2$.

By applying an IDFT upon $X_i + Y_i$ $(i = 0, \cdots, N_2 - 1)$, we generate the time-domain transmitted signal as

$$x_n + y_n = \frac{1}{\sqrt{N_2}} \sum_{i=0}^{N_2-1} (X_i + Y_i)\, e^{j2\pi ni/N_2}, \qquad n = 0, \cdots, N_2 - 1 \tag{5.1}$$

where $x_n + y_n$ is the time-domain signal at the nth sampling instant and $j^2 = -1$. In a matrix form, equation (5.1) can be expressed as

$$\mathbf{x} + \mathbf{y} = \mathbf{F}\,(\mathbf{X} + \mathbf{Y}) \tag{5.2}$$

where

$$\begin{aligned} \mathbf{X} + \mathbf{Y} &= [X_0 + Y_0 \; X_1 + Y_1 \; \cdots \; X_{N_2-1} + Y_{N_2-1}]^T \\ \mathbf{x} + \mathbf{y} &= [x_0 + y_0 \; x_1 + y_1 \; \cdots \; x_{N_2-1} + y_{N_2-1}]^T \end{aligned}$$

and $\mathbf{F} \in \mathbb{C}^{N_2 \times N_2}$ is the IDFT matrix with the (n, i)th element

$$F(n, i) = \frac{1}{\sqrt{N_2}} e^{j2\pi ni/N_2}$$

for $n, i = 0, \ldots, N_2 - 1$.

As in Chapter 2, a doubly frequency selective fading channel model is adopted in this chapter. For this system model, the discrete demodulated signal at the receiver becomes

$$z_n = e^{j2\pi\varepsilon n/N_2} \sum_{k=0}^{\mu} (x_{n-k} + y_{n-k})\, h\,(n, k) + v_n \qquad n = 0, \ldots, N_2 - 1 \tag{5.3}$$

where v_n is AWGN process with independent real and imaginary components, each of which has zero mean and variance σ^2. ε is the normalized frequency offset which is defined as (2.6).

As shown in Appendix B.3, the matrix form of (5.3) is represented as

$$\mathbf{z} = \mathbf{D}_\varepsilon \mathbf{H}\,(\mathbf{x} + \mathbf{y}) + \mathbf{n} \tag{5.4}$$

where $\mathbf{n} = [v_0\ v_1\ \cdots\ v_{N_2-1}]^T$ denotes the AWGN noise with zero mean and covariance matrix $2\sigma^2\mathbf{I}$, $\mathbf{D}_\varepsilon = \text{diag}\{1,\ e^{j2\pi\varepsilon/N_2}, \ldots,\ e^{j2\pi\varepsilon(N_2-1)/N_2}\}$, $\mathbf{z} = [z_0\ z_1\ \cdots\ z_{N_2-1}]^T$ denotes the time-domain received signal, and $\mathbf{H} \in \mathbb{C}^{N_2\times N_2}$ is the channel matrix given by

$$\begin{bmatrix} h(0,0) & 0 & 0 & \cdots & 0 & h(0,\mu) & h(0,\mu-1) & \cdots & h(0,1) \\ h(1,1) & h(1,0) & 0 & \cdots & 0 & 0 & h(1,\mu) & \cdots & h(1,2) \\ \vdots & \vdots & \vdots & \ddots & \vdots & \vdots & \vdots & \ddots & \vdots \\ h(\mu,\mu) & h(\mu,\mu-1) & \cdots & \cdots & h(\mu,0) & 0 & 0 & \cdots & 0 \\ 0 & h(\mu+1,\mu) & \cdots & \cdots & h(\mu+1,1) & h(\mu+1,0) & 0 & \cdots & 0 \\ \vdots & \vdots & \vdots & \ddots & \vdots & \vdots & \vdots & \ddots & \vdots \\ 0 & 0 & 0 & \cdots & h(N_2-1,\mu) & h(N_2-1,\mu-1) & \cdots & \cdots & h(N_2-1,0) \end{bmatrix}. \tag{5.5}$$

After removing the CP, the received signal $\mathbf{z}$ is passed through a FDT. Then we have

$$\mathbf{Z} = \mathbf{F}^H(\mathbf{x}+\mathbf{y}) = \mathbf{A}_\varepsilon(\mathbf{X}+\mathbf{Y}) + \mathbf{N}_0 \tag{5.6}$$

where $\mathbf{A}_\varepsilon = \mathbf{F}_\varepsilon^H\mathbf{H}\mathbf{F}$, $\mathbf{F}_\varepsilon^H \in \mathbb{C}^{N_2\times N_2}$ is a matrix with the (n,i)th element $F_\varepsilon^H(n,i) = \frac{1}{\sqrt{N_2}}e^{-j2\pi(n-\varepsilon)i/N_2}$ $(n,i = 0,\ldots,N_2-1)$ and $\mathbf{N}_0 = \mathbf{F}^H\mathbf{n}$.

5.2 PAPR, PICR, and OBP Problems for the System Model in Section 5.1

For the system model given in Section 5.1, the PAPR definition in (3.1) becomes

$$\text{PAPR} = \frac{\max_n\{p_n\}}{E\{p_n\}} = \frac{\|\mathbf{x}+\mathbf{y}\|_\infty^2}{E\{\|\mathbf{x}+\mathbf{y}\|_2^2/N\}} \tag{5.7}$$

where p_n denotes the power of $x_n + y_n$. We can achieve PAPR reduction by minimizing (5.7).

From (5.6), the received signal on the kth subcarrier can be expressed as

$$Z_k = (X_k+Y_k)\,A_\varepsilon(k,k) + \sum_{l=0,l\neq k}^{N_2-1}(X_l+Y_l)\,A_\varepsilon(k,l) + N_{ok} \tag{5.8}$$
$$k = 0,\cdots,N_2-1$$

where $A_\varepsilon(k,l)$ denotes the (k,l)th element of $\mathbf{A}_\varepsilon$ and N_{0k} denotes the kth element of $\mathbf{N}_0$.

For the system model given in Section 5.1, the PICR defined in (3.3) and (3.4) becomes

$$\mathrm{PICR} = \max_{N_0 \le k \le N_1 - 1} \left\{ \frac{\left| \sum_{l=0, l \neq k}^{N_2 - 1} (X_l + Y_l) A_\varepsilon(k,l) \right|}{\left| A_\varepsilon(k,k)(X_k + Y_k) \right|} \right\} \tag{5.9}$$

which specifies the worst-case ICI on any information subcarrier. Note that only the symbols on information subcarriers need to be detected at receiver and thus only the PICR on information subcarriers needs to be reduced. Therefore, in (5.9), we consider $k = N_0, \ldots, N_1 - 1$ only. We can reduce the effect of ICI and improve BER performance of OFDM systems by reducing PICR.

For the system model given in Section 5.1, OBP radiation is reduced by adding $M/2$ sidelobe cancellation subcarriers on both sides of the information spectrum. Figure 5.1 shows an example of a system with $N = 12$, $M = 4$, and $K_1 = K_2 = 7$. Thus equation (3.10) becomes

$$\mathbf{s} = \mathbf{G}(\mathbf{X} + \mathbf{Y}) \tag{5.10}$$

where $\mathbf{G} \in \mathbb{R}^{K \times N_2}$ is a real matrix with the (k,n)th element $G(k,n) = \mathrm{sinc}(w_k - \epsilon_n)$, and w_k is defined as (3.14) with N being replaced by $N_2 = M + N$. We can suppress OBP radiations by minimizing $\|\mathbf{s}\|_2$.

5.3 Joint PAPR, PICR, and OBP Design

It is noted that high PAPR of OFDM signals results in inefficient operations of nonlinear devices in the system, high PICR of received signal degrades BER performance of OFDM systems, and high OBP radiations decrease efficiency of frequency band usage. As discussed above, most previous studies consider PAPR

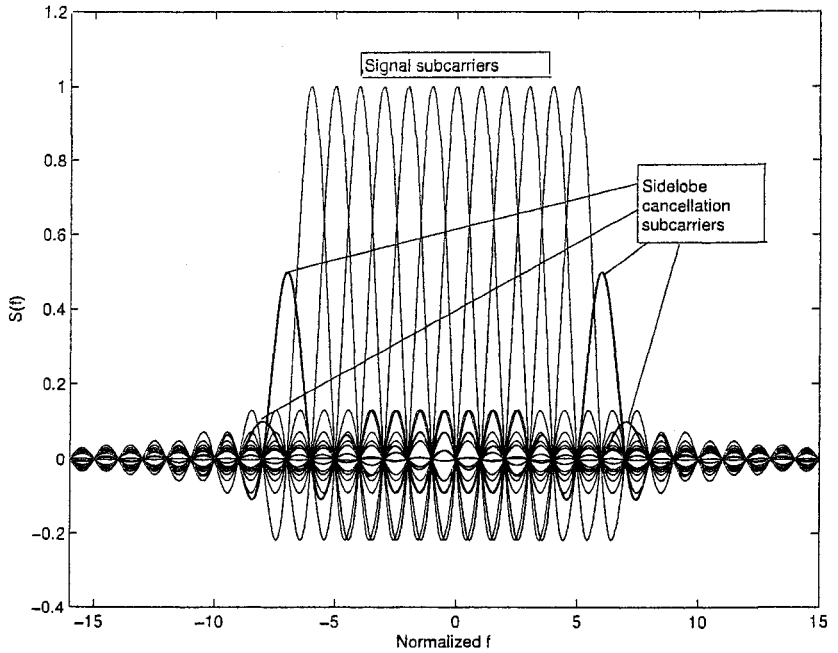

Figure 5.1: The PSD of an OFDM system with $N = 12$, $M = 4$, and $K_1 = K_2 = 7$

problem, PICR problem, or OBP problem solely, and most schemes in literature reduce PAPR, PICR, or OBP only. However, as shown later in Section 5.4, when one of the three problems is considered alone and schemes are adopted to reduce one of the three parameters solely, the performance of the other two problems of the same system can be quite bad. Therefore, it is desirable to design the system considering PAPR, PICR, and OBP problems jointly so that PAPR, PICR, and OBP are reduced and the performance of the whole system is improved. Thus, we define new joint design problems by taking PAPR, PICR, and OBP of the OFDM signals into account.

5.3.1 Problem Formulation

We note that in a practical OFDM system, sidelobe power needs to be suppressed in order to reduce the OBP radiation effects. In addition, PAPR of the OFDM signal needs to be lower than a specific threshold such that nonlinear devices used in the system always operate in their linear response regions [31]. The value of PICR is related to the BER performance of the system. In general, the lower the PICR, the better the system BER performance [14][30]. Therefore, the PICR needs to be reduced as much as it can be. On the other hand, by adopting modification vector for sidelobe suppression and PAPR and PICR reduction, part of the total transmission power is now not used for information data transmission. Therefore, generally, more power will be needed if the BER performance of the system is preserved, or in other words, the BER performance of the system will be degraded if the total transmission power is kept constant. Therefore, the increment in the transmission power after adding the modification vector needs to be limited. Thus, based on these observations, a joint PAPR-PICR-OBP design problem is defined as

$$\min \quad \text{PICR} \tag{5.11a}$$

$$\text{subject to: } \text{PAPR} \leq \tau \tag{5.11b}$$

$$\text{OBP} \leq \alpha \cdot \text{OBP}_o \quad 0 < \alpha < 1 \tag{5.11c}$$

$$\|\mathbf{X}+\mathbf{Y}\|_2^2 - \|\mathbf{X}\|_2^2 \leq \beta \|\mathbf{X}\|_2^2 \quad 0 < \beta < 1 \tag{5.11d}$$

where OBP_o denotes the OBP of the original OFDM information symbol $\mathbf{X}$, OBP denotes the OBP of the actual transmitted OFDM signal $\mathbf{X}+\mathbf{Y}$, τ is a constant parameter which depends on the linear dynamic range of the nonlinear device used

in the OFDM system, and $\alpha \in (0,1)$ is a parameter depending on the OBP suppression requirement and the number of subcarriers used for guard bands.

Two approaches are adopted in this chapter for the joint PAPR, PICR, and OBP design problem in (5.11). One approach is based on the phase rotation and the other one is based on the constellation extension.

5.3.2 Algorithm Based on Phase Rotation Approach

As shown in Figure 5.2, in the phase rotation approach, the actual transmitted symbol on the kth subcarrier, which is $X_k + Y_k$ based on the discussion in Section 5.1, is obtained by rotating the original information symbol X_k by a certain phase angle. Letting r_k be the rotation phasor on the kth subcarrier with $\|r_k\|_2 = 1$, we have

$$r_k = 1 + \frac{Y_k}{X_k} \qquad k = N_0, \ldots, N_1 - 1.$$

Denote $\mathbf{A}_\varepsilon^o \in \mathbb{C}^{N_2 \times N_2}$ as a matrix by replacing all diagonal elements of $\mathbf{A}_\varepsilon$ in (5.6)

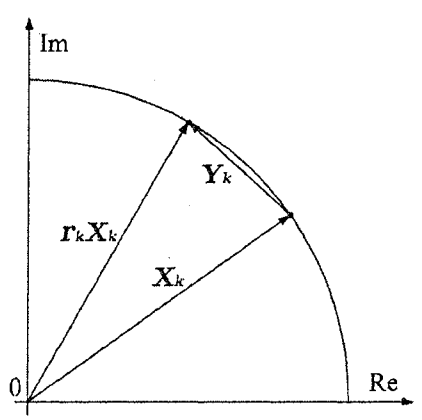

Figure 5.2: Phase rotation approach

by zeros. Then the kth row of $\mathbf{A}_\varepsilon^0$ can be expressed as

$$\mathbf{b}_k^T = \left[b_{k0} \ \cdots \ b_{k(k-1)} \ 0 \ b_{k(k+1)} \ \cdots \ b_{k(N_2-1)}\right].$$

Using the phase rotation approach, by equation (5.9), the objective function of the joint design problem in (5.11a) can be reformulated as

$$\min \qquad \text{PICR} = \min_{\mathbf{Y}} \max_{k\in[N_0,N_1-1]} \frac{\left\|\mathbf{b}_k^T(\mathbf{X}+\mathbf{Y})\right\|_2}{\left\|A_\varepsilon(k,k)(X_k+Y_k)\right\|_2} \tag{5.12a}$$

$$\text{subject to:} \quad \left\|1+\frac{Y_k}{X_k}\right\|_2 = 1, k = N_0, \cdots, N_1-1. \tag{5.12b}$$

Note that the angle of the rotation phasor r_k needs to be quantized before transmitted to the receiver, and the number of quantization levels is in general quite limited to reduce the associated overhead. In our approach, we restrict the quantization levels as $-\theta$, 0, and θ and constrain the rotation angle within the range of $[-\theta, \ \theta]$ with $\theta \in (0, \pi/2)$. Therefore, as shown in Figure 5.3, the nonconvex constraint in (5.12b) is relaxed as the shaded convex feasible region as

$$\cos\theta \leq \Re(1+Y_k/X_k) \leq 1 \tag{5.13a}$$

$$-\theta \leq \arg(1+Y_k/X_k) \leq \theta \qquad k = N_0, \ldots, N_1-1. \tag{5.13b}$$

The constraint (5.13b) is equivalent to

$$-\tan\theta \leq \frac{\Im(1+Y_k/X_k)}{\Re(1+Y_k/X_k)} \leq \tan\theta.$$

Denote the kth row of $\mathbf{F}$ as $\mathbf{f}_k^T = \left[f_{k0} \ f_{k2} \ \cdots \ f_{k(N_2-1)}\right]$. The PAPR constraint in (5.11b) can be reformulated as

$$\begin{aligned}\left\|\mathbf{f}_k^T(\mathbf{X}+\mathbf{Y})\right\|_2 &\leq \sqrt{\tau}E\left\{\|\mathbf{x}+\mathbf{y}\|_2/\sqrt{N_2}\right\} \\ &= \sqrt{\frac{\tau}{N_2}\sum_{i=0}^{N_2-1} E\left\{\|X_i+Y_i\|_2^2\right\}}, k = 0, \ldots, N_2-1. \end{aligned} \tag{5.14}$$

The OBP constraint in (5.11c) can be reformulated as

$$\|\mathbf{G}(\mathbf{X}+\mathbf{Y})\|_2 \leq \sqrt{\alpha}\,\|\mathbf{G}\mathbf{X}\|_2 . \tag{5.15}$$

For a small θ, we have $\|1+Y_k/X_k\|_2 \approx 1$ for the variable located within the relaxed solution region as shown in Figure 5.3. Therefore, we have the following approximations when θ is small

$$\begin{aligned} \|A_\varepsilon(k,k)(X_k+Y_k)\|_2 &\approx \|A_\varepsilon(k,k)X_k\|_2 \\ \frac{1}{N_2}\sum_{i=0}^{N_2-1} E\left\{\|X_i+Y_i\|_2^2\right\} &\approx \frac{1}{N_2}\sum_{i=0}^{N_2-1} E\left\{\|X_i\|_2^2\right\} = \mathcal{E} \end{aligned} \tag{5.16}$$

where $\mathcal{E}$ denotes the average power of the original information symbols.

Therefore, letting θ be a small angle chosen from the range of $(0,\pi/2)$, and denoting $\mathbf{X}=\mathbf{X}_r+j\mathbf{X}_i$, $\mathbf{Y}=\mathbf{Y}_r+j\mathbf{Y}_i$, $\mathbf{b}_k=\mathbf{b}_{r,k}+j\mathbf{b}_{i,k}$, $\mathbf{f}_k=\mathbf{f}_{r,k}+j\mathbf{f}_{i,k}$, and $\mathbf{g}=\mathbf{G}\mathbf{X}=\mathbf{g}_r+j\mathbf{g}_i$, based on the above discussion, the joint design problem in (5.11) is relaxed as

$$\min_{\hat{\mathbf{Y}}} \quad \max_{k\in[N_0,N_1-1]} \frac{\left\|\hat{\mathbf{s}}_k+\hat{\mathbf{B}}_k^T\hat{\mathbf{Y}}\right\|_2}{\|A_\varepsilon(k,k)X_k\|_2} \tag{5.17a}$$

$$\text{subject to:} \quad \left\|\hat{\mathbf{x}}_k+\hat{\mathbf{P}}_k^T\hat{\mathbf{Y}}\right\|_2 \leq \sqrt{\tau\mathcal{E}} \quad k=0,\ldots,N_2-1 \tag{5.17b}$$

$$\left\|\hat{\mathbf{g}}+\hat{\mathbf{G}}\hat{\mathbf{Y}}\right\|_2 \leq \sqrt{\alpha}\,\|\hat{\mathbf{g}}\|_2 \quad 0<\alpha<1 \tag{5.17c}$$

$$\left\|\hat{\mathbf{X}}+\hat{\mathbf{Y}}\right\|_2 \leq \sqrt{\beta+1}\left\|\hat{\mathbf{X}}\right\|_2 \quad 0<\beta<1 \tag{5.17d}$$

$$\hat{\mathbf{D}}\hat{\mathbf{Y}}+\hat{\mathbf{f}} \geq \mathbf{0} \tag{5.17e}$$

where $\hat{\mathbf{s}}_k=\left[\Re\left\{\mathbf{b}_k^T\mathbf{X}\right\}\ \Im\left\{\mathbf{b}_k^T\mathbf{X}\right\}\right]^T$, $\hat{\mathbf{x}}_k=\left[\Re\left\{\mathbf{f}_k^T\mathbf{X}\right\}\ \Im\left\{\mathbf{f}_k^T\mathbf{X}\right\}\right]^T$, $\hat{\mathbf{X}}=\left[\mathbf{X}_r^T\ \mathbf{X}_i^T\right]^T$,

$\hat{\mathbf{Y}} = \left[\mathbf{Y}_r^T\ \mathbf{Y}_i^T\right]^T$, $\hat{\mathbf{g}} = \left[\mathbf{g}_r^T\ \mathbf{g}_i^T\right]^T$,

$$\hat{\mathbf{B}}_k^T = \begin{bmatrix} \mathbf{b}_{rk}^T & -\mathbf{b}_{ik}^T \\ \mathbf{b}_{ik}^T & \mathbf{b}_{rk}^T \end{bmatrix},\ \hat{\mathbf{P}}_k^T = \begin{bmatrix} \mathbf{f}_{rk}^T & -\mathbf{f}_{ik}^T \\ \mathbf{f}_{ik}^T & \mathbf{f}_{rk}^T \end{bmatrix},\ \hat{\mathbf{G}} = \begin{bmatrix} \mathbf{G} & \mathbf{0} \\ \mathbf{0} & \mathbf{G} \end{bmatrix}$$

$$\hat{\mathbf{D}}^T = \begin{bmatrix} \mathbf{0}_{N,\frac{M}{2}} & -\mathrm{diag}\left\{\bar{\mathbf{X}}_r\right\} & \mathbf{0}_{N,M} & -\mathrm{diag}\left\{\bar{\mathbf{X}}_i\right\} & \mathbf{0}_{N,\frac{M}{2}} \\ \mathbf{0}_{N,\frac{M}{2}} & \mathrm{diag}\left\{\bar{\mathbf{X}}_r\right\} & \mathbf{0}_{N,M} & \mathrm{diag}\left\{\bar{\mathbf{X}}_i\right\} & \mathbf{0}_{N,\frac{M}{2}} \\ \mathbf{0}_{N,\frac{M}{2}} & \mathrm{diag}\left\{-\bar{\mathbf{X}}_i + \tan\theta\cdot\bar{\mathbf{X}}_r\right\} & \mathbf{0}_{N,M} & \mathrm{diag}\left\{\bar{\mathbf{X}}_r + \tan\theta\cdot\bar{\mathbf{X}}_i\right\} & \mathbf{0}_{N,\frac{M}{2}} \\ \mathbf{0}_{N,\frac{M}{2}} & \mathrm{diag}\left\{\bar{\mathbf{X}}_i + \tan\theta\cdot\bar{\mathbf{X}}_r\right\} & \mathbf{0}_{N,M} & \mathrm{diag}\left\{-\bar{\mathbf{X}}_r + \tan\theta\cdot\bar{\mathbf{X}}_i\right\} & \mathbf{0}_{N,\frac{M}{2}} \end{bmatrix}$$

$$\hat{\mathbf{f}} = \begin{bmatrix} \mathbf{0}_{N,1} \\ \mathrm{diag}\left\{\left\|\bar{X}_0\right\|_2^2, \cdots, \left\|\bar{X}_{N-1}\right\|_2^2\right\}(1-\cos\theta)\,\mathbf{E}_{N,1} \\ \mathrm{diag}\left\{\left\|\bar{X}_0\right\|_2^2, \cdots, \left\|\bar{X}_{N-1}\right\|_2^2\right\}\tan\theta\cdot\mathbf{E}_{N,1} \\ \mathrm{diag}\left\{\left\|\bar{X}_0\right\|_2^2, \cdots, \left\|\bar{X}_{N-1}\right\|_2^2\right\}\tan\theta\cdot\mathbf{E}_{N,1} \end{bmatrix}$$

with $\mathbf{0}_{l,m} \in \mathbb{R}^{l\times m}$ and $\mathbf{E}_{l,m} \in \mathbb{R}^{l\times m}$ being matrixes with all elements being zeros and ones respectively and and $\mathbb{R}$ being the real space, $\mathrm{diag}\{\mathbf{\Omega}\}$ being a diagonal matrix with diagonal elements $\mathbf{\Omega} = [\omega_0\ \cdots\ \omega_{N-1}]^T$, $\bar{X}_n$ $(n = 0, \ldots, N-1)$ being the nth element of $\bar{\mathbf{X}}$, $\bar{\mathbf{X}}_r = \Re\{\bar{\mathbf{X}}\}$, and $\bar{\mathbf{X}}_i = \Im\{\bar{\mathbf{X}}\}$. The derivation of (5.17e) is provided in Appendix D.

By introducing an upper bound ξ in the objective function (5.17a) as an additional variable, we can reformulate the problem in (5.17) as

$$\min_{\tilde{\mathbf{Y}}}\ \mathbf{d}_r^T\tilde{\mathbf{Y}} \tag{5.18a}$$

$$\text{s. t.}\ \left\|\hat{\mathbf{s}}_k + \tilde{\mathbf{B}}_k^T\tilde{\mathbf{Y}}\right\|_2 \le \mathbf{c}_{rk}^T\tilde{\mathbf{Y}} \quad k = N_0, \ldots, N_1 - 1 \tag{5.18b}$$

$$\left\|\hat{\mathbf{x}}_k + \tilde{\mathbf{P}}_k^T\tilde{\mathbf{Y}}\right\|_2 \le \sqrt{\tau\mathcal{E}} \quad k = 0, \ldots, N_2 - 1 \tag{5.18c}$$

$$\left\|\hat{\mathbf{g}} + \tilde{\mathbf{G}}\tilde{\mathbf{Y}}\right\|_2 \le \sqrt{\alpha}\left\|\hat{\mathbf{g}}\right\|_2 \quad 0 < \alpha < 1 \tag{5.18d}$$

$$\left\|\hat{\mathbf{X}} + \tilde{\mathbf{I}}\tilde{\mathbf{Y}}\right\|_2 \le \sqrt{1+\beta}\left\|\hat{\mathbf{X}}\right\|_2 \quad 0 < \beta < 1 \tag{5.18e}$$

$$\tilde{\mathbf{D}}_r\tilde{\mathbf{Y}} + \hat{\mathbf{f}} \ge \mathbf{0}. \tag{5.18f}$$

where $\tilde{\mathbf{Y}} = \left[\hat{\mathbf{Y}}^{\mathbf{T}}\ \xi\right]^T$, $\tilde{\mathbf{B}}_k^T = \left[\hat{\mathbf{B}}_k^T\ \mathbf{0}_{2,1}\right]$, $\mathbf{c}_{rk} = [\mathbf{0}_{1,2N_2}\ \|A_\varepsilon(k,k)\,X_k\|_2]^T$, $\mathbf{d}_r = [\mathbf{0}_{1,2N_2}\ 1]^T$, $\tilde{\mathbf{P}}_k^T = \left[\hat{\mathbf{P}}_k^T\ \mathbf{0}_{2,1}\right]$, $\tilde{\mathbf{I}} = [\mathbf{I}_{2N_2,2N_2}\ \mathbf{0}_{2N_2,1}]$, $\tilde{\mathbf{G}} = \left[\hat{\mathbf{G}}\ \mathbf{0}_{2N_2,1}\right]$ and $\tilde{\mathbf{D}}_r =$

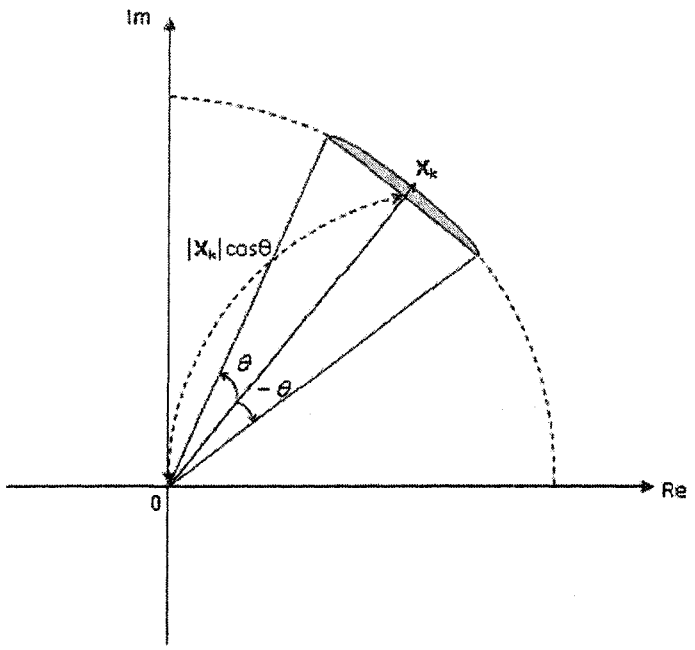

Figure 5.3: Relaxed solution region

$\left[\hat{\mathbf{D}}\ \mathbf{0}_{4N,1}\right]$.

The problem in (5.18) is an explicit SOCP problem with $2N_2 + 1$ variables, which can be solved efficiently by the well established interior point method [33].

After we obtain the solution to the problem in (5.18), which is denoted as Y_k^* ($k = 0, \ldots, N_2 - 1$), the actual transmitted symbol on the kth subcarrier is given by

$$\begin{cases} X_k e^{j\delta_k^*} & k = N_0, \ldots, N_1 - 1 \\ Y_k^* & k = 0, \ldots, N_0 - 1, N_1, \ldots, N_2 - 1. \end{cases} \tag{5.19}$$

with

$$\delta_k^* = \arg\min_{\delta_k \in \{-\theta, 0, \theta\}} \left| \arg\left(1 + \frac{Y_k^*}{X_k}\right) - \delta_k \right|$$

being the quantized rotation angle.

It is noted that sometimes no feasible solution can be found for the optimization problem in (5.18) for some OFDM symbols under the given values of the parameters including τ, α, and β, especially when N is large. In this situation, for the application of overlay cognitive radio system, we propose to identify the solution as the one that minimizes OBP with PAPR constraint and if still no solution can be found, then identify the solution as the one that minimizes OBP without PAPR constraints. They are formulated by (5.20) and (5.21) respectively.

$$\begin{array}{lll} \min \text{OBP} & = & \min_{\tilde{\mathbf{Y}}} \mathbf{d}^T\tilde{\mathbf{Y}} \\ \text{s.t.} \quad \left\|\hat{\mathbf{g}}+\tilde{\mathbf{G}}\tilde{\mathbf{Y}}\right\|_2 & \leq & \mathbf{d}^T\tilde{\mathbf{Y}} \\ \left\|\hat{\mathbf{x}}_k+\tilde{\mathbf{P}}_k^T\tilde{\mathbf{Y}}\right\|_2 & \leq & \sqrt{\frac{\tau}{N}\sum_{i=0}^{N_2-1}E\left\{\|X_i\|_2^2\right\}}, \text{for } k=0,\cdots N_2-1 \\ \left\|\hat{\mathbf{X}}+\tilde{\mathbf{I}}\tilde{\mathbf{Y}}\right\|_2 & \leq & \sqrt{1+\beta_2}\left\|\hat{\mathbf{X}}\right\|_2, 0<\beta_2<1 \\ \tilde{\mathbf{D}}^T\tilde{\mathbf{Y}}+\hat{\mathbf{f}} & \geq & \mathbf{0} \end{array} \tag{5.20}$$

$$\begin{array}{lll} \min_{\tilde{\mathbf{Y}}} & \mathbf{d}_r^T\tilde{\mathbf{Y}} & \\ \text{s. t.} & \left\|\hat{\mathbf{g}}+\tilde{\mathbf{G}}\tilde{\mathbf{Y}}\right\|_2 \leq \mathbf{d}_r^T\tilde{\mathbf{Y}} & \\ & \left\|\hat{\mathbf{X}}+\tilde{\mathbf{I}}\tilde{\mathbf{Y}}\right\|_2 \leq \sqrt{1+\beta}\left\|\hat{\mathbf{X}}\right\|_2 & 0<\beta<1 \\ & \tilde{\mathbf{D}}_r\tilde{\mathbf{Y}}+\hat{\mathbf{f}} \geq \mathbf{0}. & \end{array} \tag{5.21}$$

In this way, OBP is minimized while the values of PAPR and PICR may be large. Thus, it may result in nonlinear operations of PAs in the system and cause detection performance of the receiver degraded. From the simulation results that we obtained and will be presented in Section 5.4, the performance of PAPR and PICR reductions is not affected much since the phenomenon that no feasible solution can be found for the problem in (5.18) happens quite infrequently when the parameter values of the system are set appropriately.

It should be made clear that the problem in (5.21) is only one possibility to deal with the situation when no feasible solution could be found for the problem in (5.18) and (5.20). Depending on the specific applications, different problems may

be formulated and solved to find a solution in this special case. For instance, we may choose to minimize PICR with PAPR constraint but without considering OBP in the applications where enough guard bands have been set up in the system.

As mentioned above, the rotating phases need to be transmitted to the receiver as side information. In our proposed approach, $\log_2 3$ bits are needed to transmit side information for one information symbol. Therefore, the information efficiency, which is defined as the percentage of the bits used for transmitting information out of the total bits, is given as

$$\eta = \log_2 Q/(\log_2 Q + \log_2 (3)) \times 100\% \tag{5.22}$$

with Q being the size of the modulation constellations.

Therefore, the proposed phase rotation approach based algorithm for the joint PAPR-PICR-OBP design problem is summarized as follows.

Step 1: Solve the problem in (5.18).

If no solution is found, then go to step 2. Otherwise, go to step 4.

Step 2: Solve the problem in (5.20). If still no solution is found, then go to step 3. Otherwise, go to step 4.

Step 3: Solve the problem in (5.21), then go to step 4.

Step 4: Record the values of PAPR, PICR, and OBP of the OFDM signal under the solution and stop.

5.3.3 Algorithm Based on the Constellation Extension Approach

In the constellation extension approach, the information symbol on the kth subcarrier, which is X_k, is extended to a new constellation to optimize the design

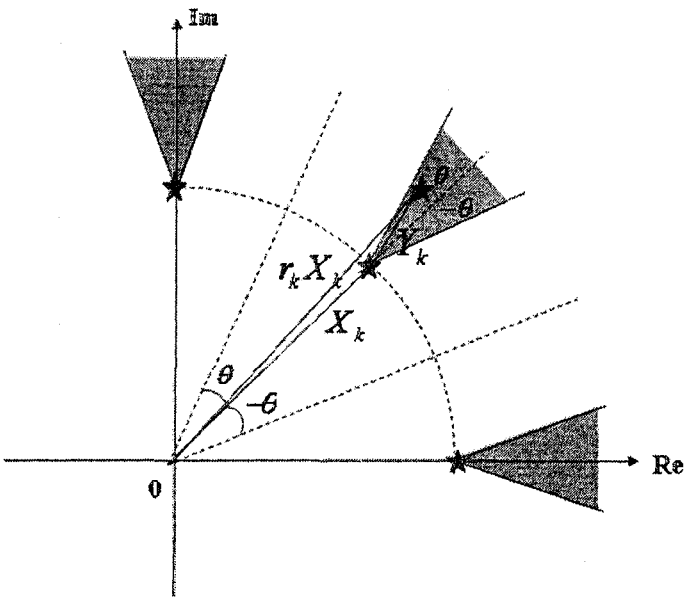

Figure 5.4: Feasible region of 8PSK for the constellation extension approach.

objectives [20] and [22]. In order to avoid from transmitting side information and to maintain the BER performance of the original signal, each new constellation must be located in a certain feasible region so that without any side information, the receiver is able to recover the original information symbol and that the nearest distance of any two new adjacent constellations is greater than or at least equal to the nearest distance of any two original adjacent constellations. For instances, the feasible regions of MPSK modulation and 16QAM are shown as the shaded areas in Figures 5.4 and 5.5, respectively.

Similar to the derivation in the phase rotation approach, the joint design based

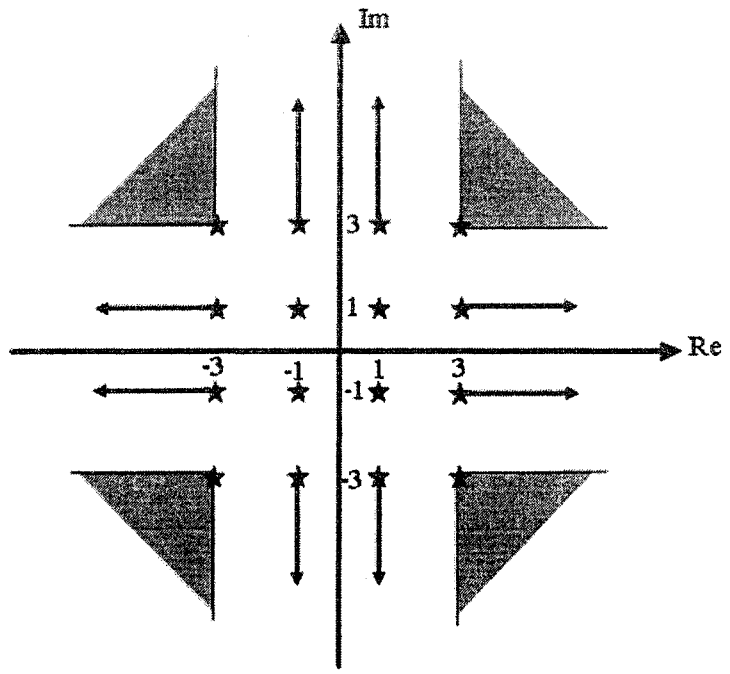

Figure 5.5: Feasible region of 16QAM for the constellation extension approach.

on the constellation extension approach can be formulated as

$$\min \text{PICR} = \min_{\hat{Y}} \max_{k\in[N_0,N_1-1]} \frac{\left\|\hat{\mathbf{s}}_k + \hat{\mathbf{B}}_k^T\hat{\mathbf{Y}}\right\|_2}{\left\|A_\varepsilon(k,k)(X_k+Y_k)\right\|_2} \tag{5.23a}$$

$$\text{subject to: } \left\|\hat{\mathbf{x}}_k + \hat{\mathbf{P}}_k^T\hat{\mathbf{Y}}\right\|_2 \leq \sqrt{\frac{\tau}{N_2}\sum_{i=0}^{N_2-1} E\left\{\|X_i+Y_i\|_2^2\right\}},\ k=0,\ldots,N_2-1 \tag{5.23b}$$

$$\left\|\hat{\mathbf{g}} + \widehat{\mathbf{G}}\hat{\mathbf{Y}}\right\|_2 \leq \sqrt{\alpha}\left\|\hat{\mathbf{g}}\right\|_2, 0<\alpha<1 \tag{5.23c}$$

$$\left\|\hat{\mathbf{X}} + \hat{\mathbf{Y}}\right\|_2 \leq \sqrt{\beta+1}\left\|\hat{\mathbf{X}}\right\|_2, 0<\beta<1 \tag{5.23d}$$

$$X_k + Y_k \text{ be feasible, } k=N_0,\ldots,N_1-1 \tag{5.23e}$$

Note that the objective function (5.23a) can be converted to

$$\begin{aligned} &\min \xi \\ \text{s. t. } &\left\|\hat{\mathbf{s}}_k + \hat{\mathbf{B}}_k^T\hat{\mathbf{Y}}\right\|_2 \leq \xi\left\|A_\varepsilon(k,k)(X_k+Y_k)\right\|_2 \\ &k=N_0,\ldots,N_1-1. \end{aligned} \tag{5.24}$$

By using Taylor expansion,

$$z = \xi \left\| (X_k + Y_k) \right\|_2 = \xi \sqrt{(X_{rk} + Y_{rk})^2 + (X_{ik} + Y_{ik})^2}$$

can be linearized at $(\xi = \xi_0, Y_k = Y_k^0 = Y_{rk}^0 + jY_{ik}^0)$ as

$$\begin{aligned} z \quad &\approx z\left(\xi_0, Y_k^0\right) + \frac{\partial z}{\partial \xi}\Big|_{(\xi_0, Y_k^0)} (\xi - \xi_0) \\ &+ \frac{\partial z}{\partial Y_{rk}}\Big|_{(\xi_0, Y_k^0)} \left(Y_{rk} - Y_{rk}^0\right) + \frac{\partial z}{\partial Y_{ik}}\Big|_{(\xi_0, Y_k^0)} \left(Y_{ik} - Y_{ik}^0\right) \end{aligned}$$

where

$$\begin{aligned} \frac{\partial z}{\partial \xi}\Big|_{(\xi_0, Y_k^0)} &= \left\| (X_k + Y_k) \right\|_2 \Big|_{(\xi_0, Y_k^0)} = \left\| X_k + Y_k^0 \right\|_2 \\ \frac{\partial z}{\partial Y_{rk}}\Big|_{(\xi_0, Y_k^0)} &= \xi \frac{X_{rk} + Y_{rk}}{\left\| X_k + Y_k \right\|_2}\Big|_{(\xi_0, Y_k^0)} = \xi_0 \frac{X_{rk} + Y_{rk}^0}{\left\| X_k + Y_k^0 \right\|_2} \\ \frac{\partial z}{\partial Y_{ik}}\Big|_{(\xi_0, Y_k^0)} &= \xi \frac{X_{ik} + Y_{ik}}{\left\| X_k + Y_k \right\|_2}\Big|_{(\xi_0, Y_k^0)} = \xi_0 \frac{X_{ik} + Y_{ik}^0}{\left\| X_k + Y_k^0 \right\|_2}. \end{aligned}$$

So we have

$$\begin{aligned} z \quad \approx \quad & -\frac{\xi_0}{\left\| X_k + Y_k^0 \right\|_2} \left(\left(X_{rk} + Y_{rk}^0\right) Y_{rk}^0 + \left(X_{ik} + Y_{ik}^0\right) Y_{ik}^0 \right) \\ & + \frac{\xi_0 \left(X_{rk} + Y_{rk}^0\right)}{\left\| X_k + Y_k^0 \right\|_2} Y_{rk} + \frac{\xi_0 \left(X_{ik} + Y_{ik}^0\right)}{\left\| X_k + Y_k^0 \right\|_2} Y_{ik} + \left\| X_k + Y_k^0 \right\|_2 \xi \end{aligned} \tag{5.25}$$

If we let $\mathbf{L} = \left[\left\| \frac{A_\varepsilon(N_0, N_0)}{X_{N_0} + Y_{N_0}^0} \right\|_2 \cdots \left\| \frac{A_\varepsilon(N_1 - 1, N_1 - 1)}{X_{N_1 - 1} + Y_{N_1 - 1}^0} \right\|_2 \right]^T$, $\bar{\mathbf{X}}_r^L = \operatorname{diag}\{\mathbf{L}\} \left(\bar{\mathbf{X}}_r + \bar{\mathbf{Y}}_r^0\right)$, $\bar{\mathbf{X}}_i^L = \operatorname{diag}\{\mathbf{L}\} \left(\bar{\mathbf{X}}_i + \bar{\mathbf{Y}}_i^0\right)$, with

$$\bar{\mathbf{Y}}^0 = \bar{\mathbf{Y}}_r^0 + j\bar{\mathbf{Y}}_i^0 = \left[\bar{Y}_0^0 \ \cdots \ \bar{Y}_{N-1}^0 \right]^T,$$

the ith element of which being the $(i + N_0)$th element of $\mathbf{Y}^0$ for $i = 0 \ \ldots \ N - 1$ and

$$\bar{\mathbf{L}} = \left[\left\| A_\varepsilon\left(N_0, N_0\right) \left(X_{N_0} + Y_{N_0}^0\right) \right\|_2 \cdots \left\| A_\varepsilon\left(N_1 - 1, N_1 - 1\right) \left(X_{N_1 - 1} + Y_{N_1 - 1}^0\right) \right\|_2 \right]^T,$$

then the constraint in (5.24) for $k = N_0, \ldots, N_1 - 1$ can be relaxed as

$$\left\| \hat{\mathbf{s}}_k + \tilde{\mathbf{B}}_k^T \tilde{\mathbf{Y}} \right\|_2 \leq \mathbf{c}_{ek}^T \tilde{\mathbf{Y}} + d_{ek} \tag{5.26}$$

where

$$d_{ek} = -\xi_0 \left\| \frac{A_\varepsilon(k,k)}{X_k + Y_k^0} \right\|_2 \left(\left(X_{rk} + Y_{rk}^0 \right) Y_{rk}^0 + \left(X_{ik} + Y_{ik}^0 \right) Y_{ik}^0 \right)$$

and $\mathbf{c}_{ek}^T$ is the kth row of the matrix

$$\mathbf{R} = \left[\mathbf{0}_{N,\frac{M}{2}} \quad \xi_0 \cdot \mathrm{diag}\left\{ \bar{\mathbf{X}}_r^L \right\} \quad \mathbf{0}_{N,M} \quad \xi_0 \cdot \mathrm{diag}\left\{ \bar{\mathbf{X}}_i^L \right\} \quad \mathbf{0}_{N,\frac{M}{2}} \quad \bar{\mathbf{L}} \right]. \tag{5.27}$$

In addition, as found in the literature, the increase of the average power in the optimally modified signal is fairly moderate for the constellation extension approach. So we will replace the average power in (5.23b) by $\mathcal{E}$, which represents the average power of the original information symbols, as defined in (5.16).

Therefore, the problem in (5.23) can be relaxed as

$$\min_{\tilde{\mathbf{Y}}} \ \mathbf{d}_e^T \tilde{\mathbf{Y}} \tag{5.28a}$$

$$\text{subject to: } \left\| \hat{\mathbf{s}}_k + \tilde{\mathbf{B}}_k^T \tilde{\mathbf{Y}} \right\|_2 \leq \mathbf{c}_{ek}^T \tilde{\mathbf{Y}} + d_{ek} \quad k = N_0, \ldots, N_1 - 1 \tag{5.28b}$$

$$\left\| \hat{\mathbf{x}}_k + \tilde{\mathbf{P}}_k^T \tilde{\mathbf{Y}} \right\|_2 \leq \sqrt{\tau \mathcal{E}} \quad k = 0, \ldots, N_2 - 1 \tag{5.28c}$$

$$\left\| \hat{\mathbf{g}} + \tilde{\mathbf{G}} \tilde{\mathbf{Y}} \right\|_2 \leq \sqrt{\alpha} \left\| \hat{\mathbf{g}} \right\|_2 \quad 0 < \alpha < 1 \tag{5.28d}$$

$$\left\| \hat{\mathbf{X}} + \tilde{\mathbf{I}} \tilde{\mathbf{Y}} \right\|_2 \leq \sqrt{1 + \beta} \left\| \hat{\mathbf{X}} \right\|_2 \quad 0 < \beta < 1 \tag{5.28e}$$

$$X_k + Y_k \text{ be feasible} \quad k = N_0, \ldots, N_1 - 1 \tag{5.28f}$$

A. MPSK Modulation Case

From Figure 5.4, the feasible region of MPSK modulation for the constellation extension approach can be expressed as

$$\begin{cases} -\theta \leq \arg\left(Y_k/X_k\right) \leq \theta \\ \Re\left(1+Y_k/X_k\right) \geq 1 \end{cases} \qquad k = N_0, \ldots, N_1 - 1 \tag{5.29}$$

where $\theta = \pi/M$. For example, $\theta = \frac{\pi}{8}$ and $\frac{\pi}{4}$ for 8PSK and QPSK, respectively.

From (5.29), similar to the derivation of (5.17e), we get the matrix form of the feasible region constraint in (5.28f) as

$$\tilde{\mathbf{D}}_e^p \tilde{\mathbf{Y}} \geq \mathbf{0} \tag{5.30}$$

where

$$\tilde{\mathbf{D}}_e^p = \begin{bmatrix} \mathbf{0}_{N,\frac{M}{2}} & \operatorname{diag}\left\{\bar{\mathbf{X}}_r\right\} & \mathbf{0}_{N,M} & \operatorname{diag}\left\{\bar{\mathbf{X}}_i\right\} & \mathbf{0}_{N,\frac{M}{2}} & \mathbf{0}_{N,1} \\ \mathbf{0}_{N,\frac{M}{2}} & \operatorname{diag}\left\{\tan\theta \cdot \bar{\mathbf{X}}_r - \bar{\mathbf{X}}_i\right\} & \mathbf{0}_{N,M} & \operatorname{diag}\left\{\tan\theta \cdot \bar{\mathbf{X}}_i + \bar{\mathbf{X}}_r\right\} & \mathbf{0}_{N,\frac{M}{2}} & \mathbf{0}_{N,1} \\ \mathbf{0}_{N,\frac{M}{2}} & \operatorname{diag}\left\{\tan\theta \cdot \bar{\mathbf{X}}_r + \bar{\mathbf{X}}_i\right\} & \mathbf{0}_{N,M} & \operatorname{diag}\left\{\tan\theta \cdot \bar{\mathbf{X}}_i - \bar{\mathbf{X}}_r\right\} & \mathbf{0}_{N,\frac{M}{2}} & \mathbf{0}_{N,1} \end{bmatrix}.$$

Thus, for the MPSK modulation case, we convert the joint design problem into an explicit SOCP problem with $2N_2 + 1$ variables. Similar to (5.19), after solving this SOCP problem and obtaining the solution Y_k^* $(k = 0, \ldots, N_2 - 1)$, the actual transmitted symbol on the kth subcarrier can be expressed as

$$\begin{cases} X_k + Y_k^* & k = N_0, \ldots, N_1 - 1 \\ Y_k^* & k = 0, \ldots, N_0 - 1, N_1, \ldots, N_2 - 1 \end{cases}. \tag{5.31}$$

B. 16QAM Case

As shown in Figure 5.5, the feasible region of 16QAM for the constellation extension approach is given as: For $N_0 \leq k \leq N_1 - 1$,

(1) If $|X_{rk}| = |X_{rk}| = 1$,then $Y_{rk} = Y_{ik} = 0$;

(2) If $|X_{ik}| = 3$ and $|X_{rk}| = 1$, then $Y_{rk} = 0, X_{ik}Y_{ik} \geq 0$;

(3) If $|X_{rk}| = 3$ and $|X_{ik}| = 1$, then $Y_{ik} = 0, X_{rk}Y_{rk} \geq 0$;

(4) If $|X_{rk}| = |X_{ik}| = 3$, then $X_{ik}Y_{ik} \geq 0, X_{rk}Y_{rk} \geq 0$.

That is, if $|X_{rk}| = 3$, then $|Y_{rk}| \neq 0$; otherwise, $Y_{rk} = 0$. Also, if $|X_{ik}| = 3$, then $|Y_{ik}| \neq 0$; otherwise, $Y_{ik} = 0$. Therefore, for 16QAM, the feasible region constrains the real and/or imaginary components of some extension subcarriers as zeros, which means the number of variables in the problem of (5.28) can be reduced.

Denote $\mathbf{I}^a \in \mathbb{R}^{N_a \times 1}$ and $\mathbf{I}^b \in \mathbb{R}^{N_b \times 1}$ as the index vectors containing the N_a and N_b increasingly sorted indexes corresponding to non-zero real and imaginary components of the variables Y_k $(N_0 \leq k \leq N_1 - 1)$, respectively. Let

$$\mathbf{I}^r = \begin{bmatrix} 0 & \cdots & N_0 - 1 & (\mathbf{I}^a)^T & N_1 & \cdots & N_2 - 1 \end{bmatrix}^T \in \mathbb{R}^{N_r \times 1}$$

with $N_r = N_a + M$,

$$\mathbf{I}^i = \begin{bmatrix} 0 & \cdots & N_0 - 1 & (\mathbf{I}^b)^T & N_1 & \cdots & N_2 - 1 \end{bmatrix}^T \in \mathbb{R}^{N_i \times 1}$$

with $N_i = N_b + M$, and $\mathbf{J} = \left[(\mathbf{I}^r)^T \ (\mathbf{I}^i)^T\right]^T \in \mathbb{R}^{(N_r + N_i) \times 1}$. Accordingly, we denote $\mathbf{X}_r^a = \left[X_{r,0}^a \ X_{r,1}^a \ \cdots \ X_{r,N-1}^a\right]^T$ with the kth element $X_{r,k}^a = \bar{X}_{r,k}$ for $k \in \mathbf{I}^a$, otherwise $X_{r,k}^a = 0$ and $\mathbf{X}_i^b = \left[X_{i,0}^b \ X_{i,1}^b \ \cdots \ X_{i,N-1}^b\right]^T$ with the kth element $X_{i,k}^b = \bar{X}_{i,k}$ for $k \in \mathbf{I}^b$, otherwise $X_{i,k}^b = 0$.

Then for 16QAM, the feasible region constraint in (5.28f) can be formulated as

$$\tilde{\mathbf{D}}_e^q \tilde{\mathbf{Y}}_e^q \geq \mathbf{0} \tag{5.32}$$

where $\tilde{\mathbf{Y}}_e^q = \left[\hat{Y}_{J_0} \ \cdots \ \hat{Y}_{J_{N_r+N_i-1}} \ \xi\right]^T$ with J_n denoting the nth element of $\mathbf{J}$ and $\hat{Y}_{J_n}$ denoting the J_nth element of $\hat{\mathbf{Y}}$ $(n = 0, \ldots, N_r + N_i - 1)$. $\tilde{\mathbf{D}}_e^q$ is given by

$$\tilde{\mathbf{D}}_e^q = \begin{bmatrix} \mathbf{0}_{N,\frac{M}{2}} & \overline{\operatorname{diag}\{\mathbf{X}_r^a\}} & \mathbf{0}_{N,M} & \mathbf{0}_{N,N_b} & \mathbf{0}_{N,\frac{M}{2}+1} \\ \mathbf{0}_{N,\frac{M}{2}} & \mathbf{0}_{N,\frac{M}{2}} & \mathbf{0}_{N,M} & \overline{\operatorname{diag}\{\mathbf{X}_i^b\}} & \mathbf{0}_{N,\frac{M}{2}+1} \end{bmatrix} \tag{5.33}$$

with $\overline{\operatorname{diag}\{\mathbf{X}_r^a\}}$ and $\overline{\operatorname{diag}\{\mathbf{X}_i^b\}}$ being the column reduced matrixes obtained by deleting the kth column from $\operatorname{diag}\{\mathbf{X}_r^a\}$ and $\operatorname{diag}\{\mathbf{X}_i^b\}$ if $X_{r,k}^a = 0$ and $X_{i,k}^b = 0$, respectively.

Thus for 16QAM, the problem in (5.28) is converted to

$$\begin{aligned} &\min_{\tilde{\mathbf{Y}}_e^q} \left(\mathbf{d}_e^q\right)^T \tilde{\mathbf{Y}}_e^q \\ \text{s. t.} \quad &\left\|\hat{\mathbf{s}}_k + \tilde{\mathbf{B}}_k^q \tilde{\mathbf{Y}}_e^q\right\|_2 \le \left(\mathbf{c}_{ek}^q\right)^T \tilde{\mathbf{Y}}_e^q + d_{ek} \quad k = N_0, \ldots, N_1 - 1 \\ &\left\|\hat{\mathbf{x}}_k + \tilde{\mathbf{P}}_k^q \tilde{\mathbf{Y}}_e^q\right\|_2 \le \sqrt{\tau \mathcal{E}} \quad k = 0, \ldots, N_2 - 1 \\ &\left\|\hat{\mathbf{X}} + \tilde{\mathbf{I}}^q \tilde{\mathbf{Y}}_e^q\right\|_2 \le \sqrt{1+\beta} \left\|\hat{\mathbf{X}}\right\|_2 \quad 0 < \beta < 1 \\ &\left\|\hat{\mathbf{g}} + \tilde{\mathbf{G}}^q \tilde{\mathbf{Y}}_e^q\right\|_2 \le \sqrt{\alpha} \left\|\hat{\mathbf{g}}\right\|_2 \quad 0 < \alpha < 1 \\ &\tilde{\mathbf{D}}_e^q \tilde{\mathbf{Y}}_e^q \ge \mathbf{0} \end{aligned} \tag{5.34}$$

where

$$\begin{aligned} \tilde{\mathbf{B}}_k^q &= \left[\mathbf{b}_0^q \ \mathbf{b}_1^q \ \cdots \ \mathbf{b}_{N_r+N_i-1}^q \ \mathbf{0}_{2,1}\right] \\ \tilde{\mathbf{P}}_k^q &= \left[\mathbf{p}_0^q \ \mathbf{p}_1^q \ \cdots \ \mathbf{p}_{N_r+N_i-1}^q \ \mathbf{0}_{2,1}\right] \\ \tilde{\mathbf{I}}^q &= \left[\mathbf{I}_0^q \ \mathbf{I}_1^q \ \cdots \ \mathbf{I}_{N_r+N_i-1}^q \mathbf{0}_{2(N+M),1}\right] \\ \tilde{\mathbf{G}}^q &= \left[\mathbf{g}_0^q \ \mathbf{g}_1^q \ \cdots \ \mathbf{g}_{N_r+N_i-1}^q \ \mathbf{0}_{2K,1}\right] \\ \tilde{\mathbf{R}}^q &= \left[\mathbf{r}_0^q \ \mathbf{r}_1^q \ \cdots \ \mathbf{r}_{N_r+N_i-1}^q\right] \end{aligned}$$

with $\mathbf{b}_n^q$, $\mathbf{p}_n^q$, $\mathbf{I}_n^q$, $\mathbf{g}_n^q$, and $\mathbf{r}_n^q$ being the J_nth ($n = 0, \ldots, N_r + N_i - 1$) columns of matrixes $\tilde{\mathbf{B}}_k^T$, $\hat{\mathbf{P}}_k^T$, $\mathbf{I}$, $\mathbf{G}$, and $\mathbf{R}$, respectively. $\left(\mathbf{c}_{ek}^q\right)^T$ is the kth row of the matrix $\tilde{\mathbf{R}}^q$.

After we obtain the solution to the problem in (5.34), which is denoted as $(\tilde{\mathbf{Y}}_e^q)^* = \left[\hat{Y}_{J_0}^* \ \cdots \ \hat{Y}_{J_{Nr+N_i-1}}^* \ \xi^*\right]^T$, we are able to reconstruct the solution Y_k^* ($k = 0, \ldots, N_2 - 1$) based on the discussion above. That is, let the I_k^rth element of $\mathbf{Y}_r^*$ be $\hat{Y}_{J_k}^*$ ($k = 0, \ldots, N_r - 1$) and the other elements be zeros, and let the I_k^ith element of $\mathbf{Y}_i^*$ be $\hat{Y}_{J_{Nr+k}}^*$ ($k = 0, \ldots, N_i - 1$) and the other elements be zeros, with I_k^r and I_k^i denoting the kth elements of $\mathbf{I}^r$ and $\mathbf{I}^i$ respectively. Then we reconstruct $\mathbf{Y}^* = \mathbf{Y}_r^* + j\mathbf{Y}_i^*$. The actual transmitted symbols are then obtained according to (5.31).

5.4 Simulation Results

Computer simulations were conducted to evaluate the efficacy of the proposed algorithms in joint PAPR, PICR, and OBP design. We considered an OFDM system with a fast time-varying frequency-selective Rayleigh fading channel with $\mu = 10$ and normalized total power in multipaths. $N = 64$, $K_1 = K_2 = 16$ and $\varepsilon = 0.1$ are used. In our simulations, we adopt 16QAM or 8PSK modulation schemes. Unless otherwise mentioned, the parameter τ is set as 10 dB for the 16QAM case, 8 dB for the 8PSK modulation case in phase rotation based approach and 9 dB in constellation extension based approach, and $M = 4$. 10^4 OFDM symbols were used to obtain the results shown in this thesis.

10^4 OFDM signals are transmitted and PICR, PAPR, and OBP values of which exceed respective values, say, $PICR_0$, $PAPR_0$, and OBP_0 are countered. The probabilities that the PICR, PAPR, and OBP are greater than those respective values then are respectively given by

$$\begin{aligned} Pr(\text{PICR} > PICR_0) &= \frac{\text{the numbers countered for PICR}}{10^4} \\ Pr(\text{PAPR} > PAPR_0) &= \frac{\text{the numbers countered for PAPR}}{10^4} \\ Pr(\text{OBP} > OBP_0) &= \frac{\text{the numbers countered for OBP}}{10^4} \end{aligned}$$

To ensure the precision of the experiment results, usually the number of experiments used at least 10 times more than the target number of experiments, otherwise we can not say that the joint design performs better than the original design does. Hence, the target probability is chosen to be 10^{-3} in this problem.

5.4.1 Algorithm Based on Phase Rotation Approach

Using the phase rotation approach based algorithm, we show in Figure 5.6 the CCDFs of PICR, PAPR, and OBP of OFDM symbols obtained by minimizing PICR, PAPR, and OBP alone respectively with 8PSK, $\theta = \pi/8$, and $\beta = 1/30$. The results with quantized solutions are also included in the figure. It can be seen that the effect of quantization on the results is quite minor. From Figure 5.6, it is shown that when one of the three problems is considered alone, the performance of the other two problems is quite bad.

The quantity of OBP reduction depends on how much power is consumed by the sidelobe cancellation subcarriers and how many sidelobe cancellation subcarriers are used. The more power is used, the greater the OBP reduction is.

For the joint design problem, we adopt $\alpha = 1/30$ in the phase rotation approach based algorithm. Figure 5.7 shows the CCDFs of PICR, PAPR, and OBP of OFDM symbols with 16QAM as a function of θ obtained by solving the joint design problem. It is shown from Figure 5.7 that the value of θ does affect the performance of the joint design problem. Smaller θ causes less quantization error but makes the constraint tighter, while larger θ makes the constraint looser but causes more quantization error. From Figure 5.7, in our simulation scenario, $\theta = \pi/8$ provides a good trade-off for the performance of PICR, PAPR, and OBP reductions. Thus in the following simulations, $\theta = \pi/8$ will be adopted.

Figures 5.8, 5.9, and 5.10 show the CCDFs of PICR, PAPR, and OBP of OFDM symbols with 16QAM. Quantized optimal solutions are also included in these figures as non-dotted curves. These figures show that there is no big difference between the optimal solutions and the quantized ones. Figures 5.11, 5.12, and 5.13 show

Table 5.1: The threshold values by using phase rotation based algorithm

	1/1000 OFDM Symbols	Joint Design(dB) Optimal	Joint Design(dB) Quantized	Original (dB)	Reduction by Qantized Joint Design (dB)
16-QAM	PICR	50.6	51.9	69.5	17.6
	PAPR	8.0	8.05	10.2	2.1
	OBP	−24.2	−24.4	−9.4	15.0
8-PSK	PICR	47.5	47.9	67.3	19.4
	PAPR	8.4	8.5	10.5	2.0
	OBP	−34.4	−34.4	−21.0	13.3

the CCDFs of PICR, PAPR, and OBP for 8PSK modulation with $\tau = 8$ dB.

For the convenience of comparison, Table 5.1 lists the PICR, PAPR, and OBP threshold values which no one out of 1000 transmitted symbols can exceed for the jointly designed and the original transmitted symbols. The reduction achieved by quantized jointly designed solution is also included in Table 5.1. From Table 5.1, for the 16QAM case, 1 out of 1000 OFDM symbols has PICR exceeding 51.9 dB by using the proposed phase rotation approach based algorithm, whereas in the original transmission, 1 out of 1000 OFDM symbols has PICR exceeding 69.5 dB. This amounts to a 17.6 dB reduction in PICR by using the proposed phase rotation approach based algorithm. Similarly, it is seen that at point 1/1000, PAPR can be reduced at least by 2.1dB and OBP can be reduced at least by 15.0 dB for the 16QAM case. For the 8PSK modulation case, PICR can be reduced by 19.4 dB, PAPR by 2.0 dB, and OBP by 13.3 dB.

Figure 5.14 shows the power spectrum of OFDM symbols with 8PSK modulation scheme. The black curve is the power spectrum of the jointly designed OFDM symbols by using the proposed phase rotation approach based algorithm and the dotted curve is the power spectrum of original OFDM symbols. The OBP radiation

reduction is obviously.

The transmission efficiency η, which is defined in (5.22), is

$$\eta = 4/(4 + \log_2(3)) \times 100\% = 71.62\%.$$

for 16QAM and

$$\eta = 3/(3 + \log_2(3)) \times 100\% = 65.4\%$$

for 8PSK modulation, respectively.

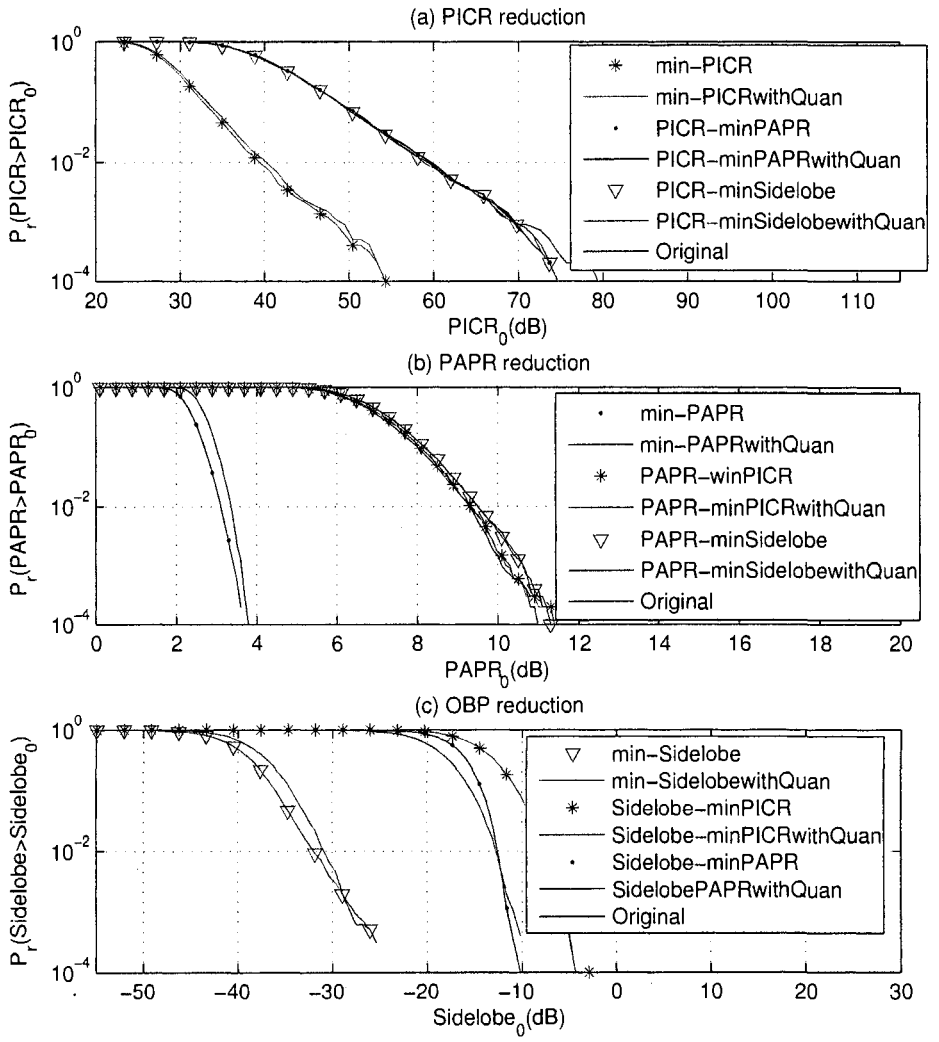

Figure 5.6: CCDFs for individual optimal problems with 16QAM (phase rotation approach)

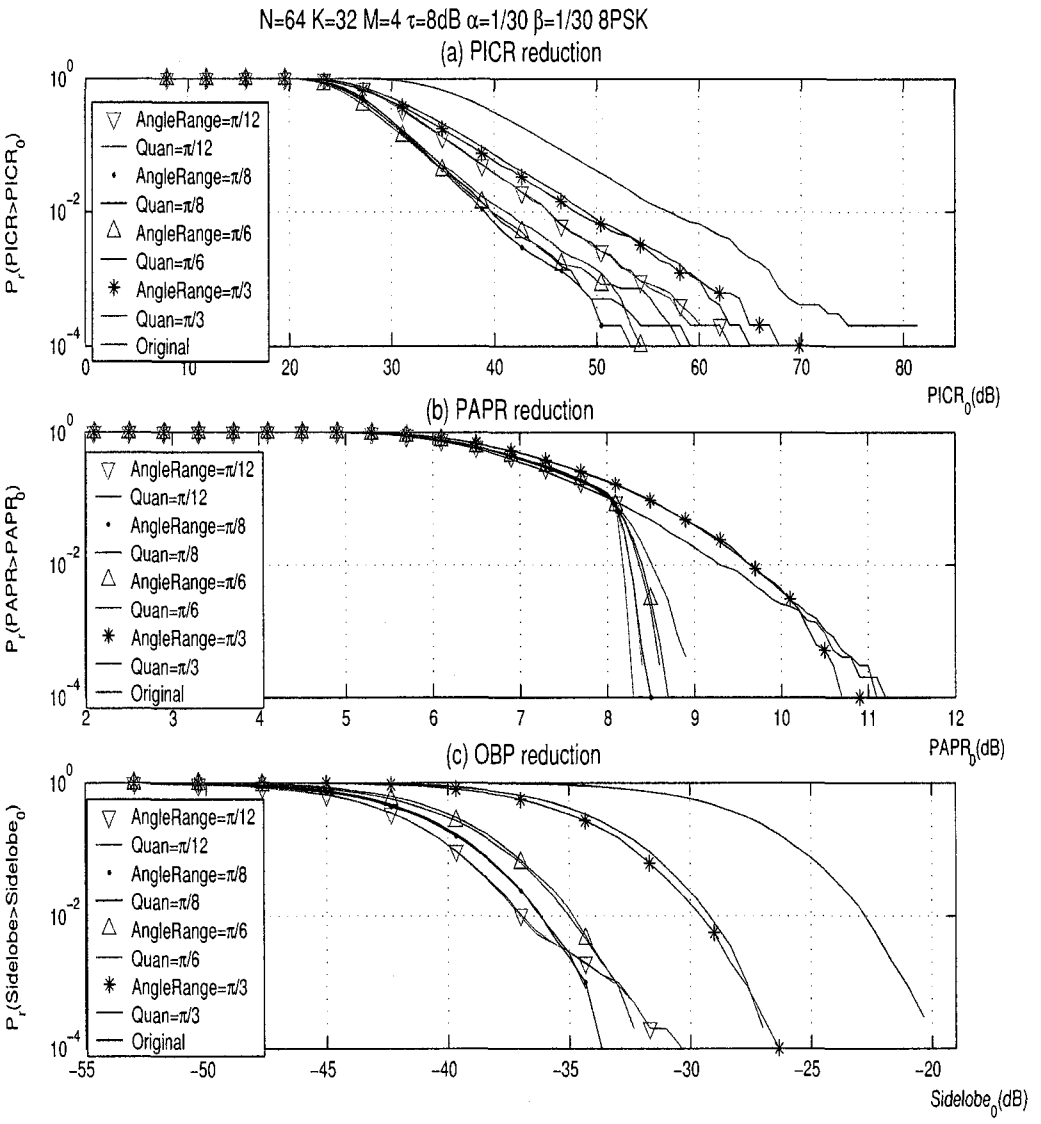

Figure 5.7: CCDFs for joint problem as a function of θ (phase rotation approach)

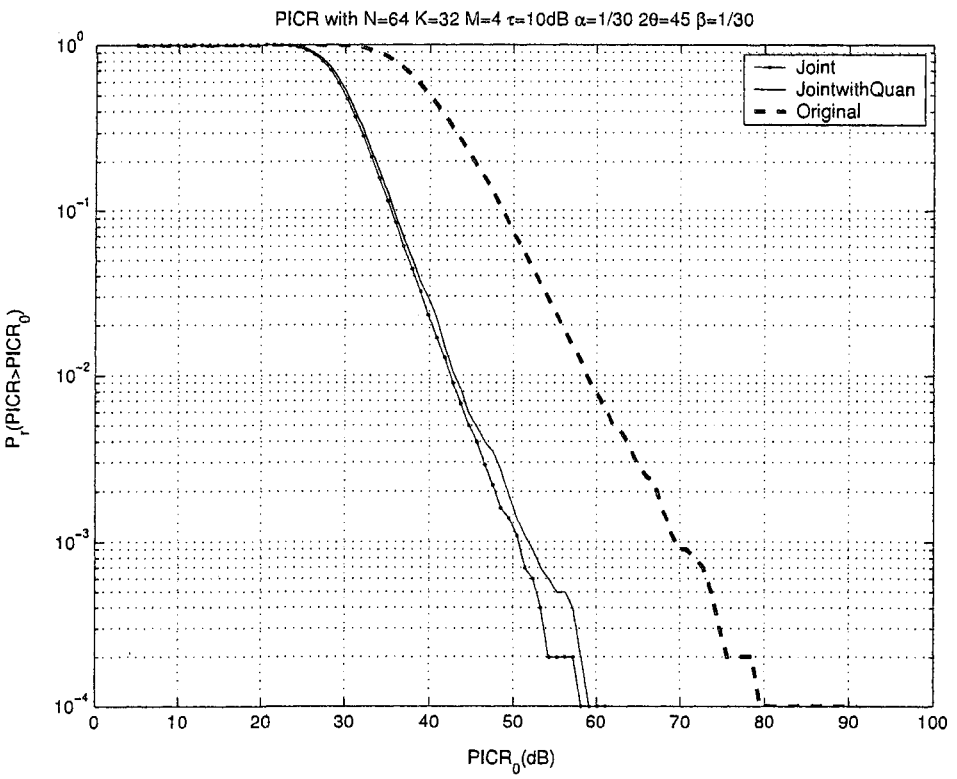

Figure 5.8: Phase rotation based PICR reduction for OFDM systems with 16QAM

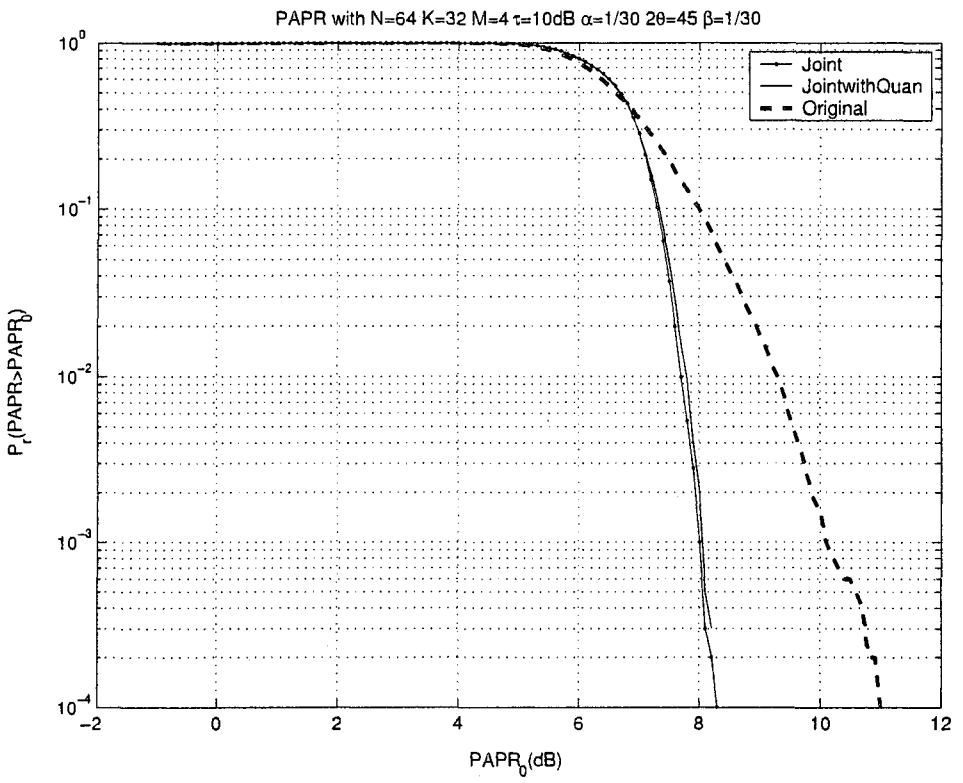

Figure 5.9: Phase rotation based PAPR reduction for OFDM systems with 16QAM

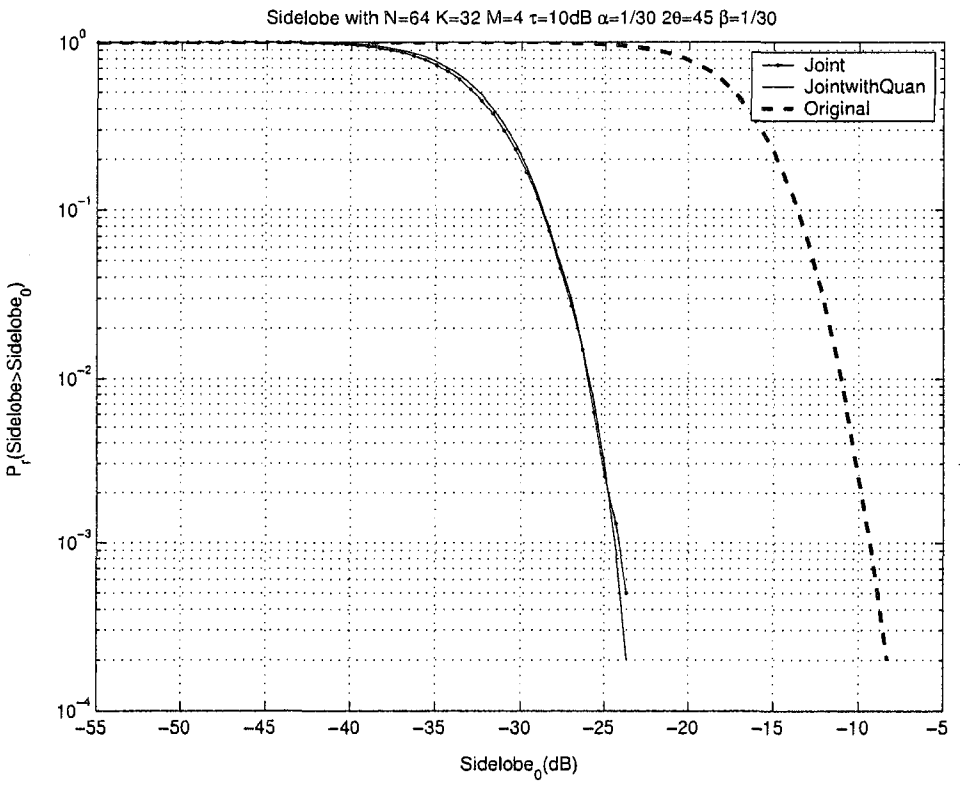

Figure 5.10: Phase rotation based OBP reduction for OFDM systems with 16QAM

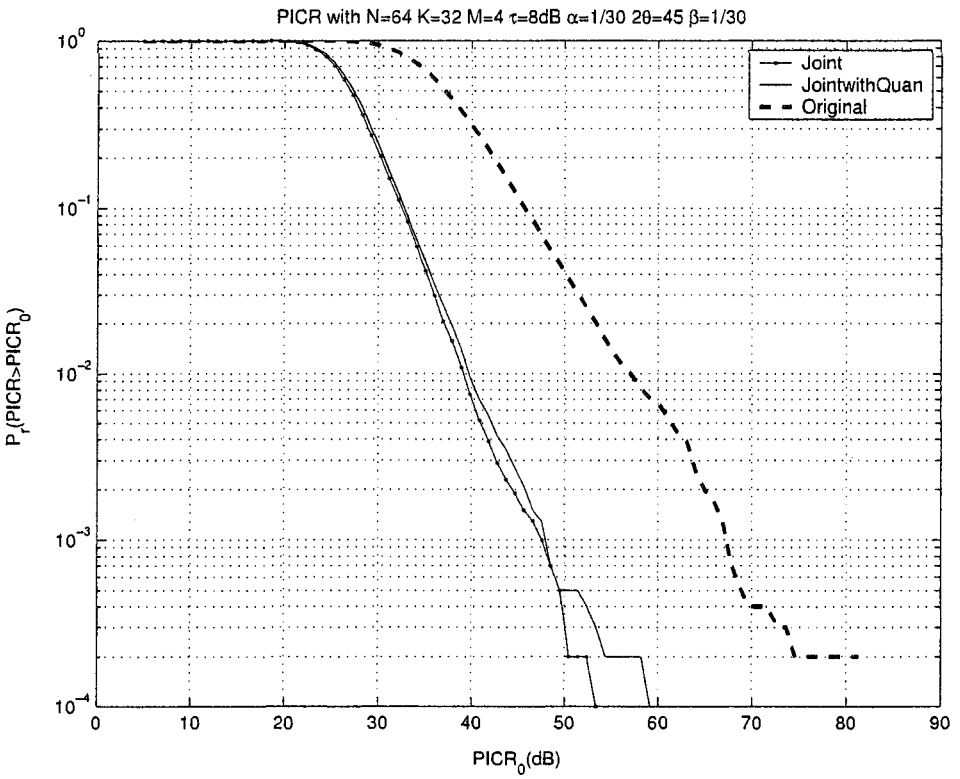

Figure 5.11: Phase rotation based PICR reduction for OFDM systems with 8PSK modulation

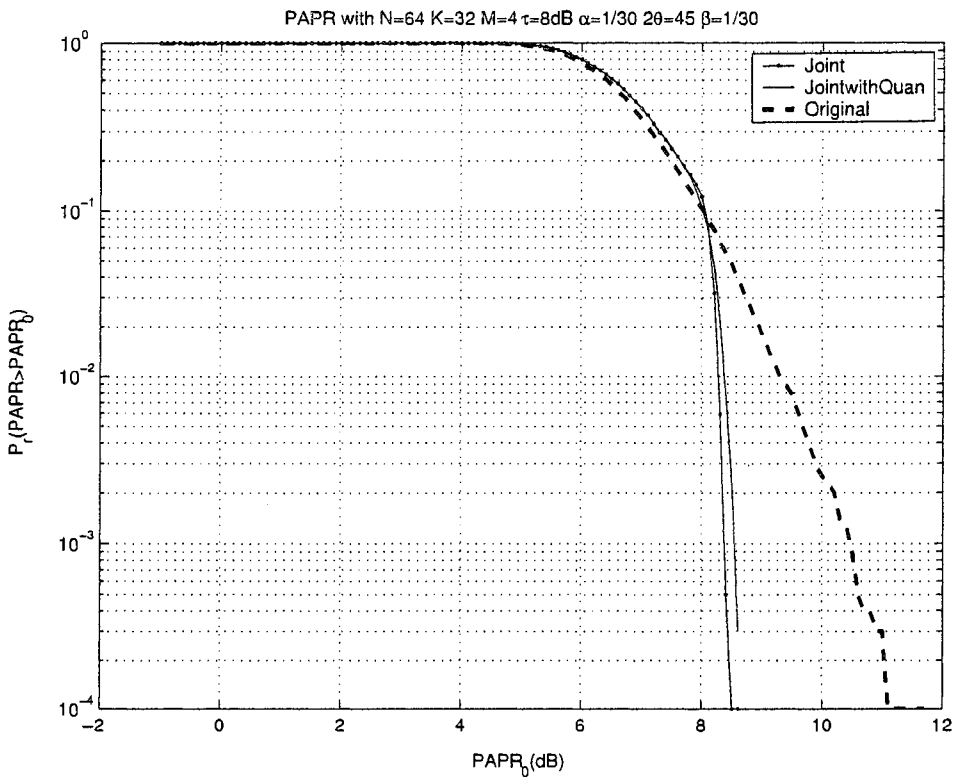

Figure 5.12: Phase rotation based PAPR reduction for OFDM systems with 8PSK modulation

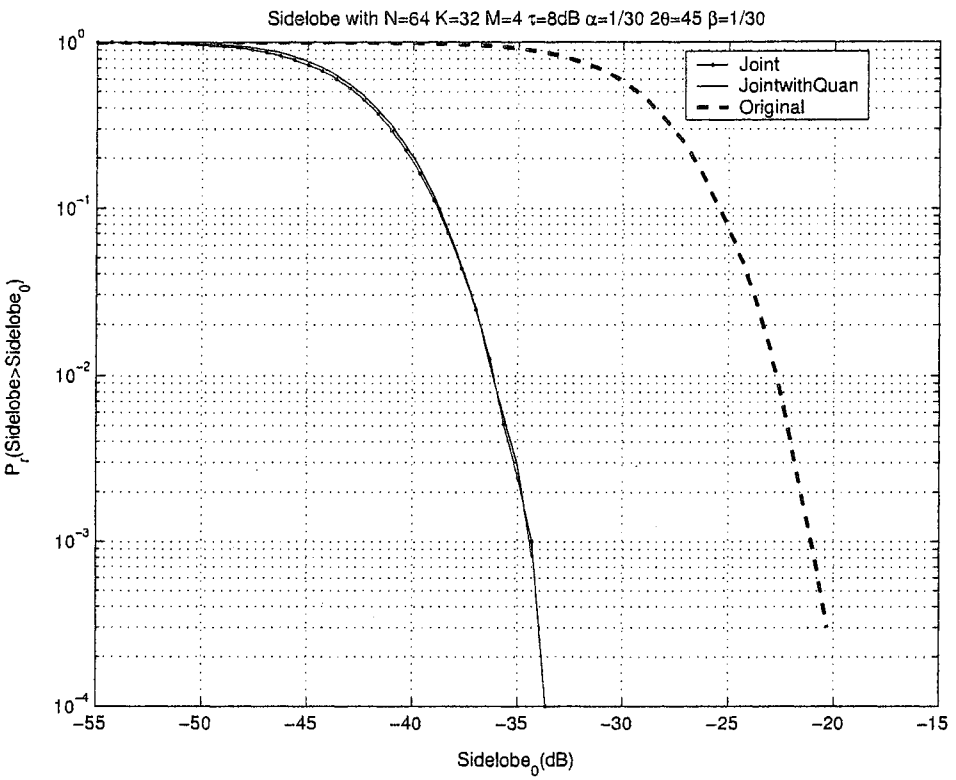

Figure 5.13: Phase rotation based OBP reduction for OFDM systems with 8PSK modulation

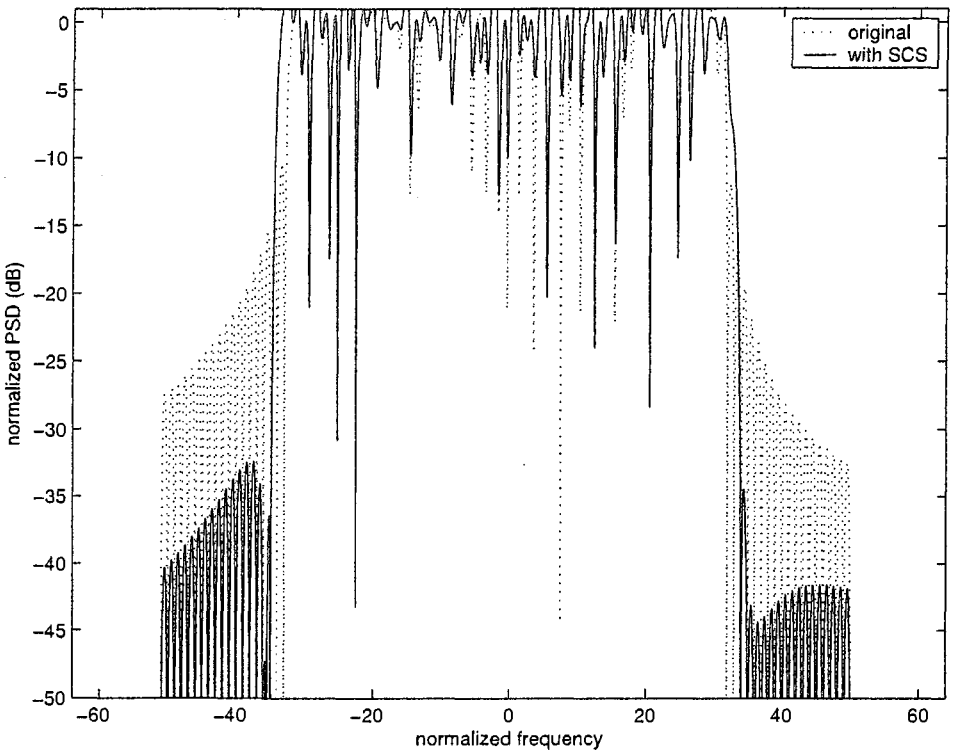

Figure 5.14: Power spectrum of the joint designed and the original OFDM symbols with 8PSK modulation (phase rotation approach)

5.4.2 Algorithm Based on Constellation Extension Approach

Using the constellation extension approach based algorithm, Figure 5.15 shows the CCDFs of PICR, PAPR, and OBP of OFDM symbols obtained by minimizing PICR, PAPR, and OBP alone respectively with 16QAM and $\beta = 1/4$. Similar to the case of the phase rotation approach, it is shown from Figure 5.15 that when one of the three problems is considered alone, the performance of the other two problems is quite bad.

As we have mentioned above, the value of α depends on how much power consumed by the sidelobe cancellation subcarriers and how many of the sidelobe cancellation subcarriers are used. When $\alpha = 1/10$ nd $\beta = 1/4$, figures 5.16, 5.17, and 5.18 show the CCDFs of PICR, PAPR, and OBP of OFDM symbols with 16QAM as a function of M. It is shown from these figures that the proposed constellation extension based joint design algorithm is efficient in reducing PAPR, PICR, and OBP of OFDM signals. In addition, as M increases, the performance of PICR, PAPR, and OBP reduction becomes better. Figures 5.19, 5.20, and 5.21 show the CCDFs of PICR, PAPR, and OBP of OFDM symbols with 8PSK modulation.

For the convenience of comparison, Table 5.2 lists the PICR, PAPR, and OBP threshold values which only one out of 1000 transmitted symbols can exceed for the constellation extension based jointly designed and the original transmitted symbols. From Table 5.2, for the 16QAM case with M=4, by using the proposed constellation extension approach based algorithm, at point 1/1000, PICR can be reduced by 9.0 dB, PAPR by 2.3 dB, and OBP by 10.7 dB. For the 8PSK modulation case with M=4, PICR can be reduced by 12.8 dB, PAPR by 2.3 dB, and OBP by 9.7 dB.

In Figure 5.22, for 16QAM modulation scheme, the circles show the constellation

Table 5.2: The threshold values by using constellation extension based algorithm with M=4

	1/1000 OFDM Symbols	Joint Design (dB)	Original (dB)	Reduction (dB)
16-QAM	PICR	60.5	69.5	9.0
	PAPR	7.9	10.2	2.3
	OBP	−20.1	−9.4	10.7
8-PSK	PICR	54.5	67.3	12.8
	PAPR	8.2	10.5	2.3
	OBP	−30.8	−21.1	9.7

of the optimal symbols and the stars show the constellation of original transmitted symbols.

5.5 Conclusion

Two approaches, the phase rotation approach and the constellation extension approach, are proposed for the joint design of PAPR, PICR, and OBP in OFDM wireless communication systems. We first model this joint design problem as a constraint optimization problem with continuous variables. This optimization problem is then converted into a SOCP problem, whose global optimal solution can be obtained efficiently. Simulation results are also presented to show that the proposed algorithms are effective in reducing PAPR, PICR, and OBP.

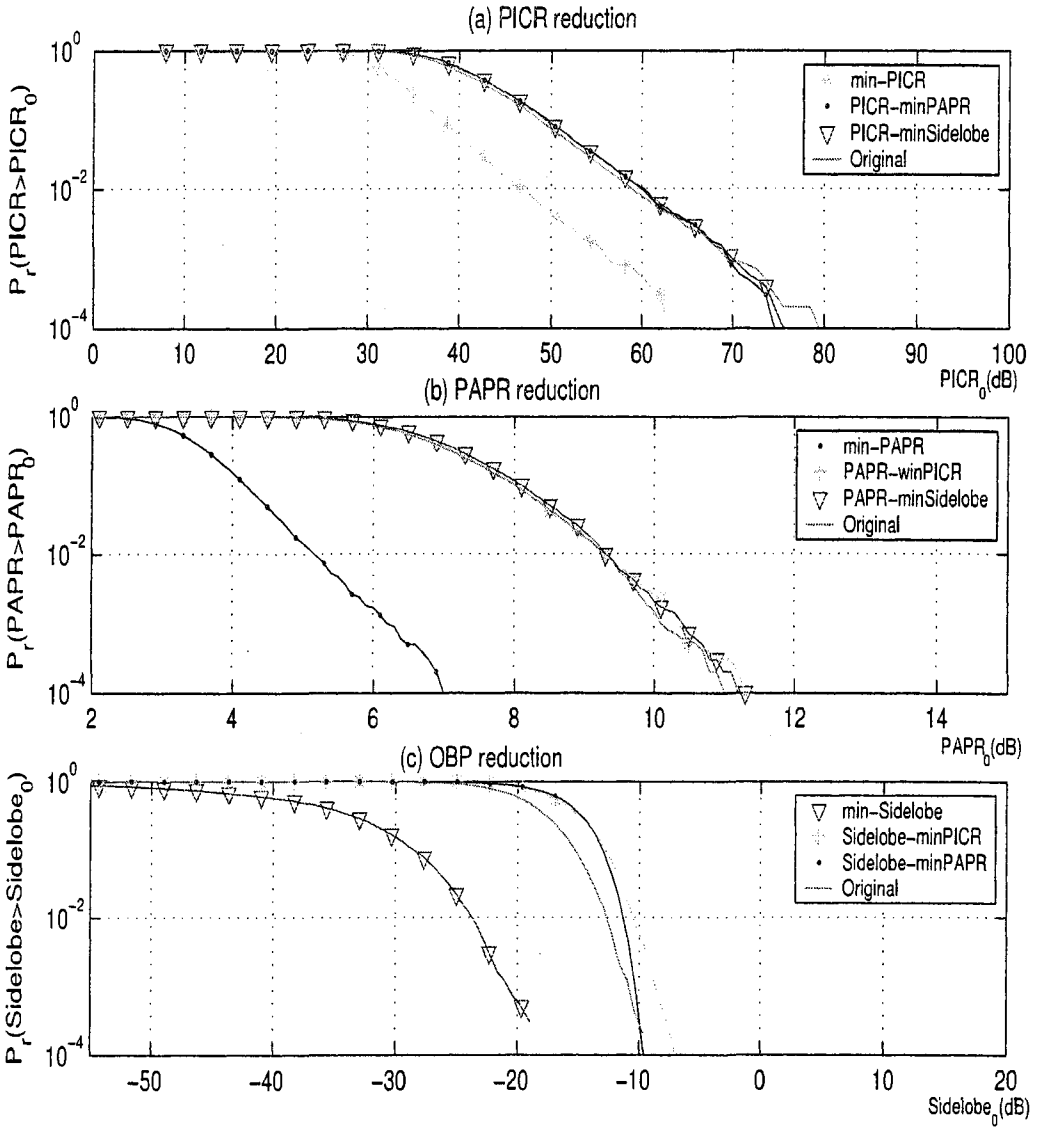

Figure 5.15: CCDFs for individual problems with 16QAM (constellation extension approach)

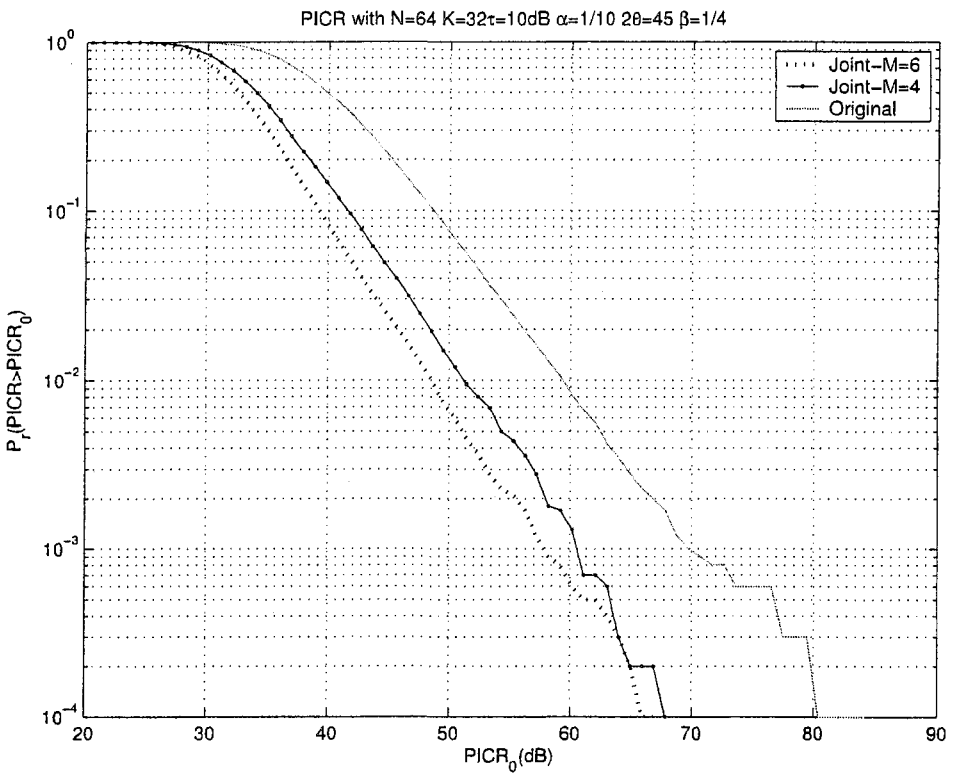

Figure 5.16: Constellation extension based PICR reduction for OFDM systems with 16QAM

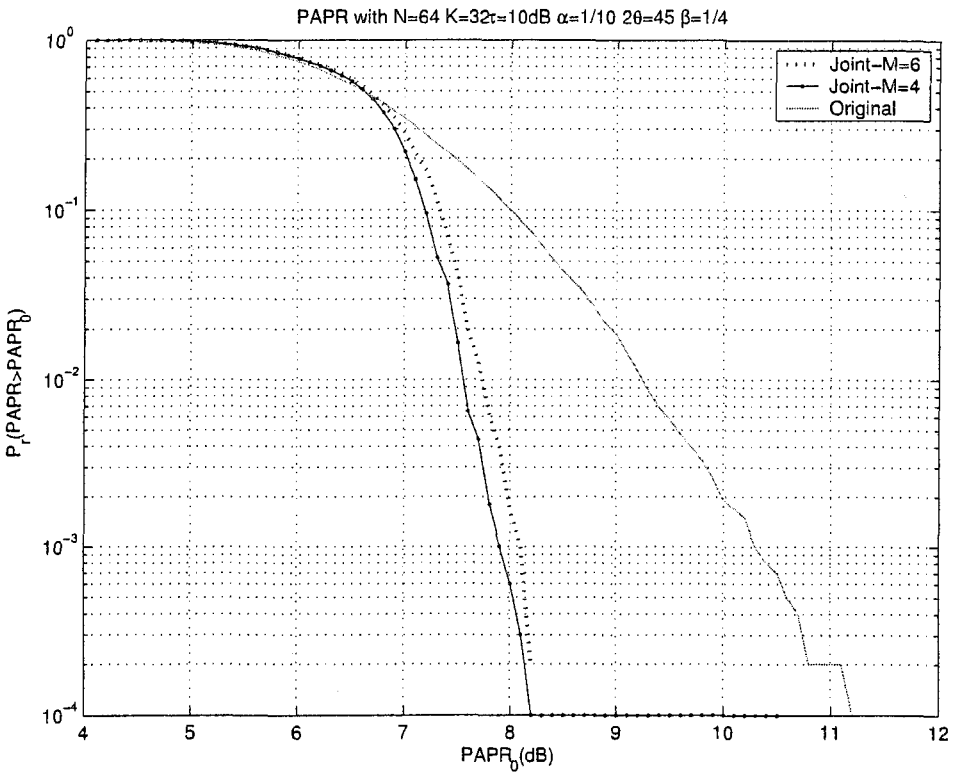

Figure 5.17: Constellation extension based PAPR reduction for OFDM systems with 16QAM

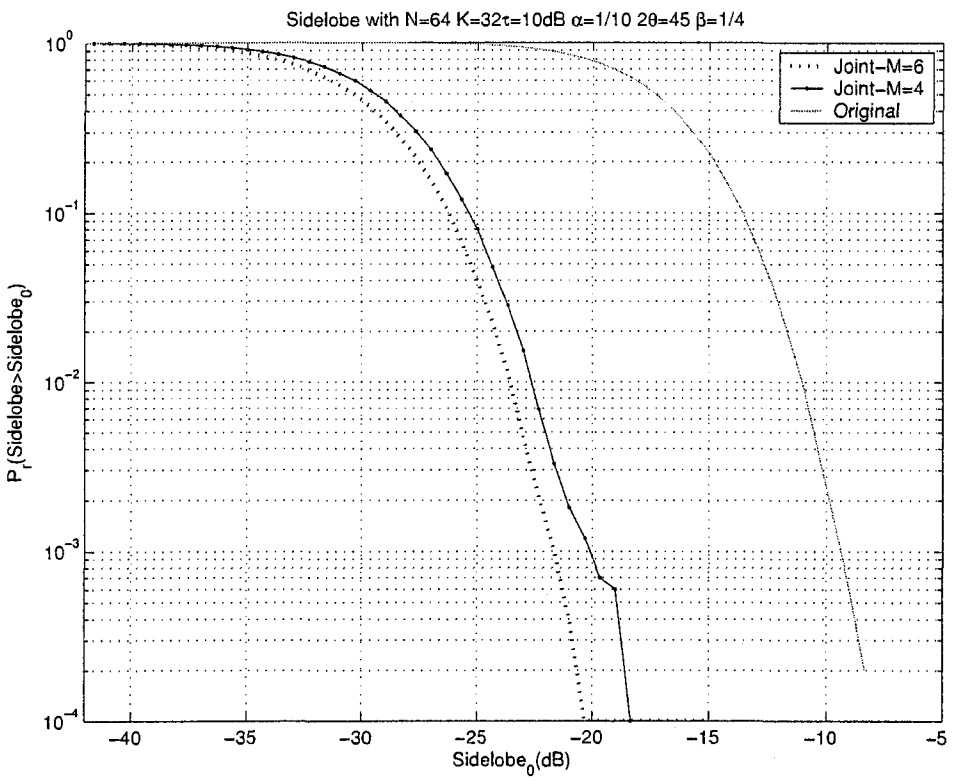

Figure 5.18: Constellation extension based OBP reduction for OFDM systems with 16QAM

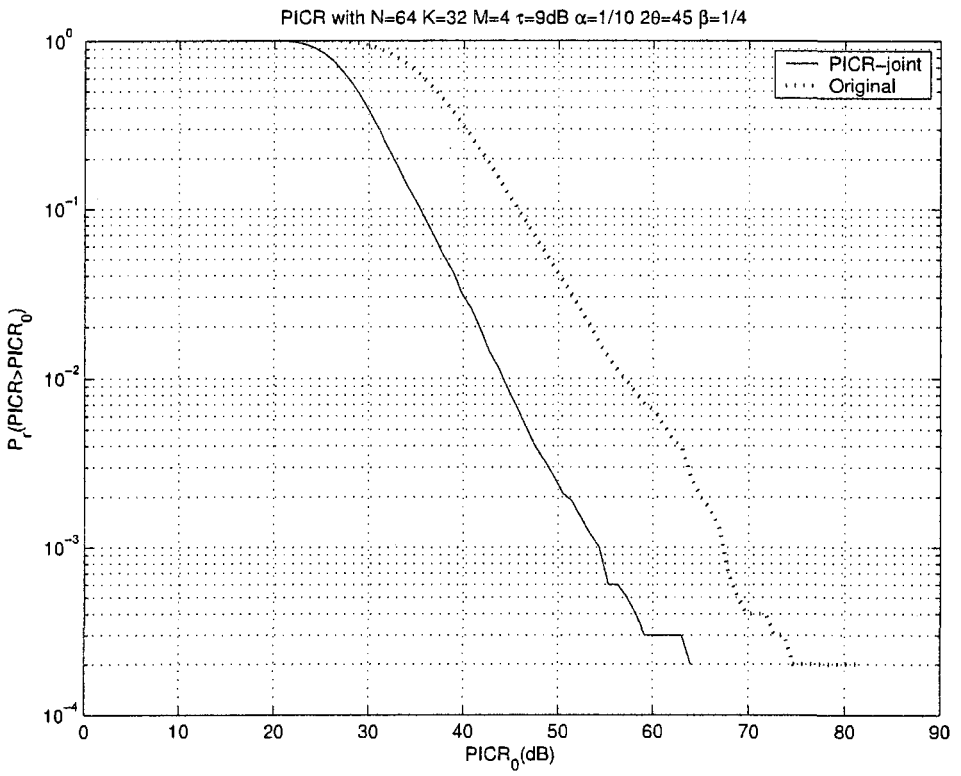

Figure 5.19: Constellation extension based PICR reduction for OFDM systems with 8PSK modulation

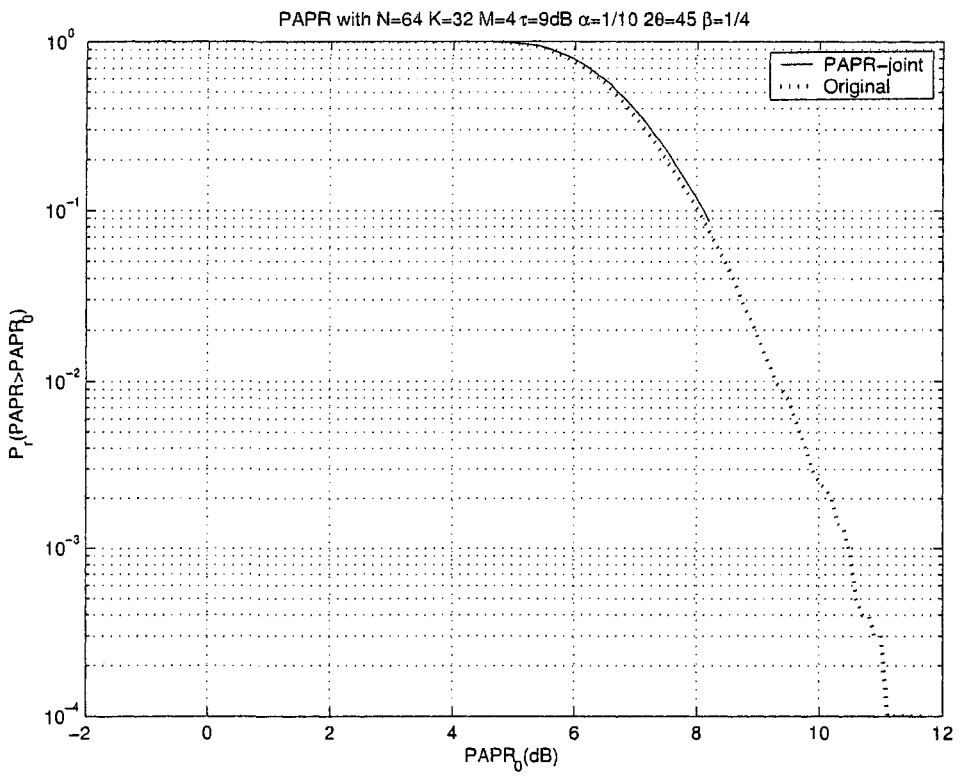

Figure 5.20: Constellation extension based PAPR reduction for OFDM systems with 8PSK modulation

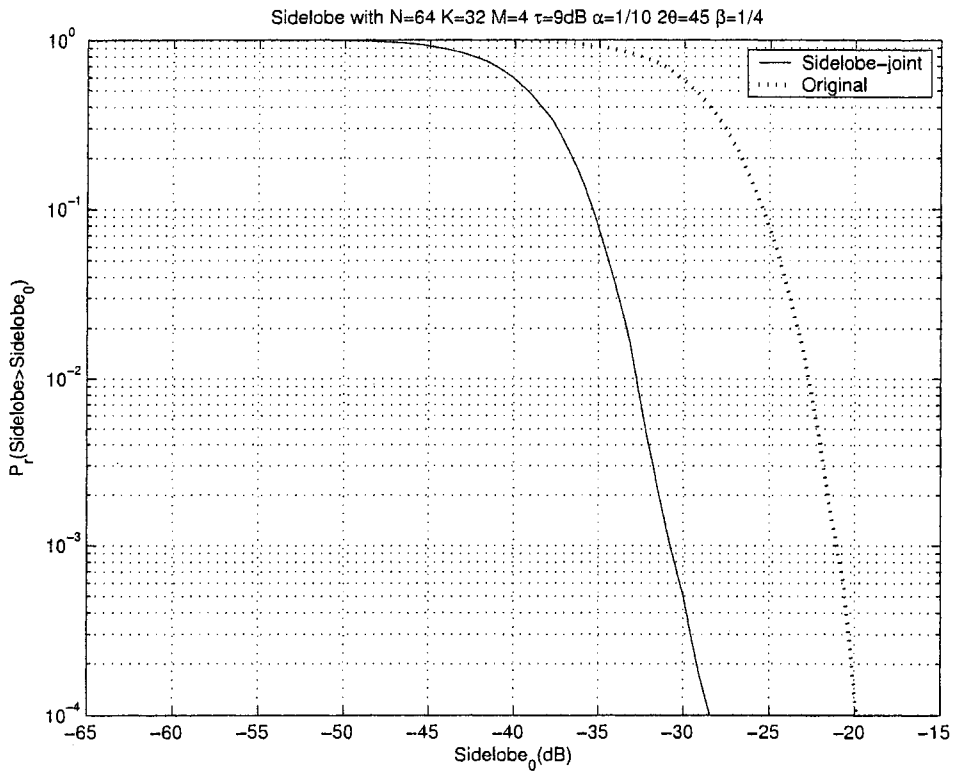

Figure 5.21: Constellation extension based OBP reduction for OFDM systems with 8PSK modulation

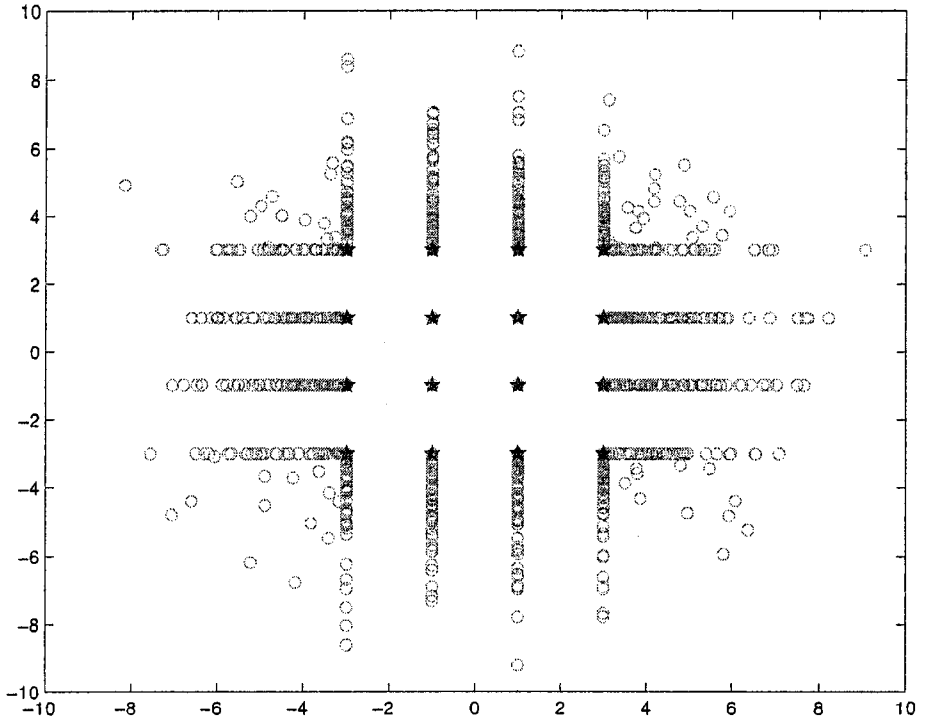

Figure 5.22: The constellations of optimal symbols

Chapter 6

Conclusions

The joint PAPR, PICR, and OBP reduction problems have been investigated for high-speed OFDM wireless communication systems in this thesis. We have first formulated a joint constrained and a joint weighted PAPR and PICR reduction problems. Algorithms with low computational complexity have also been developed to solve these joint PAPR and PICR design problems. Simulation results have shown that the proposed algorithms are effective in reducing PAPR and PICR.

In addition, we also study the joint PAPR, PICR, and OBP design problem, which has been defined as a constrained optimization problem with continuous variables based on the phase rotation approach and the constellation extension approach. The optimization problem have then been relaxed into an SOCP problem, whose global optimal solutions can be obtained efficiently. Simulation results show that the proposed schemes are effective in reducing PAPR, PICR, and OBP, and the jointly designed system has very good performance.

Chapter 7

Future Work

For joint PAPR, PICR, and OBP reduction design based on constellation extension approach, by linearizing the right side of the inequality (5.24) using Taylor expansion, the nonlinear optimization problem (5.23) is converted to SOCP optimization problem, which can be solved much efficiently than the original problem by the existing software. The designed system performs very well. However, this simplification has not been verified theoretically. This part is left for future research work.

References

[1] IEEE LAN/MAN Standards Committee, "Wireless LAN medium access control (MAC) and physical layer (PHY) specifications: high-speed physical layer in the 5 GHz band," *IEEE Standard 802.11a*, 1999.

[2] IEEE LAN/MAN Standards Committee, "IEEE standard for local and metropolitan area networks, part 16: air interface for fixed broadband wireless access systems," *IEEE Standard 802.16*, 2004.

[3] ETSI, "Radio Broadcasting Systems; Digital Audio Broadcasting (DAB) to mobile, portable and fixed receivers," *ETSI EN 300 401 V1.3.3 (2001-05)*, 2001.

[4] ETSI, "Digital Video Broadcasting (DVB): Framing structure, channel coding and modulation for digital terrestrial television," *ETSI EN 300 744 V1.5.1 (2004-11)*, 2004.

[5] Andrea Goldsmith, *Wireless Communications*, New York: Cambridge University Press, 2005.

[6] S. H. Han and J. H. Lee, "An overview of peak-to-average power ratio reduction techniques for multicarrier transmission," *IEEE Wireless Communications*, vol. 12, no. 2, pp. 56-65, Apr. 2005.

[7] A. E. Jones, T. Wilkinson, and S. Barton, "Block coding scheme for reduction of peak-to-mean envelope power ratio of multicarrier transmision schemes," *Electronics Letters*, vol. 30, no. 25, pp. 2098-2099, Dec. 1994.

[8] J. A. Davis and J. Jedwab, "Peak-to-mean power control and error correction for OFDM transmission using Golay sequences and Reed-Muller codes," *Electronics Letters*, vol. 33, no. 4, pp. 267-268, Feb. 1997.

[9] C. Robing and V. K. Tarokh, "A construction of OFDM 16-QAM sequences having low peak powers," *IEEE Trans. Information Theory*, vol. 47, no. 5, pp. 2091-2094, July 2001.

[10] M. Breiling, S. H. Müller-Weinfurtner, and J. B. Huber, "SLM peak-power reduction without explicit side information," *IEEE Commun. Letters*, vol. 5, no. 6, pp. 239-241, June 2001.

[11] P. Van Eetvelt, G. Wade and M. Tomlinson, "Peak to average power reduction for OFDM schemes by selective scrambling," *IEEE Electronics Letters*, vol. 32, no. 21, pp. 1963-1964, Oct. 1996.

[12] R. W. Bauml, R. F. H. Fischer, and J. B. Huber, "Reducing the peak-to-average power ratio of multicarrier modulation by selected mapping," *Electronics Letters*, vol. 32, no. 22, pp. 2056-2057, Oct. 1996.

[13] A. D. S. Jayalath and C. Tellambura, "SLM and PTS peak-power reduction of OFDM signals without side information," *IEEE Trans. Wireless Communications*, vol. 4, no. 5, pp. 2006-2013, Sept. 2005.

[14] K. Sathananthan and C. Tellambura, "Partial transmit sequence and selected

mapping schemes to reduce ICI in OFDM systems," *IEEE Communication Letters*, vol. 6, no. 8, pp. 313-315, Aug. 2002.

[15] S. H. Müller and J. B. Huber, "OFDM with reduced peak-to-average power ratio by optimum combination of partial transmit sequences," *Electronics Letters*, vol. 33, no. 5, pp. 368-369, Feb. 1997.

[16] C. Tellambura, "Improved phase factor computation for the PAR reduction of an OFDM signal using PTS," *IEEE Communication Letters*, vol. 5, no. 4, pp. 135-137, Apr. 2001.

[17] A. Alavi, C. Tellambura, and I. Fair, "PAPR reduction of OFDM signals using partial transmitted sequences: an optimal approach using sphere decoding," *IEEE Communication Letters*, vol. 9, no. 11, pp. 982-984, Nov. 2005.

[18] J, Tellado, *Peak to Average Power Reduction for Multicarrier Modulation*, Ph. D. dissertation, Standford University, 2000.

[19] Serdar Sezginer, Hikmet Sari, "OFDM peak power reduction with simple amplitude predistortion," *IEEE Communication Letters*, vol. 10, no. 2, pp. 65-67, Feb. 2006.

[20] Y. H. Zhang, W.-S. Lu, and T. A. Gulliver, "A successive intercarrier interference reduction algorithm for OFDM systems," *Proc. IEEE ICC*, pp. 2936-2941, 2007.

[21] Foomooljareon, P. and Fernando, W.A.C., "Input sequence envelop scaling in PAPR reduction of OFDM", *IEEE 5th international symposium on wireless personal multimedia communicatins*, Vol. 1, Oct 2002.

[22] Y. Kou, W.-S. Lu, and A. Antouniou, "New peak to average power ratio rreduction algorithms for multicarrier communications," *IEEE Transactions on Circuits and Systems-I: Regular Papers*, vol. 51, no. 9, pp. 1790-1800, Sep. 2004.

[23] B. S. Krongold and D. L. Jones, "PAR reduction in OFDM via active constellation extension," *IEEE Trans. Broadcasting*, vol. 49, no. 3, pp. 258-268, Sep. 2003.

[24] Sinja Brandes, Ivan Cosovic, and Michael Schnell, "Reduction of out-of -band radiation in OFDM systems by Insertion of cancellation carriers," *IEEE Communication Letters*, vol.10, no. 6, pp.420-422, June 2006.

[25] Martin Senst, Markus Jordan, Meik Dorpinghaus, Mechael Farber, Gerd Ascheid, and Heinrich Meyr, "Joint reduction of peak-to-average power ratio and out-of-band power in OFDM systems," *IEEE GLOBECOM 2007 Proceedings*, vol.5, no.4, pp.135-137, April 2001.

[26] K. Sathananthan and C. Tellambura, "Coding to reduce both PAR and PICR of an OFDM signal," *IEEE Communication Letters*, vol. 6, no. 8, pp. 316-318, Aug. 2002.

[27] Kewei Yuan and Zhiwei Mao,"Joint PAPR and PICR Design in OFDM Systems," accepted by the 68th IEEE Vehicular Technology Conference, September 2008, Calgary, Canada.

[28] T. S. Rappaport, *Wireless Communications: Principles & Practice*, Upper Saddle River, NJ: Prentice Hall, 1996.

[29] J. Armstrong, "Analysis of new and existing methods of reducing intercarrier interference due to carrier frequency offset in OFDM," *IEEE Trans. Commun.*, vol. 47, no. 3, pp. 365-369, Mar. 1999.

[30] Y. Zhao and S. Häggman, "BER analysis of OFDM communication systems with intercarrier interference," *Proc. International Conference on Communication Technology*, vol. 2, Oct. 1998.

[31] P. B. Kenington, *High-Linearity RF Amplifier Design*, Norwood, MA: Artech House, 2000.

[32] A. Antoniou and W.-S. Lu, *Optimization: Methods, Algorithms, and Applications*, Norwell, MA: Kluwer, 2004.

[33] J. F. Sturm, "Using SeDumi 1.02, a MATLAB toolbox for optimization over symmetric cones," *Optimization Method Software*, vol. 11-12, pp. 625-653, Aug. 1999.

[34] K. Panta and J. Armstrong, "Spectral analysis of OFDM signals and its improvement by polynomial cancellation Coding," *IEEE Trans. Consumer Electronics*, vol. 49, no. 5, pp. 625-653, Nov. 2003.

Appendix A

Basic Concepts and Properties of DFT and IDFT

The multicarrier modulation has been widely used since the development of simple and cheap implementations of DFT and IDFT. In this section, we briefly review the basic concepts and properties of DFT and IDFT which are used in the OFDM signal model.

Let $\{x_n,\ 0 \leq n \leq N-1\}$, denote a discrete time sequence. The N-point DFT of $\{x_n\}$ is defined as

$$X_i \triangleq \frac{1}{\sqrt{N}} \sum_{n=0}^{N-1} x_n e^{-j2\pi ni/N} \qquad 0 \leq i \leq N-1. \tag{A.1}$$

Let $W_N = e^{-j2\pi/N}$, then

$$X_i = \frac{1}{\sqrt{N}} \sum_{n=0}^{N-1} x_n W_N^{ni} \qquad 0 \leq i \leq N-1 \tag{A.2}$$

where

$$\sum_{n=0}^{N-1} W_N^{ni} = \begin{cases} \frac{1-\left(W_N^i\right)^N}{1-W_N^i} = \frac{1-\left(e^{-j2\pi i/N}\right)^N}{1-W_N^i} = 0 & \text{for } i = 1, \cdots, N-1 \\ \sum_{n=0}^{N-1} W_N^0 = N & \text{for } i = 0 \end{cases}. \tag{A.3}$$

The sequence $\{x_n\}$ can be recovered from $\{X_i\}$ by using IDFT:

$$x_n \triangleq \frac{1}{\sqrt{N}} \sum_{i=0}^{N-1} X_i e^{j2\pi ni/N} \quad 0 \le n \le N-1 \tag{A.4}$$

$$\text{or } x_n = \frac{1}{\sqrt{N}} \sum_{i=0}^{N-1} X_i W^{-ni} \quad 0 \le n \le N-1. \tag{A.5}$$

The IDFT operation on $\{X_i\}$ can be represented by the matrix multiplication

$$\mathbf{x} = \mathbf{F}\mathbf{X} \tag{A.6}$$

where $\mathbf{X} = [X_0\ X_1\ \cdots\ X_{N-1}]^T$, $\mathbf{x} = [x_0\ x_1\ \cdots\ x_{N-1}]^T$, and $\mathbf{F}$ is $N \times N$ matrix which is given by

$$\mathbf{F} = \frac{1}{\sqrt{N}} \begin{bmatrix} 1 & 1 & 1 & \cdots & 1 \\ 1 & W_N^{-1} & W_N^{-2} & \cdots & W_N^{-(N-1)} \\ 1 & W_N^{-2} & W_N^{-4} & \cdots & W_N^{-2(N-1)} \\ \vdots & \vdots & \vdots & \ddots & \vdots \\ 1 & W_N^{-(N-1)} & W_N^{-2(N-1)} & \cdots & W_N^{-(N-1)^2} \end{bmatrix} \tag{A.7}$$

with element $F(n,i) = \frac{1}{\sqrt{N}} W_N^{-ni}$,for $0 \le i,\ n \le N-1$.

From $(A.3)$, $\mathbf{F}$ is orthogonal matrix with $\mathbf{F}\mathbf{F}^H = \mathbf{I}$ because the (n,i)th element of $\mathbf{F}\mathbf{F}^{\mathbf{H}}$ is given by

$$\frac{1}{N} \sum_{j=0}^{N-1} W_N^{-nj} W_N^{ji} = \frac{1}{N} \sum_{j=0}^{N-1} W_N^{(i-n)j} = \begin{cases} 0, & n \ne i \\ 1, & n = i \end{cases} \quad 0 \le i, n \le N-1.$$

The DFT operation on $\{x_n\}$ can be represented by the matrix multiplication

$$\mathbf{X} = \mathbf{F}^{-1}\mathbf{x} = \mathbf{F}^H\mathbf{x}. \tag{A.8}$$

The DFT and its inverse IDFT are typically performed via hardware using FFT and IFFT.

Appendix B

Some Derivations for OFDM

B.1 Cyclic Prefix in OFDM Signals

When an input data stream $\{x_n,\ 0 \le n \le N-1\}$ is sent through a linear time-invariant discrete-time channel $\{h_n,\ 0 \le n \le \mu\}$, the output $\{z_n,\ 0 \le n \le N-1+\mu\}$ is the discrete-time convolution of the input stream and the channel impulse response, which is given as

$$z_n = x_n * h_n = \sum_{k=0}^{\mu} x_{n-k} h_k. \tag{B.1}$$

The N-point circular convolution of $\{x_n,\ 0 \le n \le N-1\}$ and $\{h_n,\ 0 \le n \le \mu\}$ is defined as

$$z_n = x_n \circledast h_n = \sum_{k=0}^{\mu} x_{n-k}^{N} h_k \tag{B.2}$$

where $(\cdot)_{n-k}^{N}$ denotes $n-k$ modulus N. In other words, x_{n-k}^{N} is a periodic version of x_{n-k} with period N. Since

$$z_{n+N} = \sum_{k=0}^{\mu} x_{n+N-k}^{N} h_k = \sum_{k=0}^{\mu} x_{n-k}^{N} h_k = x_n \circledast h_n = z_n,$$

z_n given by (B.2) is also periodic with period N.

The circular convolution in time domain leads to multiplication in frequency domain. That is,

$$Z_i = X_i H_i \quad 0 \le i \le N-1 \tag{B.3}$$

where Z_i is the N-point DFT of $\{z_n,\ 0 \le n \le N-1\}$ and H_i is the N-point DFT of $\{h_n,\ 0 \le n \le \mu\}$. From $(B.3)$, if the channel and the input are circularly convoluted, as long as $\{h_n,\ 0 \le n \le \mu\}$ is known at the receiver, the original data sequence $\{x_n,\ 0 \le n \le N-1\}$ can be recovered by using IDFT on $\{Z_i/H_i,\ 0 \le i \le N-1\}$.

Unfortunately, the channel output is not a circular convolution but a linear convolution. However, the linear convolution between the input sequence of the channel and the channel impulse response can be converted into a circular convolution by adding a cyclic prefix to the input so that we get a modified input sequence as

$$\{\widetilde{x}_n,\ -\mu \le n \le N-1\} = x_{N-\mu}, \ldots, x_{N-1}, x_0, \ldots, x_{N-\mu-1}, x_{N-\mu}, \ldots, x_{N-1}$$

where $\{x_0, \ldots, x_{N-\mu-1}, x_{N-\mu} \ldots, x_{N-1}\}$ is the input sequence of length N.

Suppose that the modified input sequence passes through a discrete time channel with impulse response $\{h_n,\ 0 \le n \le \mu\}$. The channel output $\{z_n,\ 0 \le n \le N-1\}$ is then given by

$$\begin{aligned} z_n &= \widetilde{x}_n * h_n = \sum_{k=0}^{\mu} \widetilde{x}_{n-k} h_k \qquad \text{(B.4)} \\ &= \sum_{k=0}^{\mu} x_{n-k}^{N} h_k = x_n \circledast h_n. \end{aligned}$$

Note that since the discrete time channel impulse response has a length of $\mu+1$, the first μ samples of $\{z_n,\ n = -\mu \le n \le N-1+\mu\}$ in a given block are corrupted by ISI associated with the last μ samples of $\{\tilde{x}_n,\ -\mu \le n \le N-1\}$ in the previous block. On the other hand, since a cyclic prefix of length μ is appended at the front of the input sequence, the first μ samples of the channel output affected by the ISI can be discarded without any loss of the original information. Therefore, the cyclic prefix also serves to eliminate ISI between the data blocks.

From the above discussions, it is seen that the benefits brought by a cyclic prefix come at a cost. Since μ symbols are added to the input sequence, this is an overhead to the system and results in lower efficiency of data transmission and transmission power utilization.

B.2 The Minimum Frequency Separation of Subcarriers in OFDM Signals

Assume that each subcarrier of the OFDM signal is modulated by QAM scheme. Denote f_c as the carrier frequency, Δf as the frequency separation between adjacent subcarriers, T_s as the OFDM symbol duration, E as the energy of each symbol. Then the N signals that differ in frequency of $n\Delta f$ can be represented as

$$s_n(t) = \sqrt{\frac{2E}{T_s}} r_n \cos\left(2\pi\left(f_c + n\Delta f\right)t + \theta_n\right) \qquad n = 0, \cdots, N-1$$

where $r_n = \sqrt{A_{nr}^2 + A_{ni}^2}$, $\theta_n = \arctan\left(A_{ni}/A_{nr}\right)$, with A_{nr} and A_{ni} being the amplitudes of the quadrature carriers of the information-bearing signal on the nth subcarrier.

The inner product of any two signals $s_m(t)$ and $s_n(t)$ (for $m \neq n$) over a symbol duration T_s is given by

$$\begin{aligned}
&\langle s_m(t), s_n(t)\rangle \\
&= \int_0^{T_s} \frac{2Er_m r_n}{T_s} \cos\left(2\pi\left(f_c + m\Delta f\right)t + \theta_m\right) \cos\left(2\pi\left(f_c + n\Delta f\right)t + \theta_n\right) dt \\
&= \frac{Er_m r_n}{T_s} \int_0^{T_s} [\cos\left(4\pi f_c t + 2\pi(m+n)\Delta f t + \theta_m + \theta_n\right) + \\
&\qquad \cos\left(2\pi\left(m-n\right)\Delta f t + \theta_m - \theta_n\right)] dt \\
&= \frac{Er_m r_n}{T_s} \int_0^{T_s} \cos\left(2\pi\left(m-n\right)\Delta f t + \theta_m - \theta_n\right) dt \\
&= \frac{Er_m r_n}{2\pi T_s\left(m-n\right)\Delta f} \left[\sin\left(2\pi\left(m-n\right)\Delta f T_s + \theta_m - \theta_n\right) - \sin\left(\theta_m - \theta_n\right)\right].
\end{aligned}$$

If and only if $\langle s_m(t), s_n(t)\rangle = 0$, which means $2\pi\,|m-n|\,\Delta f T_s = 2\pi k$ for any positive integer k, the signals $s_m(t)$ and $s_n(t)$ are orthogonal to each other.

Noticed that $|m-n| = 1$ corresponds to adjacent subcarriers. Therefore, as $k = 1$, $\Delta f = 1/T_s$ represents the minimum frequency separation for two subcarriers to remain orthogonal over a symbol duration.

B.3 Matrix Representation of OFDM Received Signal

The complex baseband OFDM signal can be represented as

$$x(t) = \frac{1}{\sqrt{N}} \sum_{k=0}^{N-1} X_k e^{j2\pi k\Delta f t} \quad 0 \le t \le T_s \tag{B.5}$$

where X_k is the information symbol on the kth subcarrier. As shown in Appendix B.2, the frequency separation Δf between any two adjacent subcarriers is equal to $1/T_s$ with T_s being the OFDM symbol duration.

By adding the cyclic prefix sequence, the transmitted sequence is given by

$$\{\widetilde{x}_n,\ -\mu \le n \le N-1\} = \{x_{N-\mu},\ \cdots,\ x_{N-1},\ x_0,\ \cdots,\ x_{N-\mu-1},\ x_{N-\mu},\ \cdots,\ x_{N-1}\}$$

where $\{x_n = x(t = n/NT_s),\ 0 \leqslant n \leqslant N-1\}$ is the discrete sample sequence of $x(t)$ in (B.5), which is the desired received sequence of length N.

In this thesis, a doubly frequency selective fading channel model is adopted [28]. Thus a wide-sense stationary uncorrelated scattering (WSSUS) channel is considered, whose impulse response is give by

$$h(t;\tau) = \sum_{d=0}^{\mu} h(t;\tau_d)\delta(\tau - \tau_d)$$

where τ_d is the delay of the dth path with $\tau_0 < \tau_1 < \cdots < \tau_\mu$ and $\delta(\cdot)$ represents an impulse function. A discrete version of the channel can be expressed as a tapped

delay line (TDL) filter with random taps

$$h(n,l) = h(nT_c; lT_c) \tag{B.6}$$

where $h(n,l)$ denotes the channel coefficient for the lth tap at the nth sampling instant and the delay between two taps is T_c, with $T_c = T_s/N$ being the duration of each sample.

At receiver end, the received signal is corrupted by noise and affected by the channel. After being downconverted to baseband and filtered to remove high frequency components, from (B.4), the received signals before employing DFT in continuous and discrete versions are given by

$$\begin{aligned} z(t) &= e^{j2\pi\Delta f' t}\widetilde{x}(t) * h(t;\tau) + v(t) \\ z_n &= z(t = n/NT_s) = e^{j2\pi\varepsilon n/N}\sum_{k=0}^{\mu}\widetilde{x}_{n-k}h(n,k) + v_n \quad 0 \leqslant n \leqslant N-1 \end{aligned} \tag{B.7}$$

respectively, where $v(t)$ and v_n are the continuous and discrete version AWGN noise, $\Delta f'$ being the frequency offset of the local carrier frequency at the receiver above the correct carrier frequency [29], ε is the normalized frequency offset which is defined as

$$\varepsilon = \Delta f' \cdot T_s. \tag{B.8}$$

For $n = 0, \ldots, N-1$, we have

$$
\begin{aligned}
z_0 &= e^{j2\pi\varepsilon 0/N} \sum_{k=0}^{\mu} \widetilde{x}_{-k} h(0,k) + v_0 = x_0 h(0,0) + \sum_{k=1}^{\mu} \widetilde{x}_{-k} h(0,k) + v_0 \\
&= x_0 h(0,0) + \sum_{k=1}^{\mu} x_{N-k} h(0,k) + v_0 \\
&= x_0 h(0,0) + x_{N-1} h(0,1) + \cdots + x_{N-\mu+1} h(0,\mu-1) + x_{N-\mu} h(0,\mu) + v_0 \\
z_1 &= e^{j2\pi\varepsilon/N} \sum_{k=0}^{\mu} \widetilde{x}_{1-k} h(1,k) + v_1 \\
&= e^{j2\pi\varepsilon/N} \left(\sum_{k=0}^{1} x_{1-k} h(1,k) + \sum_{k=2}^{\mu} x_{N+1-k} h(1,k) \right) + v_1 \\
&= e^{j2\pi\varepsilon/N} \left(x_1 h(1,0) + x_0 h(1,1) + x_{N-1} h(1,2) + \cdots + x_{N-\mu+1} h(1,\mu) \right) + v_1 \\
&\vdots \\
z_\mu &= e^{j2\pi\varepsilon\mu/N} \sum_{k=0}^{\mu} \widetilde{x}_{\mu-k} h(\mu,k) + v_\mu \\
&= e^{j2\pi\varepsilon\mu/N} \sum_{k=0}^{\mu} x_{\mu-k} h(\mu,k) + v_\mu \\
&= e^{j2\pi\varepsilon\mu/N} (x_\mu h(\mu,0) + x_{\mu-1} h(\mu,1) + \cdots + x_0 h(\mu,\mu)) + v_\mu \\
z_{\mu+1} &= e^{j2\pi\varepsilon\mu+1/N} \sum_{k=0}^{\mu} \widetilde{x}_{\mu+1-k} h(\mu+1,k) + v_{\mu+1} \\
&= e^{j2\pi\varepsilon\mu+1/N} \sum_{k=0}^{\mu} x_{\mu+1-k} h(\mu+1,k) + v_{\mu+1} \\
&= e^{j2\pi\varepsilon\mu+1/N} (x_{\mu+1} h(\mu+1,0) + x_\mu h(\mu+1,1) + \cdots + x_1 h(\mu+1,\mu)) + v_{\mu+1} \\
&\vdots
\end{aligned}
$$

$$
\begin{aligned}
z_{N-1} &= e^{j2\pi\varepsilon(N-1)/N} \sum_{k=0}^{\mu} \widetilde{x}_{N-1-k} h(N-1,k) + v_{N-1} \\
&= e^{j2\pi\varepsilon(N-1)/N} \sum_{k=0}^{\mu} x_{N-1-k} h(N-1,k) + v_{N-1} \\
&= e^{j2\pi\varepsilon(N-1)/N} (x_{N-1} h(N-1,0) + \cdots + x_{N-1-\mu} h(N-1,\mu)) + v_{N-1}.
\end{aligned}
$$

Thus the matrix form (B.7) is expressed as

$$\mathbf{z} = \mathbf{D}_\varepsilon \mathbf{H}\mathbf{x} + \mathbf{n} \tag{B.9}$$

where $\mathbf{z} = [z_0 \ z_1 \ \cdots \ z_{N-1}]^T$ denotes the time-domain received signal, $\mathbf{n} = [v_0 \ v_1 \ \cdots \ v_{N-1}]^T$ denotes the AWGN noise with zero mean and covariance matrix $2\sigma^2\mathbf{I}$, $\mathbf{D}_\varepsilon = \text{diag}\{1, \ e^{j2\pi\varepsilon/N}, \ \ldots, \ e^{j2\pi\varepsilon(N-1)/N}\}$, and $\mathbf{H}$ is given by

$$\begin{bmatrix} h(0,0) & 0 & 0 & \cdots & 0 & h(0,\mu) & h(0,\mu-1) & \cdots & h(0,1) \\ h(1,1) & h(1,0) & 0 & \cdots & 0 & 0 & h(1,\mu) & \cdots & h(1,2) \\ \vdots & \vdots & \ddots & \ddots & \ddots & \ddots & \ddots & \ddots & \vdots \\ h(\mu,\mu) & h(\mu,\mu-1) & \cdots & \cdots & h(\mu,0) & 0 & 0 & \cdots & 0 \\ 0 & h(\mu+1,\mu) & \cdots & \cdots & h(\mu+1,1) & h(\mu+1,0) & 0 & \cdots & 0 \\ \vdots & \vdots & \ddots & \ddots & \ddots & \ddots & \ddots & \ddots & \vdots \\ 0 & 0 & 0 & \cdots & h(N-1,\mu) & h(N-1,\mu-1) & \cdots & \cdots & h(N-1,0) \end{bmatrix}. \tag{B.10}$$

Appendix C

Second Order Cone Programming

Second Order Cone Programming (SOCP) problem is a kind of nonlinear convex problems. Linear programming (LP) problem, convex quadratic programming (QP) problem, and quadratically constrained convex quadratic programming problems can all be formulated as SOCP problems. Many engineering problems can be formulated as SOCP problems [32]. The second order cone of dimension k is defined as

$$\mathfrak{C}_k = \left\{ \begin{bmatrix} z \\ \mathbf{y} \end{bmatrix} : z \in \mathbb{R}, \mathbf{y} \in \mathbb{R}^{k-1}, \|\mathbf{y}\|_2 \leq z \right\} \tag{C.1}$$

which is also called quadratic or Lorentz cone. For $k = 1$, the second order cone is reduced to

$$\mathfrak{C}_1 = \{z : z \in \mathbb{R}, z \geq 0\}$$

Figure C.1 shows the second order cones for $k = 1,\ 2$, and 3.

The second order cone $\mathfrak{C}_k$ is a convex set in $\mathbb{R}^k$, because for any $\left[z_1\ \mathbf{y}_1^T\right]^T$, $\left[z_2\ \mathbf{y}_2^T\right]^T$ in $\mathfrak{C}_k$ and $\lambda \in [0, 1]$, we have

$$\lambda \begin{bmatrix} z_1 \\ \mathbf{y}_1 \end{bmatrix} + (1-\lambda) \begin{bmatrix} z_2 \\ \mathbf{y}_2 \end{bmatrix} = \begin{bmatrix} \lambda z_1 + (1-\lambda)\, z_2 \\ \lambda \mathbf{y}_1 + (1-\lambda)\, \mathbf{y}_2 \end{bmatrix}$$

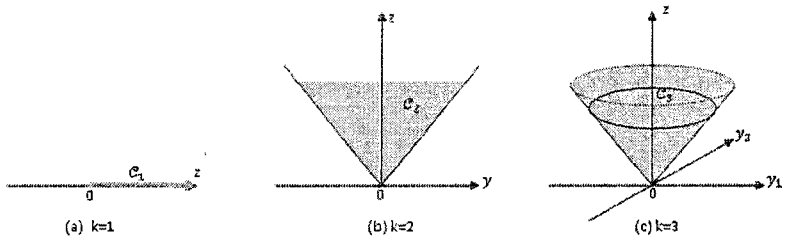

Figure C.1: Second order cones of dimension k=1, 2, and 3

where

$$\|\lambda \mathbf{y}_1 + (1-\lambda)\,\mathbf{y}_2\|_2 \leq \lambda\,\|\mathbf{y}_1\|_2 + (1-\lambda)\,\|\mathbf{y}_2\|_2 \leq \lambda z_1 + (1-\lambda)\,z_2.$$

A second order cone programming problem is a constrained minimization problem which can be formulated as

$$\text{minimize } \mathbf{d}_0^T\mathbf{x} \tag{C.2a}$$

$$\text{subject to } : \ \|\mathbf{A}_i\mathbf{x} + \mathbf{b}_i\|_2 \leq \mathbf{c}_i^T\mathbf{x} + d_i \quad i = 1, \ldots, q \tag{C.2b}$$

where $\mathbf{x} \in \mathbb{R}^{n+1}$ is the optimization vector, and $\mathbf{A}_i \in \mathbb{R}^{(n_i-1)\times n}$, $\mathbf{b}_i \in \mathbb{R}^{(n_i-1)\times 1}$, $\mathbf{c}_i \in \mathbb{R}^{n\times 1}$ and $d_i \in \mathbb{R}$ are the problem parameters.

The problem in (C.2) is called an SCOP problem because if we treat $\mathbf{c}_i^T\mathbf{x} + d_i$ and $\mathbf{A}_i\mathbf{x} + \mathbf{b}_i$ as z and $\mathbf{y}$ respectively, then each constraint in (C.2b) describes a second order cone as

$$\begin{bmatrix} \mathbf{c}_i^T\mathbf{x} + d_i \\ \mathbf{A}_i\mathbf{x} + \mathbf{b}_i \end{bmatrix} = \begin{bmatrix} \mathbf{c}_i^T \\ \mathbf{A}_i \end{bmatrix}\mathbf{x} + \begin{bmatrix} d_i \\ \mathbf{b}_i \end{bmatrix} \in \mathfrak{C}_{n_i}. \tag{C.3}$$

In other words, the set of points that satisfy the ith constraint in (C.2b) is the inverse image of the second order cone $\mathfrak{C}_{n_i}$ under an affine mapping. Since the convexity of a set is preserved under an affine mapping, the feasible region characterized by (C.2b) is convex and, therefore, the SOCP problem in (C.2) is a convex programming (CP) problem.

When $\mathbf{A}_i = \mathbf{0}$ and $\mathbf{b}_i = \mathbf{0}$ for $i = 1, \ldots, q$, the SOCP reduces to a LP problem. When $\mathbf{c}_i = \mathbf{0}$ for $i = 1, \ldots, q$, the SOCP is equivalent to a convex quadratically constrained quadratic program.

SOCP problems can be solved with great efficiency by interior point methods. As an example, the free software package, the SeDuMi toolbox, which is provided by the Advanced Optimization Lab at McMaster University, can be downloaded from the website http://sedumi.mcmaster.ca/ and used to solve the SOCP problems very efficiently.

Appendix D

Formulation of the Angle Constraint

For the convenience of discussion, the angle constraint in the phase rotation approach (5.13) is rewritten as bellow

$$\cos\theta \leq \Re\left(1 + Y_k/X_k\right) \leq 1$$
$$-\tan\theta \leq \frac{\Im\left(1 + Y_k/X_k\right)}{\Re\left(1 + Y_k/X_k\right)} \leq \tan\theta \qquad k = N_0, \ldots, N_1 - 1.$$

The rotation vector r_k is given by

$$\begin{aligned} 1 + \frac{Y_k}{X_k} &= 1 + \frac{Y_k X_k^*}{X_k X_k^*} \\ &= \left(1 + \frac{X_{rk}Y_{rk} + X_{ik}Y_{ik}}{\|X_k\|_2^2}\right) + j\frac{X_{rk}Y_{ik} - X_{ik}Y_{rk}}{\|X_k\|_2^2}. \end{aligned}$$

Therefore the angle constraints can be expressed as

$$\cos\theta \leq 1 + \frac{X_{rk}Y_{rk} + X_{ik}Y_{ik}}{\|X_k\|_2^2} \leq 1 \tag{D.1}$$

$$-\tan\theta \leq \frac{X_{rk}Y_{ik} - X_{ik}Y_{rk}}{X_{rk}Y_{rk} + X_{ik}Y_{ik} + \|X_k\|_2^2} \leq \tan\theta. \tag{D.2}$$

From (D.1) we have

$$-X_{rk}Y_{rk} - X_{ik}Y_{ik} \geq 0 \tag{D.3}$$

$$X_{rk}Y_{rk} + X_{ik}Y_{ik} + \|X_k\|_2^2\left(1 - \cos\ \theta\right) \geq 0. \tag{D.4}$$

If $-\pi/2 < \theta < \pi/2$, then $\cos\theta > 0$. From (D.4), we have

$$X_{rk}Y_{rk} + X_{ik}Y_{ik} + \|X_k\|_2^2 \geq \|X_k\|_2^2 \cos\ \theta > 0.$$

Multiplying all sides of (D.2) by $X_{rk}Y_{rk} + X_{ik}Y_{ik} + \|X_k\|_2^2$, we obtain

$$\begin{aligned} (X_{rk}\tan\theta - X_{ik})\,Y_{rk} + (X_{ik}\tan\theta + X_{rk})\,Y_{ik} + \|X_k\|_2^2 \tan\theta &\geq 0 \qquad \text{(D.5)} \\ (X_{rk}\tan\theta + X_{ik})\,Y_{rk} + (X_{ik}\tan\theta - X_{rk})\,Y_{ik} + \|X_k\|_2^2 \tan\theta &\geq 0. \qquad \text{(D.6)} \end{aligned}$$

Based on (D.3)-(D.6), for $-\pi/2 < \theta < \pi/2$, the matrix form of (5.13) can be expressed as

$$\hat{\mathbf{D}}\hat{\mathbf{Y}} + \hat{\mathbf{f}} \geq \mathbf{0}$$

where

$$\begin{aligned} \hat{\mathbf{Y}} &= \left[\mathbf{Y}_r^T\ \mathbf{Y}_i^T\right]^T \\ \hat{\mathbf{D}} &= \begin{bmatrix} \mathbf{0}_{N,N_0} & -\mathrm{diag}\left\{\bar{\mathbf{X}}_r\right\} & \mathbf{0}_{N,M} & -\mathrm{diag}\left\{\bar{\mathbf{X}}_i\right\} & \mathbf{0}_{N,N_0} \\ \mathbf{0}_{N,N_0} & \mathrm{diag}\left\{\bar{\mathbf{X}}_r\right\} & \mathbf{0}_{N,M} & \mathrm{diag}\left\{\bar{\mathbf{X}}_i\right\} & \mathbf{0}_{N,N_0} \\ \mathbf{0}_{N,N_0} & \mathrm{diag}\left\{-\bar{\mathbf{X}}_i + \tan\theta\cdot\bar{\mathbf{X}}_r\right\} & \mathbf{0}_{N,M} & \mathrm{diag}\left\{\bar{\mathbf{X}}_r + \tan\theta\cdot\bar{\mathbf{X}}_i\right\} & \mathbf{0}_{N,N_0} \\ \mathbf{0}_{N,N_0} & \mathrm{diag}\left\{\bar{\mathbf{X}}_i + \tan\theta\cdot\bar{\mathbf{X}}_r\right\} & \mathbf{0}_{N,M} & \mathrm{diag}\left\{-\bar{\mathbf{X}}_r + \tan\theta\cdot\bar{\mathbf{X}}_i\right\} & \mathbf{0}_{N,N_0} \end{bmatrix} \\ \hat{\mathbf{f}} &= \begin{bmatrix} \mathbf{0}_{N,1} \\ \mathrm{diag}\left\{\left\|\bar{X}_0\right\|_2^2, \cdots, \left\|\bar{X}_{N-1}\right\|_2^2\right\}(1-\cos\theta)\,\mathbf{E}_{N,1} \\ \mathrm{diag}\left\{\left\|\bar{X}_0\right\|_2^2, \cdots, \left\|\bar{X}_{N-1}\right\|_2^2\right\}\tan\theta\cdot\mathbf{E}_{N,1} \\ \mathrm{diag}\left\{\left\|\bar{X}_0\right\|_2^2, \cdots, \left\|\bar{X}_{N-1}\right\|_2^2\right\}\tan\theta\cdot\mathbf{E}_{N,1} \end{bmatrix}. \end{aligned}$$

Index

ADC, 11

AWGN, 12, 29, 39

BER, 2, 3, 16, 41

BPSK, 15

CCDF, 31, 71

CFO, 1

CP, 10, 11, 40

DAB, 1

DAC, 10

DFT, 13, 21, 40

DVB, 1

FDM, 9

FTV, 13

ICI, 2

ICR, 15

IDFT, 10, 16, 19, 25, 39

ISI, 1, 7

MPSK, 3, 10, 38, 55

MQAM, 10, 38

OBP, 2, 4, 5, 41, 58

OFDM, 1

P/S, 10

PA, 1

PAPR, 1, 2, 4, 14, 24, 28, 32, 40, 58

PICR, 2, 4, 15, 24, 28, 32, 41, 58

PTS, 2, 3, 19, 24

QAM, 4

QS, 13

SLM, 2, 3, 22

SOCP, 5, 48, 55

TDL, 11

TI, 3

TR, 2

WSSUS, 10